Ministère de l'Enseignement Supérieur et de la Recherche Scientifique

جامعة أكلي محند أولحاج - البويرة

Université Akli Mohand Oulhadj Bouira

كلية العلوم التطبيقية

Faculté des Sciences Appliquées

Département de Génie des Procédées

Laboratoire Matériaux et Développement Durable

THESE DE DOCTORAT

Présentée en vue de l'obtention du grade de Docteur

En : GENIE DES PROCEDES

Spécialité : Génie Chimique

Par :

MERDOUD Ryma

Intitulée :

Développement de nouveaux matériaux photocatalyseurs et leur application dans la dépollution des eaux usées

Soutenue publiquement le 0/0/ 2025 devant le Jury composé de :

LOUNICI Hakim	Prof	Président	Université de Bouira
AOUDJIT Farid	MCA	Directeur de Thèse	Université de Bouira
MOUNI Lotfi	Prof	Codirecteur de Thèse	Université de Bouira
KERNANI Ridha	MCA	Examinateur	Université de Bouira
BELHADJ Abd-Elmouneïm	Prof	Examinateur	Université de Médéa
HAMDACHE Abderrazaq	MCA	Examinateur	Université de Bouira
RANADE Vivek	Prof	Invité	Université de Limerick

2024/2025

Ministry of Higher Education and Scientific Research

جامعة أكلي محند أولحاج - البويرة

University of Akli Mohand Oulhadj Bouira

كلية العلوم التطبيقية

Applied Science Faculty

Department of Process Engineering

Laboratory of Materials and Durable Development

DOCTORAL THESIS

Presented to obtain the degree of Doctor

In: PROCESS ENGINEERING

Specialty: Chemical Engineering

By :

Ryma MERDOUD

Entitled:

Development of new photocatalyst materials and their application in wastewater treatment

Publicly defended on 0/0/ 2025 in front of the Jury composed of:

LOUNICI Hakim	Prof	President	Bouira University
AOUDJIT Farid	MCA	Supervisor	Bouira University
MOUNI Lotfi	Prof	Co-supervisor	Bouira University
KERNANI Ridha	MCA	Examiner	Bouira University
BELHADJ Abd-Elmouneïm	Prof	Examiner	Medea University
HAMDACHE Abderrazaq	MCA	Examiner	Bouira University
RANADE Vivek	Prof	Guest	Limerick University

2024/2025

Scientific publications

Merdoud, R., Aoudjit, F., Mouni, L., & Ranade, V. V. (2024). Degradation of methyl orange using hydrodynamic Cavitation, H2O2, and photo-catalysis with TiO2-Coated glass Fibers: Key operating parameters and synergistic effects. *Ultrasonics Sonochemistry*, *103*, 106772.

International internships

- ✓ **September 2024-October 2024:** Internship at the University of Limerick, Ireland, focusing on developing new synthesis methods for photocatalytic materials and their application in water treatment using hybrid photocatalytic systems. Supervised by Prof. Vivek V. Ranade, Bernal Chair, at the Bernal Institute.
- ✓ **February 2023-Aougust 2023:** Internship at the University of Limerick, within the framework of the Erasmus+ International Credit Mobility Exchange Program on "Wastewater Treatment by Hydrodynamic Cavitation," supervised by Professor Vivek V Ranade (Bernal Chair) and a member of the M-Ring (Multiphase Reactors and intensification group) group at the Bernal Institute.

Communications

- ✓ Ryma MERDOUD, AOUDJIT Farid, MOUNI Lotfi. Synergetic degradation of azo dyes in wastewater: improved efficiency using advanced hybrid oxidation processes. The 1st National Seminar on BIODIVERSITY, ENVIRONMENTAL RISKS AND PUBLIC HEALTH (SNBRESP 2024), University of TARF, Algeria.
- ✓ Ryma MERDOUD, AOUDJIT Farid. Application of TiO2 photocatalysis for wastewater treatment. The 1st National Seminar on Materials Science NSMS'23, University of Bouira, Algeria.
- ✓ Ryma MERDOUD, AOUDJIT Farid. Algeria's energy policy and challenges. The 17th International Exhibition of Water Equipment, Technologies and Services, International Conference Center, CIC, Club des pins- Algiers, Algeria. SIEE-Pollutec'2022.

Acknowledgments

I am profoundly grateful to **my parents**, whose constant support, sacrifices, and encouragement have been the cornerstone of my academic progress. To **Maria**, **Abdou,** and **Sarah**, whose presence and support have been invaluable. To my entire family, thank you for your belief in me and for standing by my side throughout this work. This achievement would not have been possible without you.

Special thanks to my best friends: **Meriem**, a dear and trusted friend; **Adel**, a cherished friend whose unwavering support and assistance have been invaluable; and **Mouna**, for her help and encouragement.

I extend my sincere appreciation to my supervisor, **Mr. Farid Aoudjit**, for his guidance, expertise, and continuous support throughout my research. His supervision has been essential in shaping the direction of this work.

I am also grateful to **Prof. Lotfi Mouni**, whose support, both moral and practical, has greatly contributed to this research. His generosity in providing laboratory access and necessary resources has been instrumental in accomplishing this work.

Special thanks to **Prof. Soulimane Tewfik** for facilitating my integration into the University of Limerick and for his continuous support, both academically and personally. His assistance was crucial in enabling me to carry out my research in Ireland.

My sincere appreciation goes to **Prof. Vivek Ranade**, whose professionalism and dedication have been a true inspiration. I am immensely grateful for the opportunity to work within his research group, for the valuable experience gained in his laboratory, and for his continuous support, which has significantly contributed to my professional and scientific development.

I would also like to acknowledge **Hadioushe Dalila** for her advice and support, particularly at the beginning of my doctoral studies.

I am sincerely thankful to my colleagues and friends in Ireland: **Vaishnavi, Jagddep, Roja, Amol, Manoj**, **Chinmey, Mukesh,** and all the members of the **MRing research group**, whose collaboration and support have been greatly appreciated.

A heartfelt acknowledgment to **Hanane, Lekbira, and Ismahane** for their kindness and encouragement.

I am truly thankful to my thesis jury members for their insightful feedback and support. My heartfelt thanks to the president, **Mr. Hakim Lounici**, and to the examiners, **Mr. Redha Kernani, Mr. Abderrazaq Hamdache, and Mr. Abd Elmouneïm Belhadj,** for their time, expertise, and valuable feedback

To all those who have contributed to this research in any way, I extend my deepest appreciation.

Table of Contents

List of Figures

List of Tables

List of Abbreviations

Nomenclature

β	Ratio of flow rate through the cavitation device and working volume (Q/V, s^{-1}).
C_{in}	Inlet concentration of MO (ppm)
C	Concentration of MO in the holding tank (ppm)
Ca	cavitation number (-)
COD_0	Chemical oxygen demand at t=0
COD_t	Chemical oxygen demand at t(min)
d_T	Characteristic diameter of the vortex based-HC device (m)
ΔP	Pressure drop across cavitation device (bar)
Eu	Euler number (–)
Φ	per pass degradation factor (-)
k	First-order rate constant (min−1)
n	Number of passes through cavitation device (–)
Q	Recirculating flow rate through cavitation device (LPM)
P	Liquid density (kg/m3)
P_2	Pressure at the outlet (kPa)
P_v	vapour pressure (kPa)
Re	Reynolds number (-)
t	Treatment time (min)
v	Throat velocity for vortex-based cavitation device (m/s)
V	Volume of the solution in all the setup (including the holding tank, the pump and the pipes) (L)
$Y_{cav,HC}$	The cavitation yield (mg/kJ)
γ_1	Synergy coefficient of the combined effect of PC and H_2O_2
γ_2	Synergy coefficient of the combined effect of PC, H_2O_2, and HC

General introduction

Although water covers more than 71% of the earth's surface, the scarcity of clean, high-quality drinking water has emerged as one of the most urgent global challenges, nowadays **[1, 2]**.

This situation is exacerbated by the rapid growth of the global population, and expanding industrial activities, which have significantly increased the demand for clean water **[3]**.

Among these industries, the textile sector stands out as a major contributor to water consumption **[4]**. It has been investigated that the textile industry alone consumes 79 billion cubic meters of freshwater annually **[4, 5]**, contributing to nearly 20% of global water pollution by generating large volumes of wastewater **[6-8]**. This wastewater contains high concentrations of persistent and toxic pollutants, which degrade water quality **[9]**, disrupt aquatic ecosystems **[10]**, and alter ecological balances, ultimately posing serious health risks to both humans and the environment **[11]**.

Considering these challenges, traditional wastewater treatment methods are widely employed owing to their ability to handle a diverse range of pollutants **[12]**. While they can be effective in reducing pollutant concentrations and improving water quality, these methods often have significant drawbacks. A major limitation is their tendency to transfer pollutants from one medium to another rather than degrading and mineralizing them, which results in secondary, complex toxic pollution **[13]**. This limitation emphasizes the need for the development of advanced wastewater treatment methods to ensure sustainable access to clean water **[14]**.

Among these technologies, advanced oxidation processes (AOPs), such as photocatalysis (PC), have gained widespread attention due to their ability to generate highly reactive radicals **[15]**, which mineralize complex organic pollutants partially or completely into carbon dioxide (CO_2), and water (H_2O), offering more effective and eco-environmental alternatives **[16]**.

To further enhance the efficiency of these processes, innovative strategies and material modifications are essential **[17, 18]**.

Within this framework, the current study focuses on optimizing the PC process for the degradation of organic pollutants, specifically methyl orange (MO), a model dye pollutant in this work. This involves using a supported TiO_2 photocatalyst instead of its powdered form. Additionally, composite-based TiO_2 photocatalysts are synthesized to further enhance the

photocatalytic performance. The study also explores the synergistic effects of combining PC with other AOPs, such as the hydrodynamic cavitation (HC) process, to enhance the performance and effectiveness of dye-containing wastewater treatment. Thus, this work addresses both photocatalyst optimization and process enhancement, facilitating practical application.

The thesis is structured into three chapters, each focusing on different aspects of wastewater treatment:

- **Chapter I** provides a comprehensive review of water pollution and wastewater treatment, focusing on dyes and their environmental and health risks. It discusses the limitations of conventional treatment methods and introduces heterogeneous photocatalysis as a promising alternative for dye degradation. Special emphasis is placed on titanium dioxide (TiO_2), a commonly used photocatalyst, exploring its properties, limitations, and strategies for enhancing its performance, including immobilization and doping. The chapter also highlights innovative techniques for optimizing the efficiency of the PC process in wastewater treatment applications.

- **Chapter II** is divided into three main parts. The first part focuses on the degradation of MO using HC alone. The second part examines the impact of combining HC with varying concentrations of hydrogen peroxide (H_2O_2). The third part explores the coupling of HC, H_2O_2, and PC using TiO_2-coated glass fibers tissue (TiO_2-coated GFT), evaluating the synergistic effects and overall performance of this integrated treatment system, including a mineralization study to assess the extent of MO degradation.

- **Chapter III** is structured into three main sections. The first section investigates the degradation of MO using PC alone, emphasizing the optimization of the synthesis method and the photocatalyst type, light intensity, and photocatalyst loading. The second section examines the synergistic effect of combining PC using different H_2O_2 concentrations to enhance the degradation of MO. The third section explores the coupling of PC, H_2O_2, and HC, evaluating the overall performance and synergistic effects of this integrated system in MO degradation.

- **General Conclusion** summarizes the key findings of the thesis, discusses their implications, and suggests potential directions for future research.

Chapter I : Literature Review

I.1 Introduction

This chapter provides a comprehensive review of the literature concerning textile wastewater and its treatment methods. It begins by providing an overview of dyes including their classification, highlighting their environmental impacts such as toxicity to aquatic ecosystems, as well as their potential adverse effects on human health.

The chapter then examines some traditional wastewater treatment methods, discussing their limitations and introducing advanced alternatives, such as heterogeneous photocatalysis for dye removal. Emphasis is placed on TiO_2-based PC, a widely recognized photocatalyst for dye degradation. Its historical development, crystalline structures, applications, and limitations are discussed. Some strategies for enhancing its performance, such as immobilization on supports and doping with metal elements like silver (Ag), are explored.

Finally, the chapter presents some strategies to further improve the PC process, including the addition of oxidants and coupling PC with other AOPs, such as the HC process.

This literature review aims to identify some of the existing knowledge gaps, establish the pivotal role of PC within the framework of advanced wastewater treatment, and highlight the importance of innovative strategies in developing effective, efficient, and sustainable solutions to mitigate dye pollution.

I.2 Overview of dyes

The historical development of synthetic dyes is a captivating narrative that highlights the blend of scientific advancement, technological progress, and artistic creativity. Dyes, whether natural, derived from plants such as the root of madder (Rubia tinctorum), served as a primary source of red and orange dyes utilized in ancient civilizations such as Egypt and Greece **[19]**, animals like the Murex Trunculus, and Murex brandaris, a sea snails, used to produce Tyrian purple, produced from their secretions, highly prized in Rome **[20]**, or minerals such as Lapis lazuli, used to produce ultramarine blue **[21]**, or synthetic, created through chemical processes such as tartrazine (E102), a lemon-yellow synthetic dye **[22]**, are substances designed to impart color to various materials, including textiles, paper, cosmetics, pharmaceutical, and food products **[23].** Their ability to absorb and reflect light at specific wavelengths enables them to produce a diverse spectrum of colors.

Before synthetic dyes led to birth in the late 19th century, various civilizations depended on natural materials, which were often limited in both availability and color variety, for coloring fabrics, and materials **[24].**

The accidental discovery of the first synthetic dye, mauveine, by the British chemist, William Henry Perkin in the mid-1800s, was a pivotal moment in this journey. Perkin stumbled upon mauveine while trying to synthesize quinine from coal tar derivatives, paving the way for the synthetic dye industry **[25].** This new dye offered consistent and striking colors that natural sources could not match, sparking significant interest and further research **[26].**

In 1863, François-Emmanuel Verguin, A French chemist, synthesized alizarin, the first synthetic red dye, from coal tar **[27],** while Carl Graebe and Carl Liebermann, German chemists, made strides with fuchsine in 1858 **[28].**

The late 19th century marked the global establishment of the dye industry, as chemists systematically explored the relationship between chemical structures and color. Innovators like Paul Friedländer and Adolf von Baeyer played crucial roles in identifying the molecular structures of various dyes **[29].**

The 20th century witnessed groundbreaking advancements in dye chemistry, leading to the advancement of a diverse range of synthetic dyes that offered improved color fastness, brightness, and a broader spectrum of hues.

These innovations were driven by the growing demands of the textile industry, as well as the need for dyes in other applications such as plastics, inks, and coatings. For example, the introduction of reactive dyes in the 1950s, revolutionized the dyeing process for cellulose fibers, providing more intense and long-lasting colors **[30].**

Today, the synthetic dye industry continues to thrive, driven by the demand for high-quality colors in various sectors **[31].** Despite growing awareness of environmental issues, many industries still rely heavily on synthetic dyes owing to their cost-effectiveness, wide range of available colors, and superior performance characteristics **[32],** making them indispensable in mass production processes **[23].**

Consequently, the global market for synthetic dyes is expected to expand dramatically due to the fast industrialization and urbanization of emerging economies **[33].**

Dyes are primarily composed of two key components: chromophores, and auxochromes **[34].** Chromophores are the part of the dye molecule responsible for light absorption and color production. They typically contain conjugated systems of double bonds, such as -C=C-, -C=N, or aromatic rings, along with specific functional groups like nitro ($-NO_2$), azo (-N=N-), carbonyl (C=O), or quinoid groups. Auxochromes, on the other hand, are functional groups attached to the chromophore that do not themselves generate color, but enhance the dye's properties, such as color intensity, solubility, and the dye's ability to bind to substrates. These groups include hydroxyl (-OH), amino ($-NH_2$), carboxyl (-COOH), and sulfonic acid ($-SO_3H$) **[35, 36].**

I.2.1 Classification of dyes

Dyes are classified according to their chemical structure and intended application, which reflects their versatility across industrial and commercial sectors. The chemical structure classification is based on the chromophore **[29].** This classification system is crucial for comprehending the behavior of dyes in various contexts, such as their stability under different environmental conditions, their interaction with various chemicals, and their performance on different materials. On the other hand, classification by application considers how dyes are selected based on their compatibility with specific materials and the dyeing processes they require **[37].**

Each classification is crucial for selecting the appropriate dye for use in various industrial applications, ensuring optimal performance and quality

I.2.1.1 Classification based on chemical structure

Among the chemical classifications, azo dyes are the most prevalent, making up approximately 50 % of commercial dyes, known for their vibrant and diverse colors due to nitrogen-to-nitrogen double bonds (–N=N–) **[38].** Other groups include nitro dyes, defined by nitro groups ($–NO_2$)**. [39],** anthraquinone dyes**,** characterized by unique chromophore containing two carbonyl groups positioned on either side of a benzene ring **[40],** phthalocyanine dyes, synthesized through the reaction of dicyanobenzene with metal ions, such as copper, nickel, cobalt, or platinum **[41]**, trimethylmethane dyes, defined by a structure in which a central carbon atom is bonded to three aryl groups **[42],** and xanthene dyes, characterized by a

xanthenone backbone with an oxygen atom linking two aromatic rings **[43]. Table I.2.1** summarizes these classifications.

Table I.2.1 Classification of synthetic dyes based on chemical structure

Type	Chromophore	Examples
Azo Dyes		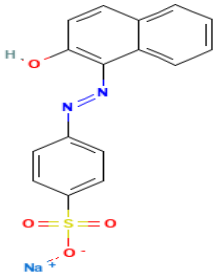 Acid orange
Nitro Dyes	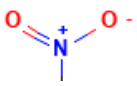	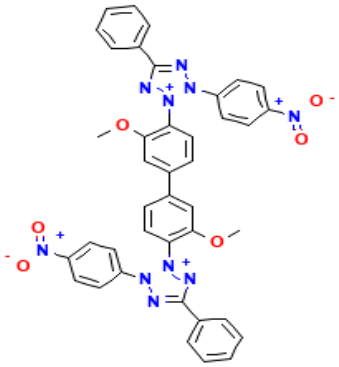 Nitroblue tetrazolium
Anthraquinone Dyes	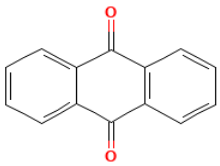	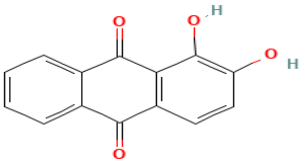 Alizarin

Phthalocyanine dyes	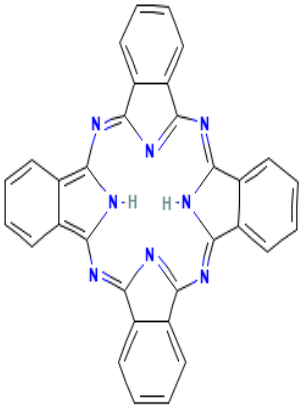	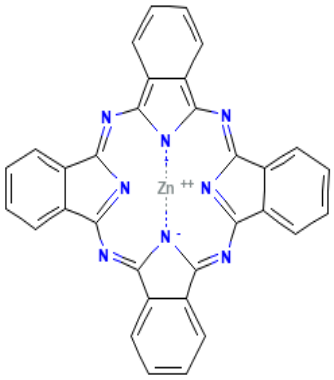 Zinc phthalocyanine
Trimethylmethane dyes	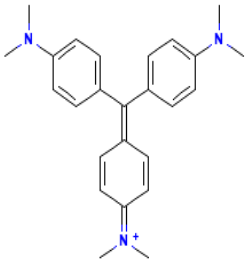	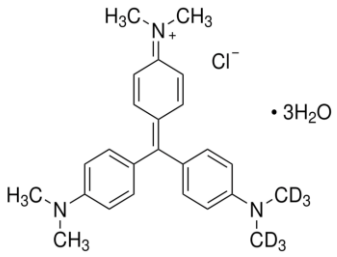 Crystal Violet-d_6 trihydrate
Xanthane dyes	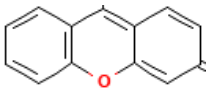	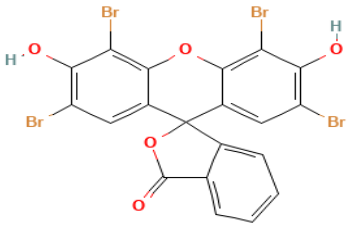 Solvent Red 43

I.2.1.2 Classification based on application

Dyes are also classified based on their application to optimize their use in various processes. This classification helps in selecting the appropriate dye for different types of fibers and desired outcomes. **Table I.2.2** outlines these application-based classifications.

Table I.2.2 Classification of synthetic dyes based on application.

Type	Description	Examples
Direct Dyes	Water-soluble dyes applied directly to cellulose fibers (e.g., cotton) without the need for a mordant. They may have lower wash fastness.	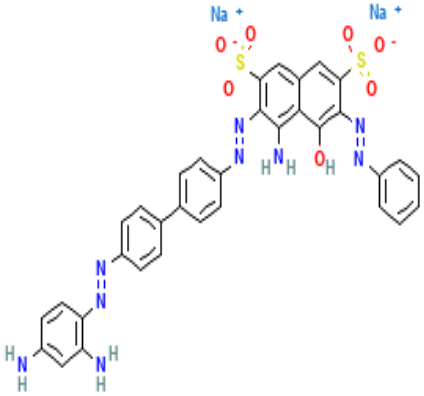 Direct Black
Acid Dyes	Used in acidic conditions to dye protein fibers (e.g., wool, silk, nylon). Ideal for bright colors in textiles and biological staining.	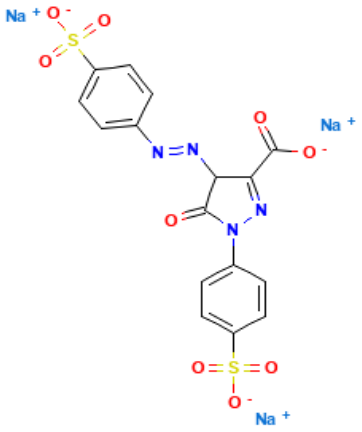 Acid Yellow
Basic Dyes	Cationic dyes that bind to negatively charged synthetic fibers (e.g., acrylics). Known for vivid colors but maybe less wash and light-resistant.	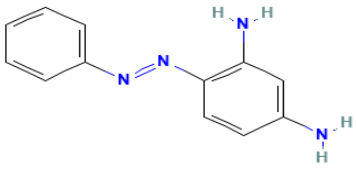 Chrysoidine

Reactive Dyes	Form a strong covalent bond with fibers in an alkaline solution. Used for dyeing wool, cotton, and silk. Offers vibrant colors and durability.	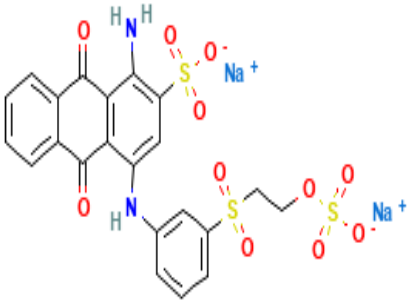 Reactive Blue 19
Vat Dyes	Insoluble in water and require a reduction process to dye cellulose fibers (e.g., cotton). Durable and stable, used in products like denim.	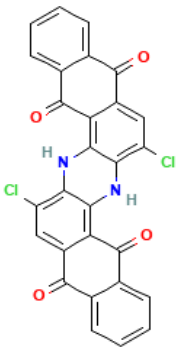 Vat Blue 6
Disperse Dyes	Used for synthetic fibers (e.g., polyester, acetate). Insoluble in water and applied at high temperatures, suitable for sportswear and activewear.	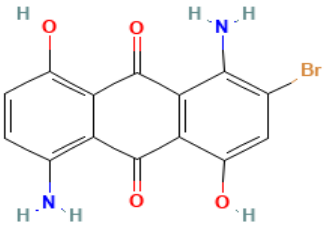 Disperse Blue 56

I.2.2 Environmental impact and health concerns of synthetic dyes

Although synthetic dyes provide substantial benefits, they raise environmental concerns **[44]**. These dyes contain aromatic amines, which are associated with cancer and genetic mutations. Exposure to these synthetic dyes can result in serious health issues **[45].**

It has been reported that approximately 800,000 tons of dyes are produced annually, with 10–15% of this amount released into the environment during manufacturing and application processes. Among more than 10,000 synthetic dye types, azo dyes represent nearly 70%, highlighting their predominance in industrial usage **[46].**

The textile sector, one of the largest consumers of water and chemicals, utilizes over 8,000 chemical species in its processes **[47].** Consequently, it represents a significant source of dye-contaminated wastewater, often discharged untreated or partially treated into natural water

bodies **[48],** which severely damage aquatic ecosystems and pose long-term health risks to exposed populations **[49].** For instance, in Malaysia alone, textile-finishing wastewater accounts for 22% of industrial effluents, with some facilities consuming up to 3000 m^3 of water per day **[50].**

These figures underscore the scale of resource consumption and environmental damage associated with textile production **[51].** Consequently, dye pollution has become a critical environmental challenge.

I.2.2.1 Toxicity to aquatic ecosystems

Textile wastewater, particularly when inadequately treated and discharged into aquatic ecosystems, represents considerable threats to aquatic ecosystems. The visible coloration of the water resulting from dye contamination causes a depletion of dissolved oxygen levels and obstructs sunlight penetration. This disruption hinders photosynthesis, which is essential for the survival of aquatic plants and algae, ultimately damaging the entire aquatic ecosystem **[52].**

This issue is evident in many regions. For instance, in Italy the reported characterization of real textile effluents from dyeing baths indicated a high organic load, with TOC levels reaching 158.0 ± 9.8 mg/L and COD at 1017 ± 58 mg/L. These values reflect the substantial presence of organic contaminants in the discharged wastewater, **[53].** Similarly, in China, the Haicheng River has been subjected to significant industrial wastewater discharge, with 8.5×10^6 tons from textile and paper industries, and 36 billion tons of untreated wastewater each year, affecting rivers, lakes, and coastal waters **[54].**

Other regions also face similar challenges such as the Yamuna River in India, which faces severe pollution due to daily discharges of approximately 15,000 million liters of effluent from textile industries, with dye concentrations reaching up to 200 mg/L and COD (Chemical Oxygen Demand**)** levels exceeding 500 mg/L, far surpassing the permissible limit of 120 mg/L **[55].**

These pollutants create hypoxic conditions in the water, significantly harming aquatic life **[56]. Table I.2.3** summarizes the effects of some dyes on some aquatic organisms. The LC_{50} (lethal concentration for 50% of organisms) is a critical measure of toxicity that indicates the concentration of a substance required to cause death in 50% of a test population of organisms. This value highlights that even relatively low concentrations of certain dyes can be highly toxic to aquatic life.

Table I.2.3 Impact of certain dyes on aquatic organisms

Dye name	Fish species/ Algea	Effects	LC_{50}	Ref
Reactive Red 120	*Catla catla*	Erratic behavior, skin darkening, scale loss, anemia with low hemoglobin/RBC and high WBC.	-	**[57]**
Sudan Black B	Zebrafish larvae	Hepatotoxicity, developmental defects, liver dysfunction, increased mortality.	0.65 mM	**[58]**
Solvent Violet 47	Zebrafish embryos	Mortality, developmental defects, malformations, edema, impaired swimming, BBB disruption.	4.37 mg/L	**[59]**
Trypan Blue	*Cirrhinus mrigala*	Mortality, hepato-renal toxicity, weight loss, hemolysis, congestion, necrosis, tubular/glomerular damage.	40 mg/L	**[60]**
Methylene Blue	*Chlorella vulgaris*	Reduced chlorophyll-a/b and photosynthetic capacity.	-	**[61]**
Disperse Blue 79	Zebrafish (*Danio rerio*)	Decreased ↓Fecundity (−65% at 500 µg/L), reduced growth, impaired hatching, altered metabolome/transcriptome.	500 µg/L	**[62]**

I.2.2.2 Adverse effects on human health

Synthetic dyes have been associated with numerous adverse health effects in humans. **[63].** These effects are due to the chemical composition of synthetic dyes, which can contain toxic, carcinogenic, or biologically disruptive contaminants. When textile dyes and heavy metals are released into water bodies, these pollutants are taken up by the tissues of fish and other seafood. Through the food chain, they ultimately accumulate in human organs or directly through drinking water **[64].**

The exposure to synthetic dyes has been associated with allergic reactions, such as asthma, skin rashes, and other skin irritations **[65].** Certain dyes, such as Tartrazine (Yellow No. 5), and Sunset Yellow (Yellow No. 6), have been linked to hyperactivity and behavioral changes, especially in children with Attention Deficit Hyperactivity Disorder (ADHD) **[66, 67].**

Studies have shown that long-term exposure to some synthetic dyes can bind to DNA and proteins inside cells, potentially leading to mutations and cancer, mainly bladder cancer, particularly for dyes that contain carcinogenic impurities, such as Citrus Red 2 **[68,69].**

Additionally, some dyes act as endocrine disruptors, interfering with hormone systems, which could result in reproductive health issues **[70]. Table I.2.4** illustrates the adverse health effects associated with several commonly used synthetic dyes.

Table I.2.4 Summary of the effects of various synthetic dyes on human health.

Dye name	Use	Adverse health effects	Ref
Congo Red	Cosmetics, leather, food, pharmaceuticals, and paper	Genotoxic, hemotoxic, neurotoxic, carcinogenic, and mutagenic	**[71]**
Methylene Blue	Coloring silk, wool, cotton, paper, cosmetics, and pharmaceuticals	Carcinogenic, respiratory distress, abdominal disorders, blindness, digestive and mental disorders, methemoglobinemia	**[72]**
Amaranth	Food coloring	Genotoxic, cytotoxic, and cytostatic	**[73]**

Disperse Red 1	Textile dye	Mutagenic effects on human hepatoma cells and lymphocytes, leading to cancer	**[74]**
Basic Red 9	Textile dye, biological stain, and cosmetics	Skin irritation, allergic dermatitis, mutations, liver sarcoma, bladder cancer	**[13]**
Crystal violet	Biological stain, pharmaceuticals, textile, and paper	Skin irritation, digestive tract failure, respiratory and renal organ failure, genotoxicity, and carcinogenicity	**[75]**

I.3 Traditional wastewater treatment methods

I.3.1 Overview and application

Traditional wastewater treatment methods have been developed and refined over many decades to satisfy the growing demand for effective water purification **[76].** These techniques employ physical, chemical, and biological processes to remove different contaminants from wastewater. Common methods include adsorption **[77]**, coagulation-flocculation **[78],** filtration **[79],** electrocoagulation **[80],** and biological treatments **[81].**

These methods have been extensively studied and applied for the removal of several pollutants such as synthetic dyes, demonstrating varying degrees of success. Their performance depends on different factors such as pollutant concentration, process time, and other operating conditions **[82]**. A summary of the application of some traditional methods for the removal of dyes is presented in **Table I.3.1.**

Table I.3.1 Application of traditional treatment methods for dye removal

Method	Dye	Operating Conditions	Concentration (mg/L)	Degradation Rate (%)	Time	Ref
Adsorption (Activated carbon)	MB	pH 9, adsorbent dosage: 60 mg/100 mL, max adsorption capacity: 322 mg/g	100	99.9	60 min	**[83]**
		pH 6, Polyferric-silicate-acetate				

Coagulation-Flocculation	CR	coagulant: 0.1 g/L, 300/60 rpm mixing, 16 mg/L dosage	100	93.3	32 min	**[84]**
Electro-coagulation	MO	pH 7, Al/Ni anodes, Fe cathode, 8 mA/cm², 1 g/L NaCl Energy consumed: 36.299 kWh/kg	100	97.74	30 min	**[85]**
Biological treatment (Yeast)	MO	Saccharomyces, pH 5, 37 °C, NaCl 4 g/L, glucose 60 mL/L	50	94.5	48 h	**[86]**
Membrane filtration	Blue Coracazol	Polyethersulfonepolyethylenei ine–graphene oxide membrane, flat sheet, pore size: 0.2 µm, pH: 6-10, 3 bar, water flux: 99 L/m²·h	Initial dye concentration: 10 mg/L, real dye bath concentration: 40 mg/L	97.8 / 96	50 h	**[87]**
Sedimentation	MB	Palygorskite material	0.001 w/v	100	24h	**[88]**

I.3.2 Challenges of traditional wastewater treatment methods

Despite their widespread use, traditional wastewater treatment methods have notable limitations that hinder their performance and sustainability **[89].** One of the major drawbacks is the generation of large amounts of sludge, which requires additional treatment and safe disposal **[12].** For instance, adsorption using activated carbon is not only costly but also energy-intensive due to the need for adsorbent regeneration **[90]**. In addition, coagulation-flocculation generates substantial amounts of chemical sludge, increasing the burden on waste management systems **[91].** Furthermore, electrocoagulation, though efficient, consumes considerable energy and is prone to electrode corrosion, which affects operational efficiency **[92].** Biological treatment methods, such as those utilizing yeast, often have lower degradation time, low biodegradability for azo dyes, and vulnerability to dye harmfulness, limiting their application in variable settings **[93].** Similarly, membrane filtration, despite its effectiveness, suffers from issues like

membrane fouling, which reduces its long-term viability, and it also incurs high operational costs **[94].** The sedimentation, while a common and simple process for separating solid particles from liquids, often requires a long settling time and also leads to the generation of sludge **[88].**

Therefore, these limitations highlight the need for ongoing research and development to improve the efficiency and sustainability of wastewater treatment methods.

I.4 Heterogeneous photocatalysis for wastewater treatment

Photocatalysis, a notably advanced oxidation process (AOP), relies on the use of light-activated catalysts to promote chemical reactions that break down complex organic pollutants in water **[96].** Among its various forms, heterogeneous photocatalysis has gained significant attention as an effective method for wastewater treatment, particularly for its potential to mineralize organic pollutants while maintaining an eco-friendly profile **[97, 98].**

This process relies on the capacity of semiconductor materials to absorb photons with energies equal to or exceeding their band gap energy. This absorption results in the excitation of electrons from the valence band to the conduction band, generating electron-hole pairs (e^-- h^+). These photogenerated charge carriers play a crucial role in facilitating redox reactions at the surface of the photocatalyst, leading to the formation of reactive oxygen species (ROS) such as hydroxyl radicals (·OH) and superoxide ions ($\cdot O_2^-$). These highly reactive species can mineralize pollutants, adsorbed onto the semiconductor's surface, completely or partially, by breaking down their chemical bonds, into carbon dioxide (CO_2), water (H_2O), and other simpler by-products **[99]. Fig. I.4.1** depicts the photocatalytic mechanism of a semiconductor for the degradation of organic pollutants.

Common semiconductor materials used in PC, such as titanium dioxide (TiO_2), zinc oxide (ZnO), and cadmium sulfide (CdS), are favored for their efficient ability to facilitate the generation of ROSs, and the subsequent degradation of pollutants **[100-102].**

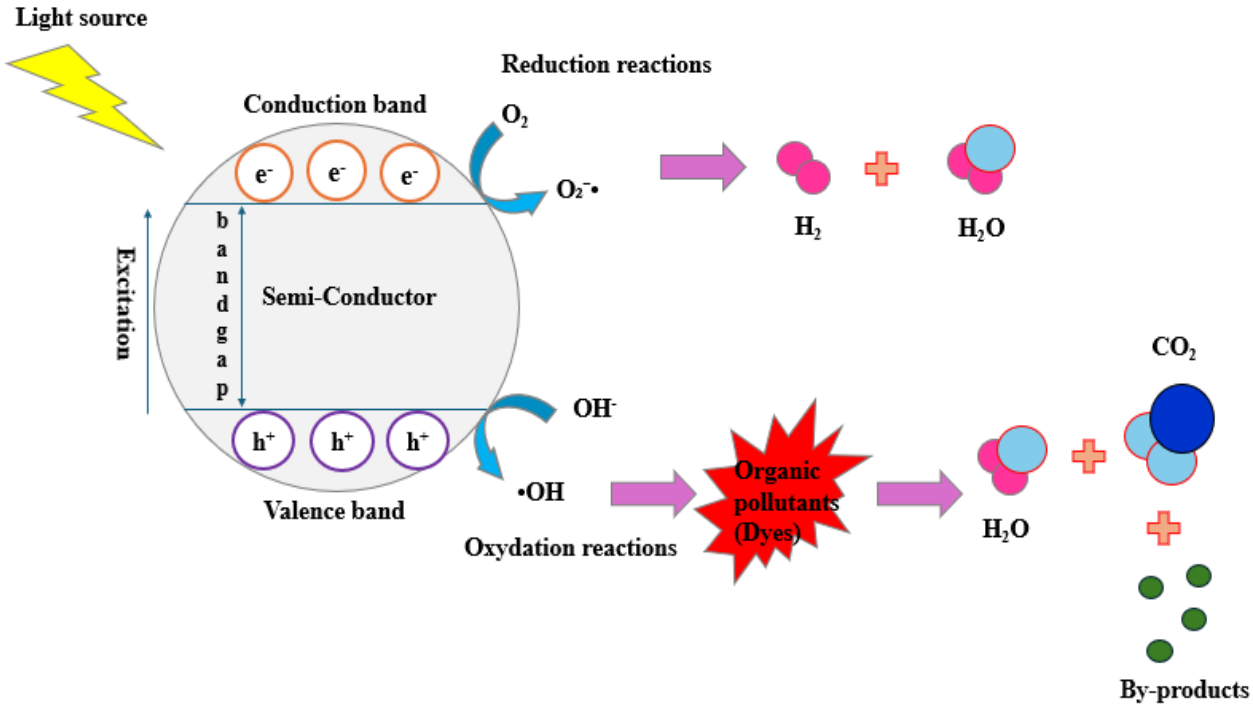

Fig. I.4.1 Photocatalytic mechanism of semiconductor-mediated degradation of organic pollutants

The mechanism of PC can be described through the following steps **[103]:**

$$\text{Catalyst} + h\nu \longrightarrow e_{cb}^{-} + h_{vb}^{+}$$

$$H_2O + h_{vb}^{+} \longrightarrow OH^{-} + H^{+},$$

$$O_2 + e_{cb}^{-} \longrightarrow O^{-2},$$

$$O^{-2} + H^{+} \longrightarrow OH^{-2},$$

$$2OH^{-2} \longrightarrow H_2O_2 + O_2,$$

$$H_2O_2 \longrightarrow 2OH^{\cdot},$$

$$OH^{\cdot} + \text{Dye} \longrightarrow CO_2 + H_2O + \text{by} - \text{products}.$$

1.4.1 Factors influencing the PC process

Several key factors significantly impact the photocatalytic efficiency in the removal of organic dyes. These parameters are essential in determining the performance of catalysts for pollutant degradation, as they directly influence the photocatalytic activity of the composites. Among these factors are the light source's nature and intensity, dye concentration, catalyst dosage, pH levels, and temperature. Understanding and optimizing these variables is vital to achieve high photocatalytic performance while minimizing costs **[104].**

- **The light source's wavelength and intensity**

The choice of a suitable light source is a critical factor in designing and optimizing photocatalytic processes. This choice should align with the properties of the photocatalyst and the goals of the photocatalytic reaction. Several aspects of light sources influence the efficiency of PC. First, the wavelength of light plays a key role, as different sources emit photons in specific ranges, such as ultraviolet (UV) or visible light. PC occurs when photons possess sufficient energy to excite the electrons in the photocatalyst, triggering the desired reactions. Additionally, the intensity of light, which refers to the amount of light emitted over time, can significantly impact the process. Higher light intensity increases the number of photons interacting with the catalyst, enhancing its reactivity. The duration of exposure to light, or irradiation time, also affects the reaction's progress. Prolonged illumination can lead to more complete reactions, ensuring better results. Finally, the type of light source, such as UV lamps, LEDs, fluorescent lamps, halogen lamps, or natural sunlight, influences photocatalytic performance due to their distinct spectral profiles. The choice of the light source should match the optical properties of the photocatalyst to maximize its efficiency **[105-107].**

- **Effect of pH**

pH significantly affects photocatalytic degradation by modifying the surface charge of the catalyst. The point at which the catalyst surface charge becomes neutral is known as the point of zero charge (pH_{PZC}), which for TiO_2 is typically around 6 ± 0.5 **[108].** According to Dutta et al., **[109]** when the pH is lower than the pH_{PZC}, the catalyst surface becomes positively charged, attracting anions. On the other hand, when the pH exceeds the pH_{PZC}, the surface becomes negatively charged, attracting cations. This variation in charge influences the adsorption of pollutants and, consequently, the efficiency of the photocatalytic process. Anionic dyes, for instance, tend to adsorb more effectively onto positively charged surfaces in acidic conditions, while cationic dyes are more likely to adsorb onto negatively charged surfaces in basic environments **[110].** These interactions are crucial in determining the overall photocatalytic activity, as the surface charge affects the catalyst's ability to interact with and degrade different pollutants.

- **Photocatalyst loading**

To optimize the photocatalytic process, it is important to avoid using an excessive amount of photocatalyst. From an economic perspective, the photocatalytic process should achieve maximum efficiency with the minimum amount of photocatalyst used **[111]**. It has been observed that increasing the amount of photocatalyst generally enhances photocatalytic activity, as more active sites are available on the surface of the catalyst. This leads to the generation of higher quantities of hydroxyl radicals (•OH) and other reactive oxygen species (ROS), thus enhancing the PC. However, beyond a certain threshold, using too much photocatalyst can decrease efficiency. Excessive photocatalyst leads to reduced light penetration within the solution, as the reactor becomes cloudy, ultimately diminishing photocatalytic performance **[112].**

- **Pollutant concentration**

The concentration of the contaminant in the solution is another significant factor that influences the photocatalytic process. There is typically an inverse relationship between dye concentration and photocatalytic degradation efficiency **[112].** As the dye concentration increases, more dye molecules adsorb onto the photocatalyst's surface, decreasing the number of available active sites for photon absorption and decreasing the generation of hydroxyl radicals (•OH) **[113].** This reduction in active sites and radical generation leads to a decrease in overall dye degradation. Additionally, higher dye concentrations limit the distance photons can travel through the solution, reducing the amount of light reaching the catalyst and further hindering photocatalytic activity. At elevated concentrations, dye molecules can also cause surface blocking by occupying active sites and competing with photons and reactive species, further diminishing catalytic efficiency. According to Mamun et al., **[114]** a 23% decrease in the photocatalytic degradation of MO dye, was observed at an initial concentration of 50 mg/L when using a doped TiO_2 composite under solar light irradiation, attributing the reduction to the limited penetration of simulated solar light into the dye solution

- **Effect of temperature**

The photocatalytic process is activated by photons and does not require heat, typically functioning at room temperature **[115].** However, there exists an optimal temperature range that

strikes a balance between improving reaction rates and minimizing the adverse effects of increased recombination rates **[116].** Generally, elevated temperatures can accelerate photocatalytic reactions by providing additional kinetic energy to molecules, promoting more frequent and effective collisions between reactants and the photocatalyst. Studies have shown that temperatures ranging from 20°C to 80°C tend to offer optimal conditions for pollutant photodegradation **[117].** However, excessive heating can lead to a rise in the recombination rate of electron-hole pairs, thereby reducing photocatalytic efficiency. Furthermore, temperature variations can alter the adsorption-desorption equilibrium of pollutants on the photocatalyst surface, with higher temperatures potentially diminishing adsorption due to an increase in desorption rates. Thus, while moderate heating can enhance photocatalytic activity, excessive temperatures may adversely affect the overall process efficiency **[115].**

I.5 TiO_2 as a photocatalyst

I.5.1 Key functional advantages of TiO_2Titanium dioxide is widely used in photocatalysis due to its unique combination of properties such as an chemical stability, low-toxicity [118], high corrosion resistance [119], and strong oxidative ability under UV light [120]. It operates effectively at low temperatures and is abundant, cost-effective [121]. These advantages make TiO_2 a preferred practical material for real-world applications, such as water purification systems **[122].**

Today, TiO_2 remains indispensable in diverse applications, from environmental remediation to renewable energy technologies.

I.5.2 Crystalline forms

TiO_2 exists in three primary crystalline forms, each with distinct structural properties and varying photocatalytic performances **[123],** as illustrated in **Fig. I.5.1.**

- **Anatase**

Characterized by its tetragonal crystal structure and relatively open atomic arrangement, features Ti^{4+} ions coordinated with six O^{2-} ions in distorted octahedra **(Fig. I.5.1 (a))**. This structure facilitates efficient pathways for electron mobility, enhancing its photocatalytic activity. With a density of 3.894 g/cm³ **[124],** anatase is less dense compared to the rutile phase of TiO_2 (density of 4.25 g/cm³) owing to its more open atomic packing. This less dense structure

reduces recombination sites for charge carriers, boosting photocatalytic efficiency. Its bandgap of approximately 3.2 eV makes anatase highly effective under UV light, and its refractive index of 2.5 further contributes to its optical properties **[125,126].** Due to its high photocatalytic activity, anatase is commonly used in environmental purification applications, such as water purification systems. Its efficiency under UV light also makes it suitable for solar cells **[127].**

- **Rutile**

Also possessing a tetragonal structure, rutile is the most stable phase, due to its dense crystal structure, in which Ti^{4+} ions are closely packed in an octahedral configuration **(Fig. I.5.1 (b))**. This phase is thermodynamically stable and typically forms at high temperatures (600–700°C) **[128].** Rutile is the densest phase of TiO_2, with a density of 4.25 g/cm³ **[129],** and a refractive index of 2.7 **[130]**. The dense packing results in fewer surface sites, reducing its photocatalytic efficiency compared to anatase, but it enhances durability, making rutile suitable for industrial applications as a white pigment for paints, plastics, and papers **[131].** With a bandgap of about 3.0 eV, rutile is less efficient under UV light for photocatalytic applications but is valued for its stability and robustness **[132].**

- **Brookite**

The rarest polymorph of TiO_2, exhibits an orthorhombic structure with a more complex atomic arrangement **(Fig. I.5.1 (c))**. It has a density of 4.12 g/cm³ **[133]** and is less stable compared to anatase and rutile. It transforms into the rutile phase at 800°C**. [134,135].** The optical and catalytic properties of brookite remain the least explored, primarily due to the challenges associated with synthesizing a pure brookite phase **[136].**

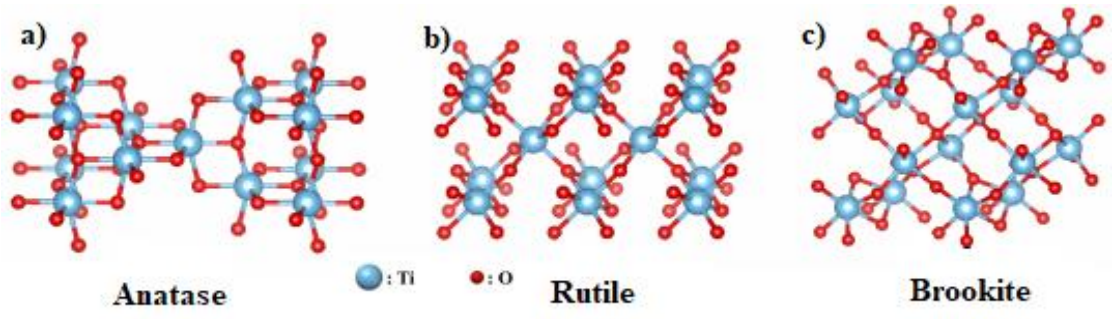

Fig. I.5.1 Crystallographic structures of a) anatase, b) rutile, and c) brookite TiO_2, visualized and represented using the VESTA software package **[137]**

I.5.3 Applications of TiO_2

Titanium dioxide (TiO_2) is a white, crystalline powder known for its chemical stability, photocatalytic activity, and corrosion resistance, making it invaluable across various industries. In environmental applications, TiO_2 is widely used in PC for water and air purification due to its ability to degrade organic pollutants under UV light **[138].** In the textile industry, it is applied as a coating to provide UV protection and improve fabric durability **[139].** TiO_2 also finds extensive use in the food industry as a whitening agent (E171) in confectionery and other products **[140],** and in pharmaceuticals, where it serves as a light-protective coating for tablets **[141].** In cosmetics, it is a key ingredient in sunscreens and makeup products due to its UV-blocking properties and skin safety **[142].** Furthermore, TiO_2 is integral to dye-sensitized and perovskite solar cells, serving as an efficient photoanode material **[143].** Its applications extend also to paints and coatings, where TiO_2 is used as a pigment to provide enhanced opacity, whiteness, and weather resistance **[144].**

I.5.4 Limitations of TiO_2

- **High Electron-Hole Recombination Rates**

Photocatalytic activity in TiO_2 is largely hindered by the rapid recombination of photogenerated electron-hole pairs. This process reduces the availability of charge carriers for key reactions, such as the generation of reactive oxygen species (ROS), limiting its overall efficiency **[145].**

- **Limited Visible Light Absorption**

Because of its large band gap (approximately 3.2 eV for anatase), TiO_2 primarily absorbs UV-A light, which makes up only about 5% of the solar spectrum. This restricts its photocatalytic performance under natural sunlight, requiring modification to extend its absorption into the visible light range for better applicability in outdoor settings **[146].**

- **Challenges in Recovery and Reusability**

When used in powder form, TiO_2 particles are challenging to recover from treated water due to agglomeration. This complicates recycling processes, making it less feasible for large-scale applications **[147].**

Therefore, optimizing these parameters is crucial for consistent and reliable photocatalytic performance.

I.5.5 Strategies to improve TiO_2 photocatalytic performance

I.5.5.1 Immobilization of TiO_2 on support materials

The use of support materials for TiO_2 is a widely studied strategy to improve its photocatalytic performance while addressing challenges such as nanoparticle aggregation, difficulty in recovery, and mechanical instability. Various materials have been explored for this purpose, each offering distinct advantages.

- Zeolites **[148],** have been extensively studied due to their high surface area, porous structure, and significant adsorption capacity, making them effective at adsorbing and concentrating pollutants near TiO_2 active sites **[149].** This synergistic effect has been observed in wastewater treatment applications, particularly for the photodegradation of synthetic dyes **[150].**
- Carbon-based materials **[151]**, including graphene and carbon nanotubes (CNTs), offer excellent electrical conductivity that facilitates effective charge separation and minimizes electron-hole recombination. This property, combined with their ability to absorb visible light, extends TiO_2's photocatalytic spectrum **[152].**
- Polymeric materials **[153],** like polyvinyl alcohol (PVA) and polyethylene are favored for their flexibility, lightweight nature, and ease of fabrication into various shapes. Their chemical stability makes them suitable for continuous-flow systems **[154].**
- Glass fibers tissue, stands out as a good choice for immobilizing TiO_2 due to its unique combination of mechanical strength, thermal stability, and optical characteristics. Its high surface area ensures uniform TiO_2 distribution, providing abundant active sites for photocatalytic reactions **[155].** Yu et al., **[156]** have reported that TiO_2 particles deposited on glass fibers exhibited stable photocatalytic activity over 4 reactive cycles, with minimal deactivation under repeated UV exposure. The TiO_2- coated GFT achieved a consistent nitrogen monoxide degradation rate of approximately 67% throughout the cycles, highlighting its potential for long-term photocatalytic applications.

  Additionally, its excellent thermal stability enables it to withstand high-temperature treatments **[157,158],** unlike polymeric materials that exhibit poor thermal stability, with

maximum resistance temperatures of approximately 150°C for PVA **[159]**, and 80°C for polyethylene **[160],** which limits their use in high-temperature processes like calcination, which requires temperatures above 400°C to enhance TiO_2 crystallinity **[161].** GFT's transparency to UV and visible light enables efficient light penetration, maximizing the activation of TiO_2, thus enhancing photocatalytic performance in photoreactor systems. Moreover, GFT's lightweight, flexible, and easy to handle, make it adaptable to various reactor configurations, including flat-panel and tubular systems. Its chemical inertness further contributes to its durability across diverse operational environments, ensuring long-term performance without interference with the catalytic process. Compared to zeolite, and carbon-based materials, which face challenges in large-scale water treatment processes due to their complex fabrication requirements, GFT offers a simpler, and more economical solution. Zeolite requires a complex synthesis process involving high temperatures, specialized conditions, and chemical treatments to achieve properties like high surface area or ion exchange capacity, making it expensive and less practical for large-scale applications **[162,163],** while carbon-based materials including graphene, and CNTs, involve multiple steps like purification and functionalization to enhance their properties **[164,165].** These complexities and costs make zeolite and carbon-based materials less suitable for large-scale applications.

While various supports offer distinct advantages, GFT provides an unmatched combination of mechanical strength, thermal stability, light transparency, and practicality. These characteristics make it a superior choice for TiO_2-based photocatalytic systems, ensuring efficient pollutant degradation, catalyst recovery, and long-term stability, thereby contributing significantly to the economic and environmental sustainability of advanced wastewater treatment technologies.

To immobilize TiO_2 on glass fibers, the dip-coating method is a commonly used technique due to its low cost, simplicity, and effectiveness **[166].**

This process involves preparing a homogeneous suspension by dissolving powdered titanium in an alcohol, such as ethanol, and stirring the mixture thoroughly. Prior to coating, the glass fibers are cleaned with specific solutions, such as acids **[167]** organic solvents, or neutral detergents **[168]** to enhance the adhesion of TiO_2 to the substrate. After stirring for a set period, the glass fibers are immersed in the solution, allowing the titanium precursor to uniformly coat their surface. According to the literature **[169], t**he immersion duration and number of dip-

coating cycles significantly influence the coating thickness. Longer immersion times allow more TiO_2 to be absorbed, leading to a thicker coating. Similarly, increasing the number of dip-coating cycles results in additional layers of TiO_2 being deposited, further enhancing the coating thickness. These factors are key to controlling the final thickness of the TiO_2 layer on the fibers. After immersion, the glass fibers are washed multiple times with distilled water to eliminate unadsorbed or weakly adsorbed TiO_2, then dried to evaporate the solvent, followed by the calcination at high temperatures (300°C to 500°C) **[170],** to improve TiO_2 crystallinity and eliminate any organic impurities, and then cooled at room temperature. In some cases, the immersion and drying steps are repeated to achieve a thicker and more uniform coating **[171].**

Proper control of dip-coating cycles and annealing parameters ensures optimal coating thickness, and photocatalytic performance, maximizing active sites and providing durable, stable coatings for wastewater treatment applications **[172].**

I.5.5.2 Ag as dopant of TiO_2 photocatalyst

Ag stands out as a highly effective dopant for improving the photocatalytic performance of TiO_2 compared to other elements such as copper, zinc, or lanthanum. This is due to its excellent catalytic properties, electrical conductivity, surface area, and durability, which enable it to facilitate highly selective and efficient redox reactions, particularly in the degradation of organic contaminants **[173,174].**

The practicality of Ag-doped TiO_2 for wastewater treatment relies heavily on its stability and reusability. For instance, Nguyen, et al., **[175]** have shown that the photocatalytic efficiency remains above 85% even after 5 reactive cycles, with negligible silver leaching. This high durability, and stability, make Ag-doped TiO_2 a promising candidate for long-term water treatment applications, minimizing the necessity for frequent catalyst replacement.

The enhancement of TiO_2 photocatalytic performance by Ag occurs through two primary mechanisms. Firstly, silver acts as an electron transfer center, capturing electrons from the conduction band of TiO_2 and transferring them to O_2 molecules, generating reactive superoxide radicals. Secondly, under light irradiation, the increased generation of holes in the valence band of TiO_2 promotes their reaction with H_2O molecules to produce (·OH), which are crucial in oxidizing dyes **[176].**

Furthermore, Ag nanoparticles play a dual role as electron mediators and photosensitizers. As electron mediators, they trap excited electrons from TiO_2's conduction band, reducing charge recombination and prolonging the lifetime of charge carriers **[177].** As photosensitizers, Ag nanoparticles absorb low-energy photons and inject excited electrons into TiO_2, enhancing photocatalytic efficiency. This dual functionality leads to the formation of a more stable electron-hole pair and significantly improves the overall efficiency of photocatalytic reactions **[178].**

In addition to these properties, Ag-doped TiO_2 exhibits excellent thermal stability **[179]**. Amrani et al., **[180]** have shown that the incorporation of silver into the TiO_2 matrix enhances its thermal stability, allowing it to maintain its crystalline structure and photocatalytic activity even at elevated temperatures.

Moreover, Ag-doped TiO_2 exhibits remarkable optical effects. The incorporation of silver nanoparticles into the TiO_2 matrix modifies its optical properties, particularly by increasing the absorption of visible light, in some cases. This is due to the surface plasmon resonance of silver nanoparticles, which allows TiO_2 to absorb a broader range of light wavelengths, thereby enhancing its photocatalytic efficiency under solar irradiation, **[180].** These optical effects are crucial for practical applications, as they enable more efficient use of solar light for photocatalytic reactions.

These properties, including enhanced charge separation, improved stability, superior thermal properties, and broadened light absorption, collectively contribute to a significant improvement in the overall photocatalytic efficiency of TiO_2, making Ag-doped TiO_2 a highly promising material for applications such as in pollutant degradation.

With all the exceptional properties of silver as a dopant for TiO_2, the synthesis method remains crucial in highlighting the photocatalytic performance.

Numerous methods have been utilized to synthesize the Ag-doped TiO_2 photocatalysts with diverse morphologies, including sol-gel **[181]**, photodeposition **[182]**, hydrothermal **[183]**, Electrospinning **[184],** and microwave-assisted processes **[182]. Table I.5.1** summarizes the common synthesis methods for Ag-doped TiO_2 nanoparticles and their efficiency in dye degradation via PC. Each method presents unique advantages and limitations in terms of cost, efficiency, and material properties such as morphology, crystallinity, particle size, and

dispersion of silver within the TiO_2 matrix. These properties significantly affect the photocatalytic efficiency and stability of the catalyst.

However, optimizing these techniques or exploring more innovative, cost-effective, and time-efficient synthesis methods remains essential to further enhance the practical application of Ag-doped TiO_2 photocatalysts.

Table I.5.1 Overview of Ag-doped TiO_2 nanoparticles synthesis and photocatalytic efficiency

Materials used	Synthesis Method	pollutant	Photocatalytic performance	Ref
Titanium (IV) isopropoxide, silver nitrate	Sol gel	MB	95% in 60 min under visible light	**[185]**
Titanium (IV) isopropoxide, silver nitrate	Hydrothermal	Tartrazine	87% in 180 min under visible light	**[183]**
TiO_2 powder, silver nitrate	photodeposition	RhB	100% in 60 min UV light	**[182]**
TiO_2 powder, silver nitrate	Formaldehyde assisted microwave synthesis	RhB	100% in 30 min under UV light	**[182]**
Titanium (IV) isopropoxide, silver nitrate	Electrospinning-calcination	MB	77% in 1.33 h under visible light	**[184]**

I.6 Strategies to improve the PC process

1.6.1 Add of oxidant

The addition of oxidants, such as H_2O_2, is a well-established strategy to enhance the efficiency of photocatalytic systems. H_2O_2 demonstrates remarkable oxidative performance when coupled with TiO_2 for the degradation of organic pollutants. For instance, Wu et al., **[186]** have

highlighted the significant synergistic effect of TiO_2/H_2O_2 systems in the photodegradation of tartrazine, MO, and rhodamine B.

Under light source, in the presence of the photocatalyst, H_2O_2 can act as an electron acceptor, effectively reducing the recombination of photogenerated electron-hole pairs (**Equation I.1)** and further boosting the generation of ROS (**Equation I.2 and I.3**)

$$H_2O_2 + h\nu \longrightarrow 2OH^{\cdot} \quad \text{I.1}$$

$$H_2O_2 + e^- \longrightarrow OH^{\cdot} + OH^- \quad \text{I.2}$$

$$H_2O_2 + O_2^{\cdot -} \longrightarrow OH^{\cdot} + OH^- + O_2 \quad \text{I.3}$$

However, the effectiveness of H_2O_2 in PC is influenced by its concentration. An optimum concentration is crucial to maximize ROSs production while minimizing the scavenging of reactive species or competitive adsorption on the catalyst surface, ensuring optimum photocatalytic efficiency **[187-189].**

I.6.2 PC coupled HC

Hydrodynamic cavitation (HC) is the phenomenon involving the formation, growth, and subsequent violent collapse of vapor-filled cavities (microbubbles) within a liquid, induced by local pressure variations. These cavities are nucleated in regions where the static pressure of the liquid falls below its vapor pressure, often due to geometric constrictions or flow acceleration. As the fluid moves into higher-pressure zones, the cavities collapse (implode) rapidly, resulting in localized extreme conditions.

Under specific conditions, the collapse of these microbubbles leads to the generation of localized hotspots with temperatures exceeding 2000 K and pressures surpassing 100 MPa. This implosion generates intense turbulence, shockwaves, high-shear zones, and liquid microjets traveling at velocities of several hundred meters per second. These mechanical effects, combined with the extreme thermodynamic conditions, induce the homolytic cleavage of water (H_2O) and dissolved gases (e.g., O_2), thereby forming highly reactive radical species, such as •OH (hydroxyl), •H (hydrogen), and O• (atomic oxygen). These reactive oxygen species (ROSs) are powerful oxidants that play a central role in the degradation of organic pollutants. **[190-192].**

Fig. I.6.1 depicts a schematic representation of the mechanisms involved in the cavitation process, illustrating bubble growth, implosion, and the subsequent formation of oxidative radicals responsible for pollutant degradation.

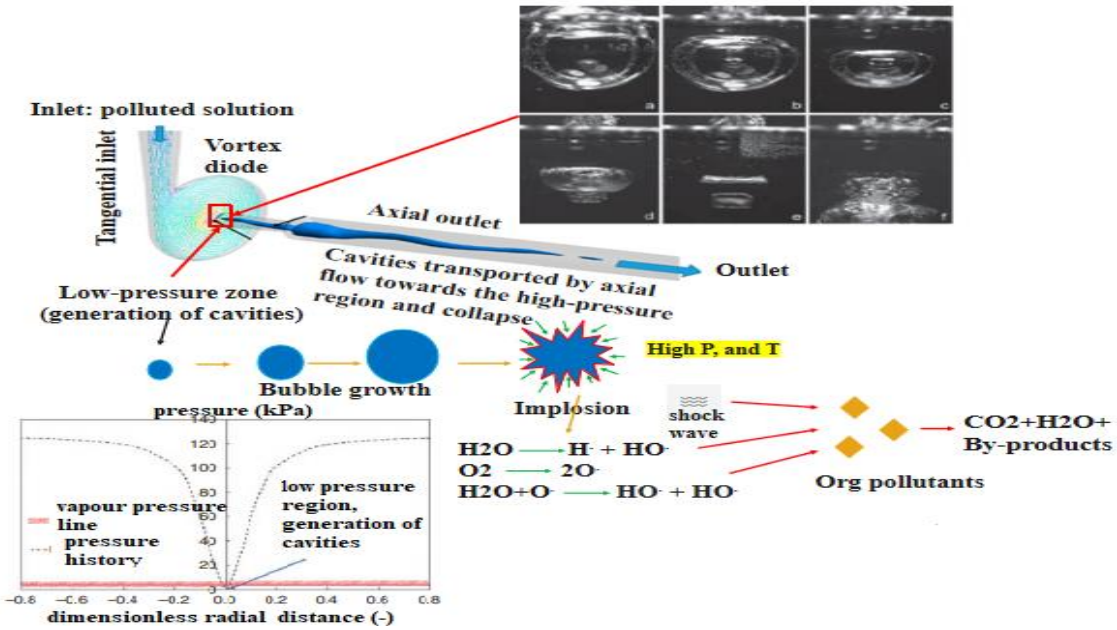

Fig. I.6.1 Schematic representation of HC process using a vortex diode, including a graphic depiction of bubble formation, expansion, and collapse during the cavitation process **[193],** and pressure profile **[194].**

HC devices are generally categorized into two main types:

1. Active cavitation devices, which contain moving parts (e.g., rotor-stator systems), generate cavitation through mechanical shear and turbulence induced by high-speed rotating components and roughened surfaces. While effective, these systems are expensive, energy-intensive, and require frequent maintenance, limiting their practical application despite their high cavitation efficiency **[195].**

2. Passive cavitation devices, which have no moving parts, include venturi tubes, orifices, and vortex diodes. These rely on flow geometry to induce pressure drops and cavitation. Among them, vortex-based systems are gaining prominence due to their ability to confine cavitation in the core of the liquid, thereby minimizing wall erosion, avoiding clogging, and prolonging device lifespan **[196,197].**

Passive devices, such as vortex-based or constriction-based systems, generate cavitation through controlled flow dynamics. While constriction devices risk clogging and erosion due to

wall-bubble collapse, vortex-based designs reduce these issues by confining cavitation to the liquid's core **[196,197].**

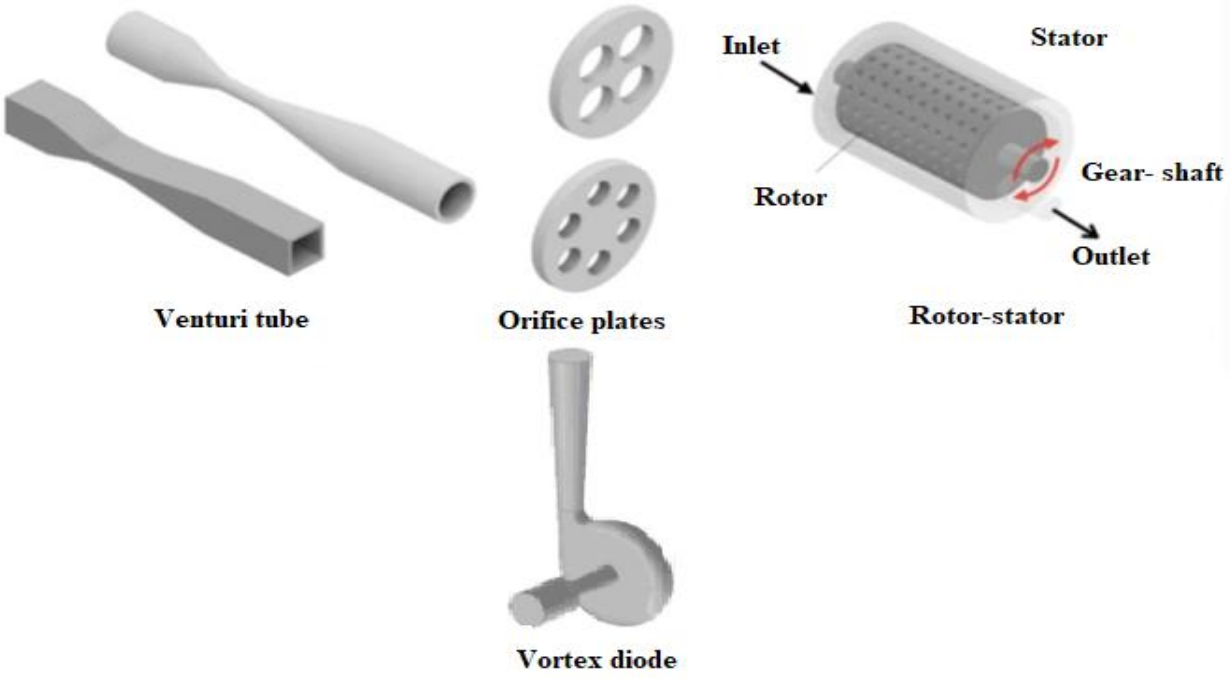

Fig. I.6.2 Hydrodynamic-based cavitation devices **[198,199]**

Applications of HC are increasingly diversified and include:

- Wastewater treatment, where ROSs degrade dyes, pharmaceuticals, pesticides, and other recalcitrant compounds **[200].**
- Water disinfection, through the disruption of microbial cell walls and oxidative inactivation of pathogens **[201].**
- Biomass pre-treatment, where cavitation enhances cell wall disruption, promoting the release of fermentable sugars for bioenergy applications **[202].**

This technique is particularly attractive due to its green and chemical-free nature, scalability, low operational footprint, and the ability to intensify chemical reactions through both physical (microjets, shockwaves, turbulence) and chemical (ROS generation) mechanisms. Moreover, HC can be integrated with other Advanced Oxidation Processes (AOPs) to enhance performance.

When combined with photocatalysis (PC), HC dramatically boosts degradation efficiency through synergistic effects—enhancing mass transfer, generating additional active sites, and accelerating radical formation, thereby improving overall kinetics of pollutant degradation.

Combining this technique with PC will further boost degradation efficiency by increasing radical generation and improving reaction kinetics.

Chapter II: Degradation of methyl orange using hydrodynamic Cavitation, H_2O_2, and photo-catalysis with TiO_2-Coated glass Fibers: Key operating parameters and synergistic effects

Ultrasonics Sonochemistry 103 (2024) 106772

Contents lists available at ScienceDirect

Ultrasonics Sonochemistry

journal homepage: www.elsevier.com/locate/ultson

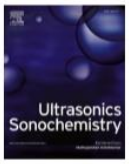

Degradation of methyl orange using hydrodynamic Cavitation, H_2O_2, and photo-catalysis with TiO_2-Coated glass Fibers: Key operating parameters and synergistic effects

Ryma Merdoud [a,b,c], Farid Aoudjit [a], Lotfi Mouni [b], Vivek V. Ranade [c,*]

[a] Laboratoire Matériaux et Développement Durable, Faculté des Sciences et Sciences Appliqués, Université de Bouira, 10000 Bouira, Algeria
[b] Laboratoire de Gestion et Valorisation des Ressources Naturelles et Assurance Qualité, Faculté SNVST, Université de Bouira, 10000, Algeria
[c] Department of Chemical Sciences and Bernal Institute, University of Limerick, Ireland

ARTICLE INFO

Keywords:
Degradation rate
External oxidant
TiO_2-coated glass fibers
Mineralization

ABSTRACT

Advanced oxidation processes (AOPs) are eco-friendly, and promising technology for treating dye containing wastewater. This study focuses on investigating the removal of methyl orange (MO), an azo dye, from a synthetic wastewater through the use of hydrodynamic cavitation (HC), both independently and in combination with hydrogen peroxide (H_2O_2), as an external oxidant, as well as photocatalysis (PC) employing catalyst coated on glass fibers tissue (GFT). The examination of various operating parameters, including the pressure drop and the concentration of H_2O_2, was systematically conducted to optimize the degradation of MO. A per-pass degradation model was used to interpret and describe the experimental data. The data revealed that exclusive employment of HC using a vortex-based cavitation device at 1.5 bar pressure drop, resulted in a degradation exceeding 96 % after 100 passes, equivalent to 230 min of treatment (cavitation yield of 3.6 mg/kJ for HC), with a COD mineralization surpassing 12 %. The presence of a small amount of H_2O_2 (0.01 %) significantly reduced the degradation time from 230 min to 36 min (16 passes), achieving a degradation of 99.8 % (cavitation yield of 6.77 mg/kJ for HC) with COD mineralization rate twice as much as HC alone, indicating a synergistic effect of 4.8. The degradation time was further reduced to 21 min by combining HC with PC using TiO_2-coated glass fibers and H_2O_2, (cavitation yield of 11.83 mg/kJ for HC), resulting in an impressive synergistic effect of 9.2 and COD mineralization twice as high as the HC/H_2O_2 system. The results demonstrate that HC based hybrid AOPs can be very effective for treating and mineralizing azo dyes in water.

1. Introduction

One of the major contributors to water contamination are the textile industries, because of their large quantities of dye containing wastewater; a problem that needs to be remedied on a global scale. On an annual basis, ~ 10^8 tons of dyes are manufactured, and a significant fraction of it is used by the textile sector around the world [1]. This extensive utilization gives rise to a substantial volume of wastewater, laden with persistent organic pollutants (POPs), primarily comprising azo dyes [2]. The environmental repercussions of such wastewater are profound, as it poses a considerable threat to ecosystems [3] and human health [4], attributed to the high toxicity, mutagenicity, and carcinogenicity [5].

Several conventional wastewater treatment techniques, such as adsorption [6], biological treatment [7], coagulation [8], membrane filtration [9] etc., involve the transfer of the pollutant from one medium to another without destroying it, in addition to the high operational cost and time-consuming, with low efficiency. Recognizing these shortcomings, there is a compelling need to explore advanced and eco-friendly alternatives to treat dye-containing wastewater, and herein lies the significance of advanced oxidation processes (AOPs). AOPs such as Fenton process [10], ozonation [11], hydrogen peroxide [12], photocatalysis [13], and others, are capable to degrade and mineralize complex organic pollutants in aqueous solutions, by the generation of powerful non-selective radicals like $OH^{\cdot}$ [14]. These AOPs are eco-friendly since they focus on complete mineralization of pollutants with high efficiencies.

In recent years, one of the promising AOPs for the treatment of wastewater is hydrodynamic cavitation (HC) [15–17]. HC is a process of

* Corresponding author.
E-mail address: Vivek.Ranade@ul.ie (V.V. Ranade).

https://doi.org/10.1016/j.ultsonch.2024.106772
Received 18 November 2023; Received in revised form 1 January 2024; Accepted 14 January 2024
Available online 18 January 2024

Abstract

Advanced oxidation processes (AOPs) constitute green and promising technological advancements for the treatment of dye-laden wastewater. This research investigates the elimination of methyl orange (MO), a type of azo dye, From synthetic wastewater through hydrodynamic cavitation (HC) independently and in conjunction with hydrogen peroxide (H_2O_2) as an external oxidant, along with photocatalysis (PC) using a catalyst immobilized on glass fiber tissue (GFT). A systematic analysis of operating conditions, including pressure drop and H_2O_2 concentration, was conducted to enhance MO degradation. To interpret and describe the experimental data, a per-pass degradation model was applied. The findings indicated that HC alone, utilizing a vortex-based cavitation device at a pressure drop of 1.5 bar, achieved over 96% degradation after 100 passes (corresponding to 230 min of treatment), with a cavitation yield of 3.6 mg/kJ and a COD mineralization rate exceeding 12%. The addition of a small amount of H_2O_2 (0.01%) significantly decreased the treatment duration from 230 minutes to 36 minutes (16 passes), leading to 99.8% degradation with a cavitation yield of 6.77 mg/kJ. This also resulted in a COD mineralization rate twice as high as that of HC alone, demonstrating a synergistic effect of 4.8. The integration of HC with PC, using TiO_2-coated glass fibers in the presence of H_2O_2, further reduced the treatment time to 21 minutes, yielding a cavitation efficiency of 11.83 mg/kJ. This approach exhibited a remarkable synergistic effect of 9.2 and achieved a COD mineralization rate twice that of the HC/H_2O_2 system. These findings confirm the high effectiveness of HC-based hybrid AOPs for the degradation and mineralization of azo dyes in wastewater.

Keywords: Degradation rate, external oxidant, TiO_2-coated glass fibers, mineralization

II.1 Introduction

Among the primary sources of water pollution, the textile industry stands out due to the large volumes of dye-laden wastewater it generates, posing a significant environmental challenge worldwide. Annually, an estimated 10^8 tons of dyes are produced, with a substantial portion being consumed by the textile sector worldwide **[203]**. As a result, this widespread use leads to the discharge of considerable amounts of wastewater containing POPs, predominantly azo dyes **[204]**. The impact of this wastewater on the environment is severe, as it represents a serious

risk to ecosystems **[205]** and human health **[206]**, due to its high toxicity, mutagenic potential, and carcinogenic properties **[207]**.

Several traditional methods for wastewater treatment, including adsorption **[208]**, biological treatment **[209]**, coagulation **[210]**, and membrane filtration **[211]**, typically transfer pollutants from one medium to another without degrading them. These techniques also tend to be costly, time-intensive, and often lack high efficiency.

Given the limitations of traditional methods, the demand for exploring advanced and eco-friendly solutions to treat dye-contaminated wastewater is needed. This highlights the importance of AOPs. Techniques like the Fenton process **[212],** ozonation **[213]**, hydrogen peroxide **[214],** and photocatalysis **[215]** are effective at breaking down and mineralizing complex organic pollutants in water by generating highly reactive and non-selective radicals such as hydroxyl (OH) **[216].**

In recent years, HC has emerged as a promising AOP for wastewater treatment **[217, 218, 200]**. HC involves the formation, growth, and collapse of gas/vapor-filled cavities (microbubbles) within a low-pressure zone, close to the vapor pressure of water at the working temperature, inside a cavitation device. The turbulence in this low-pressure environment generates cavities, which then travel to higher-pressure regions. When exposed to pressure fluctuations, these cavities collapse, creating local hot spots and generating highly reactive oxidizing radicals **[219]**. HC has demonstrated its efficiency in removing POPs from both real synthetic and real wastewater (on an industrial scale) **[220]**, sourced from various industries, including agriculture **[221]**, food **[222]**, textiles **[223]**, and pharmaceuticals **[224].**

Although numerous studies have explored the use of HC for dye-contaminated wastewater treatment, its independent application has demonstrated limitations in attaining high levels of degradation **[225-227]**. As a result, considerable attempts are being undertaken to combine HC with other AOPs **[228-230]**. Recent research has highlighted the synergistic benefits of pairing HC with PC **[225, 231]**, while HC combined with H_2O_2 has also proven to be an effective strategy for dye removal **[226]**. Major studies examining the integration of HC with various AOPs to enhance pollutant degradation are presented in **Table II.1.**

Table II.1 Overview of key research on combined AOPs.

Oxidation processes used	Pollutant (s)	Results	Reference
HC (Venturi), zero-valent iron (ZVI), and sulfite	Direct Red 83 (DR83)	The HC/ZVI/sulfite process achieved 95.54% dye degradation, significantly outperforming individual processes (ZVI and sulfite <6%, HC 68.21%)	**[232]**
HC (orifice), potassium persulfate (KPS), and H_2O_2	Ponceau 4R, Tartrazine, and Coomassie Brilliant Blue (CBB)	Degradation rates of 92.27%, 50.1%, and 42.3% were achieved for Tartrazine, CBB and Ponceau 4R, respectively. A synergetic index of 2.51 confirmed the effectiveness of the combined HC-KPS-H_2O_2 process, which outperformed HC alone, by 98%	**[233]**
HC (orifice), $Na_2S_2O_8$ and O_3	Methylene blue	The HC/O_3 combination showed better results than $Na_2S_2O_8$ for methylene blue degradation, achieving over 99% degradation with a synergy coefficient of 3.58	**[234]**
HC (orifice), H_2O_2, Fenton, photo-Fenton, photolytic (UV irradiation), and photocatalytic (UV irradiation + TiO_2)	Methylene blue, MO, and Rhodamine-B	The HC/H_2O_2 process achieved 100% decolorization in 40 minutes (ternary dye: H_2O_2 ratio 1:40), with a synergetic effect of 28.97. HC/Fenton and HC/photo-Fenton achieved 98% decolorization with synergetic effects of 6.285 and 4.923, respectively, while HC/photolytic and HC/photocatalytic processes resulted in 74.53% and 82.13% decolorization, respectively.	**[235]**

HC (venturi), Fe^{3+}-doped TiO_2	Rhodamine B	The combination of HC with Fe^{3+}-doped TiO_2 resulted in the highest degradation (91.11%) a a Fe:Ti ratio of 0.05:1.00 M	**[228]**
HC (venturi), NaCl, H_2O_2 and NaCl, NH4Cl, and Na2SO4	MO	HC alone resulted in 30% degradation, HC/H_2O_2 achieved 70%, while HC/NaCl also showed improvement. The combination of NaCl, NH_4Cl, and Na_2SO_4 enhanced the dye decolorization to 90%	**[236]**

The key goal of this study is to examine the degradation and mineralization of MO, a harmful azo dye **[237].** In this study, we present results from HC, HC coupled with H_2O_2, and the combination of HC/H_2O_2 with PC. This approach integrates a vortex-based HC system using an innovative immobilized photocatalyst, which consists of TiO_2-coated GFT.

Vortex-based cavitation has been recognized for its advantages compared to conventional orifice or venturi-based methods, as demonstrated by Ranade and his colleagues **[190, 238, 239]**. This technology facilitates earlier inception of cavitation and requires considerably less energy than conventional systems. Several studies consistently comparing the efficiency of these devices show that vortex-based cavitation devices achieve a much higher cavitation yield, measured in terms of the amount (in milligrams) of pollutant degraded per unit of energy **[240]**.

This study is the first to demonstrate the synergistic effect of combining vortex-based HC, H_2O_2, and a fiber-coated TiO_2. The use of TiO_2- GFT not only addresses the challenges of traditional cavitation systems but also provides an innovative approach to issues related to suspended TiO_2 powder, like agglomeration, which often necessitates additional post-treatment steps like filtration **[241]**. The per-pass degradation model was utilized to interpret the experimental data on MO degradation in batch systems and to assess the efficiency of HC, both individually and in conjunction with H_2O_2 and PC. The treatment efficiency was assessed by determining the cavitation yield, expressed as the weight of dye degraded per unit of energy consumed. These results offer important insights for the potential large-scale application of this method for treating dye-contaminated wastewater.

II.2 Material and methods

II.2.1 Materials

Methyl orange (molecular weight: 327.334 g mol^{-1}; molecular formula: $C_{14}H_{14}N_3NaO_3S$) was obtained from Thermo Fisher Scientific. Synthetic MO solutions were prepared using distilled water for all experiments. Sulfuric acid (Sigma Aldrich, 98%) was employed to adjust the solution's pH. Hydrogen peroxide (Thermo Fisher Scientific, 30% v/v) was utilized to evaluate its effect on enhancing the oxidizing capacity of the process. The TiO_2-coated GFT, sourced from Ahlstrom Research and Services, was used as the photocatalyst, prepared by impregnating the GFT—pre-coated with 6.5 $g \cdot m^{-2}$ of colloidal silica with an aqueous suspension of TiO_2 P25 (80% anatase, 20% rutile) using an industrial size-press technique. The colloidal silica served as a binding agent to ensure uniform TiO_2 deposition. The resulting composite exhibited a specific surface area of 20.6 $m^2 \cdot g^{-1}$, as determined by BET analysis **[242]**. All chemicals were utilized as received from the suppliers.

II.2.2 Experimental setup

The degradation experiments were conducted in a lab-scale setup, schematically illustrated in **Fig. II.2.1.** The system was specifically designed to facilitate the independent evaluation of HC and PC, as well as their combined effect. Photographs of the experimental setups are depicted in the SI as **Fig. S1** and **Fig. S2**, respectively.

The combined system includes a 2.5 L holding tank, from which liquid is circulated utilizing a centrifugal pump with a power rating of 0.75 kW. The system includes an integrated manual pressure drop control to regulate the liquid flow through a vortex-based cavitation device (throat diameter: 3 mm). The cavitation device is constructed from aluminum, following the design approach outlined by Ranade et al. **[238].** The temperature of the liquid in the holding tank was monitored throughout the experiments but was not actively controlled. For the photocatalytic process, a 60W LED 395 nm UV light was positioned horizontally at the top of an aluminum photoreactor (volume: 43.952 cm^3, dimensions: 41H × 32L × 33.5W cm), maintaining a 13 cm distance from the liquid surface. The TiO_2-coated GFT was immersed diagonally within the solution. To ensure proper mixing, the solution was kept under continuous stirring at 200 rpm. The liquid flow rate at various pressure drops was calculated by recording the time needed to

collect 1L of liquid The pressure drop versus flow rate characteristics of the vortex-based cavitation device are provided in **Fig. S3.**

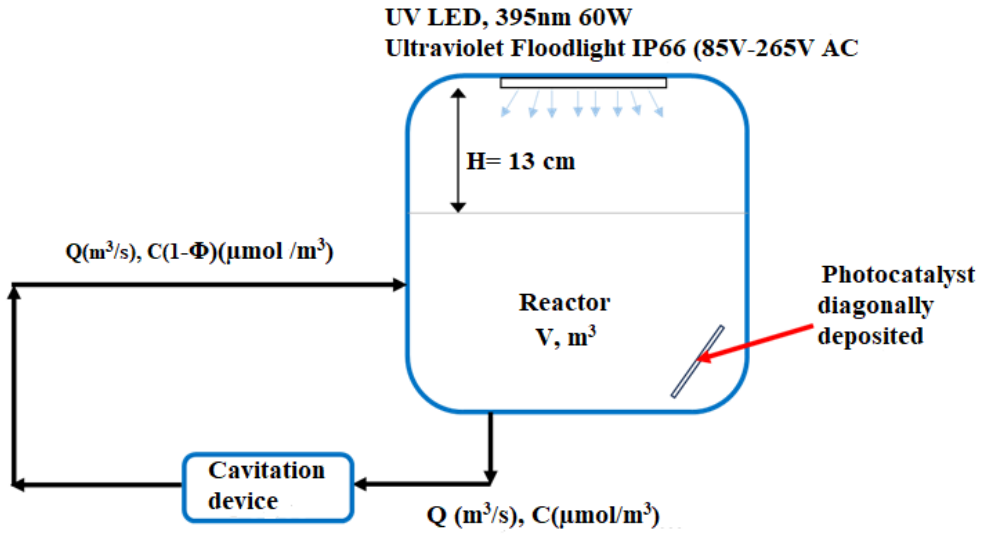

Fig. II.2.1 Schematic of the experimental set-up

II.2.3 Experimental Methodology

All experiments were conducted using 2.5 L of MO aqueous solution, with concentrations varying between 10 and 20 ppm. The solution pH was adjusted to approximately 2.0, in alignment with prior studies **[236, 243].**

Initial trials revealed that the efficiency of vortex-based HC remains unaffected by the initial concentration, as observed in previous studies by Ranade et al. **[217]**. To optimize chemical consumption while maintaining the reliability of analytical measurements, an initial dye concentration of approximately 10 ppm was selected, ensuring accurate detection and evaluation.

The temperature during the experiments ranged from 30 °C to 47 °C. Three sets of experiments were performed in this study. The first set focused on dye degradation using only HC, with inlet pressures varying from 1.5 to 3.5 bar for 100 passes. This approach aimed to identify the optimal inlet pressure for achieving the highest degradation efficiency.

Since the outlet is open to atmospheric pressure, the inlet pressure (expressed as gauge pressure) directly corresponds to the pressure drop across the cavitation device. The experimental conditions for the HC trials are detailed in **Table II.2.2**. Determining the cavitation number for vortex-based cavitation devices is complex and not easily defined. According to Ranade et al.

[190], the cavitation number for vortex-based cavitation devices can be estimated using the maximum tangential velocity within the vortex chamber. More recently, Gode et al. **[244],** established a correlation between the pressure drop across the cavitation device and the maximum tangential velocity. Using this approach, the cavitation numbers were determined as follows:

$$Ca = 2\left(\frac{P_2 - P_v}{\Delta P}\right) = \sim \frac{2}{\Delta P \text{ in } bar} \qquad \text{II.1}$$

Table II.2.2: Operational parameters for HC experiments.

d_T is characteristic diameter, ΔP is pressure drop across the HC device, V_T is velocity based on characteristic diameter, Re is Reynolds number and, Q is the flow rate through the HC device, Ca is cavitation number, P_2 is the pressure at the outlet and P_v is vapor pressure

$\boldsymbol{\Delta P}$ (bar)	1.5	2	2.5	3	3.5
$\boldsymbol{Q}$ (L/min)	1.1	1.3	1.5	1.7	1.9
$\boldsymbol{V_T}$ (m/s)	2.6	3.1	3.5	4.0	4.5
$\boldsymbol{Re}$ $\left[\left(\frac{d_T\ V_T\ \rho}{\mu}\right)\right]$	7785	9200	10616	12031	13447
$\boldsymbol{Ca}$ $\left[\sim 2\left(\frac{P_2 - P_v}{\Delta P}\right)\right]$	1.33	1	0.8	0.67	0.57

In the second set of experiments, the effect of HC in combination with varying amounts of H_2O_2 (0% v/v, 0.001% v/v, 0.005% v/v, 0.01% v/v, 0.1% v/v, and 1% v/v) was examined to evaluate its impact on dye degradation. The tests were conducted over a duration of 60 min, utilizing the optimal inlet pressure determined from the initial sets of experiments.

Finally, the degradation of MO was assessed utilizing a hybrid system combining HC and PC, under the optimal inlet pressure and H_2O_2 concentration. The experiment was conducted over 60 minutes with TiO_2-coated GFT (5 cm × 5 cm) (**Fig. S4**). Prior to initiating the PC process, the MO solutions were maintained in darkness and stirred at 200 rpm for 60 minutes to establish adsorption-desorption equilibrium, as described in previous studies **[245],** before turning on the UV lamp to begin the photocatalytic treatment.

To assess the contribution of adsorption, aliquots were collected before and after the dark equilibration period. The results showed that dye adsorption onto the TiO_2-coated GFT was minimal, with removal not exceeding ~5%, in line with the well-established limited adsorption capacity of TiO_2-based photocatalysts.

TiO_2-coated GFT catalyst was characterized using X-ray diffraction (XRD) with an Empyrean X-ray diffractometer. XRD patterns were collected using Cu-Kα radiation at a scan rate of 0.1° 2θ s^{-1}, with an accelerating voltage of 45 kV and a current of 40 mA. Scanning electron microscopy (SEM) images were obtained using a Hitachi SU70 microscope at 5 kV after gold coating the sample for 1 minute at 20 mA. Detailed characteristics of the catalyst are provided in Section S1 of the SI. All experiments on dye degradation were conducted in triplicate, with errors found to be less than 5%.

II.2.4 Analysis and processing of data

The samples collected during the experiments were analyzed with a UV-Vis spectrophotometer (Shimadzu UV1800) **(Fig. S5**) to follow the changes in absorbance over time at a wavelength specific to the pH of the solution. For the MO solution at pH 2, the maximum absorbance peak was observed at 507 nm. Immediately after each sampling, the sample was directly analyzed using the spectrophotometer, while the experimental setup was paused to avoid further reaction during analysis. MO concentrations were indirectly determined using a calibration curve **(Fig. S6).** These UV-measured concentrations were considered accurate and were utilized in all subsequent calculations.

Pseudo-first-order kinetics have been widely used in the literature to model pollutant degradation through HC, as seen in numerous studies **[226-236]**. However, Ranade et al., **[217]** pointed out that this model has certain limitations that may affect its accuracy in describing the degradation process. For instance, the pseudo-first-order kinetics model, when applied under the same operational conditions, could predict two distinct values for the effective rate constant in same HC reactors but with varying containment volumes. To address this issue, we adopted the per-pass degradation factor (Φ), which depends on the operating conditions and the reactor design but remains independent of the holding tank volume used during the experiments. This approach proves particularly useful for understanding and interpreting pollutant degradation

and optimizing essential operating parameters to achieve the most efficient HC performance **[219].**

However, to compare the efficiency of the HC system with other hybrid methods and to quantify the synergistic effects, we employed the pseudo-first-order kinetics approach, aligning with the commonly used methodology in most published studies on hybrid AOPs.

The overall efficiency of a typical cavitation-based water treatment system, as illustrated in **Fig. II.2.1**, can be modeled as **[192]**:

$$V\frac{\mathrm{dC}}{\mathrm{dt}} = \mathrm{Q\Phi C} \quad \text{or} \quad V\frac{\mathrm{dC}}{\mathrm{dt}} = -\mathrm{k}_{eff}\mathrm{C} \qquad \text{II.2}$$

Where C represents the pollutant concentration, V denotes the effective volume (which includes both the holding tank volume and the volume of the piping system, including the pump), Q is the flow rate through the cavitation device, $\mathrm{k}_{eff}is$ the apparent degradation rate constant and Φ is the per-pass degradation factor. While the effect of temperature could be incorporated by considering activating energy, this study has not factored in activation energy. Instead, we have presented the effective per-pass degradation factor (Φ) or the effective rate constant (k_{eff}), which were determined across the range of temperatures employed in the experiments.

The number of passes through the cavitation device is linked to the residence time in the holding tank, which is calculated as the ratio of the holding tank volume to the flow rate through the cavitation device(V/Q), and operating time. This relationship can be expressed as:

$$\mathrm{n} = \beta\mathrm{t} \qquad \text{II.3}$$

Where n represents the number of passes, and β is the inverse of the residence time (Q/V, in s^{-1}). The Chemical Oxygen Demand (COD) of the MO solutions was measured using a DR 1900 spectrophotometer (Hach) for all sample analyses. For this, 2 mL of the sample was digested using commercial cuvette tests COD reagent (LCI400, 0–1000 mg/L) for 120 minutes at 148 °C in an LT 200 digester (Hach-Lange, Germany) (Fig. S7 and Fig. S8). The percentage of COD destroyed was calculated as:

$$\%\mathrm{COD} = \frac{COD_0 - COD_t}{COD_0} \times 100 \qquad \text{II.4}$$

Where COD_0 and COD_t refer to the COD values of the MO solutions before and after treatment respectively.

HC is less complex in operation compared to PC. To improve the accuracy of assessing system efficiency, we suggest focusing on the cavitation yield of HC ($Y_{cav,HC}$), providing a practical and cost-efficient metric for evaluating performance. The cavitation yield (($Y_{cav,HC}$) is an essential factor in determining the effectiveness of the HC process. It is defined as the amount of pollutant degraded per unit of energy consumed and can be calculated using the following equation:

$$Y_{cav,HC} = \frac{V\,(C_{in}-C)}{\Delta P\; Q\; t} \qquad \text{II.5}$$

Where C_{in} is the initial dye concentration, and C is the dye concentration at time t. The cavitation yield ($Y_{cav,HC}$) is expressed in units of milligrams of dye degraded per kilojoule (mg/kJ) of energy consumed during the HC process.

II.3 Results and discussion

The initial discussion focuses on the results obtained from experiments conducted only HC for dye degradation. Following this, the impact of incorporating H_2O_2 into the HC process on MO degradation is explored, considering the optimal conditions derived from the HC-only experiments. The potential synergy between the added H_2O_2 and HC was also assessed. Before conducting the PC experiments, the catalyst's physical properties were characterized. Diffraction analysis, a non-destructive technique, was employed to identify the crystalline structure of TiO_2-coated GFT (**Fig. S9**). This technique allowed for the determination of the crystallite size of the TiO_2 nanoparticles, which is crucial for influencing the material's electrical and optical properties. The sample's surface structure and composition were further examined utilizing SEM (**Fig. S10**). After the catalyst characterization, the potential application of the hybrid HC/H_2O_2/PC system was investigated, focusing on the degradation of MO under the optimal conditions determined for HC and H_2O_2. The mineralization degree was also established. The findings are discussed in the upcoming sub-sections.

II.3.1 Application on only HC for degradation of MO

The flow rate through the HC device, or equivalently, the pressure drop across the HC device, is a crucial factor influencing the efficiency of HC in degrading organic pollutants [**246]**. According to Ranade et al. **[190]**, vortex-based cavitation devices typically initiate cavitation at a pressure drop in the range of 0.8-1 bar. Nevertheless, the precise inception point may deviate slightly from the stated value, influenced by operating temperature, dissolved gas concentration, the presence of impurities, etc. To eliminate any ambiguity regarding the starting point and guarantee reproducibility while minimizing error bars on the data, the effect of inlet pressure or pressure drop across the cavitation device was examined within the range of 1.5 to 3.5 bar. The pH was maintained at 2 for all experiments. The samples were taken at various

intervals (0, 10, 30, 60, 80, and 100 passes) and analyzed for MO concentration. HC induces the formation and collapse of cavities within the cavitation device, resulting in extremely high local temperature and pressure, which in turn generates highly reactive radicals responsible for the degradation of pollutants in the solution. Sarvothaman et al. **[192]**, have provided a simplified representation of the pollutant degradation reactions as follows:

$$\text{Cavity collapse} \longrightarrow OH^{\cdot} \text{ and other radicals } (R^{\cdot}) \qquad \text{II.6}$$

$$R^{\cdot} + \text{pollutant} \longrightarrow \text{intermediates} \longrightarrow CO2 + H_2O \qquad \text{II.7}$$

As the dye solution flows through the HC device, each pass exposes the dye molecules to the collapsing cavities, which results in the degradation of the dye molecules through the reaction outlined in **Equation II.7**. The decrease in MO concentration in relation to the number of passes at varying pressure drops is illustrated in **Fig. II.3.1**.

The maximum degradation of 96.4% was achieved at an inlet pressure of 1.5 bar. At pressures exceeding this value, a notable decline in the degradation rate was observed. Given that energy consumption per unit mass of treated wastewater is proportional to the pressure drop, the optimal pressure drop can be identified as 1.5 bar, as it also yielded the highest degradation. It is essential to highlight that the overall efficiency of pollutant degradation via HC depends on the product of two factors: the number density of collapsing cavities (number per m^3) and the intensity of cavity collapse. As the pressure drop across the cavitation device increases, the

driving force for cavitation increases, which in turn raises the number density of cavities. However, as more cavities coexist in the liquid, the effective compressibility of the medium increases, reducing the intensity of cavity collapse. This leads to a decrease in the generation of hydroxyl radicals, thus lowering the rate of pollutant degradation **[190]**. The degradation extent for pressure drops ranging from 2 to 3.5 bar varied by no more than 10%.

Building on the approach outlined by Ranade et al. **[192, 219],** the per-pass degradation model was applied to interpret the batch experimental data. As shown in **Fig. II.3.1**, the per-pass degradation factor, which is dependent on hydroxyl radical generation, decreases as the pressure drop increases. The observed values range between 0.029 and 0.045. The maximum degradation efficiency was obtained at a pressure drop of 1.5 bar, corresponding to a per-pass degradation factor of 0.045. Based on this, 1.5 bar was chosen as the optimal pressure drop for subsequent experiments.

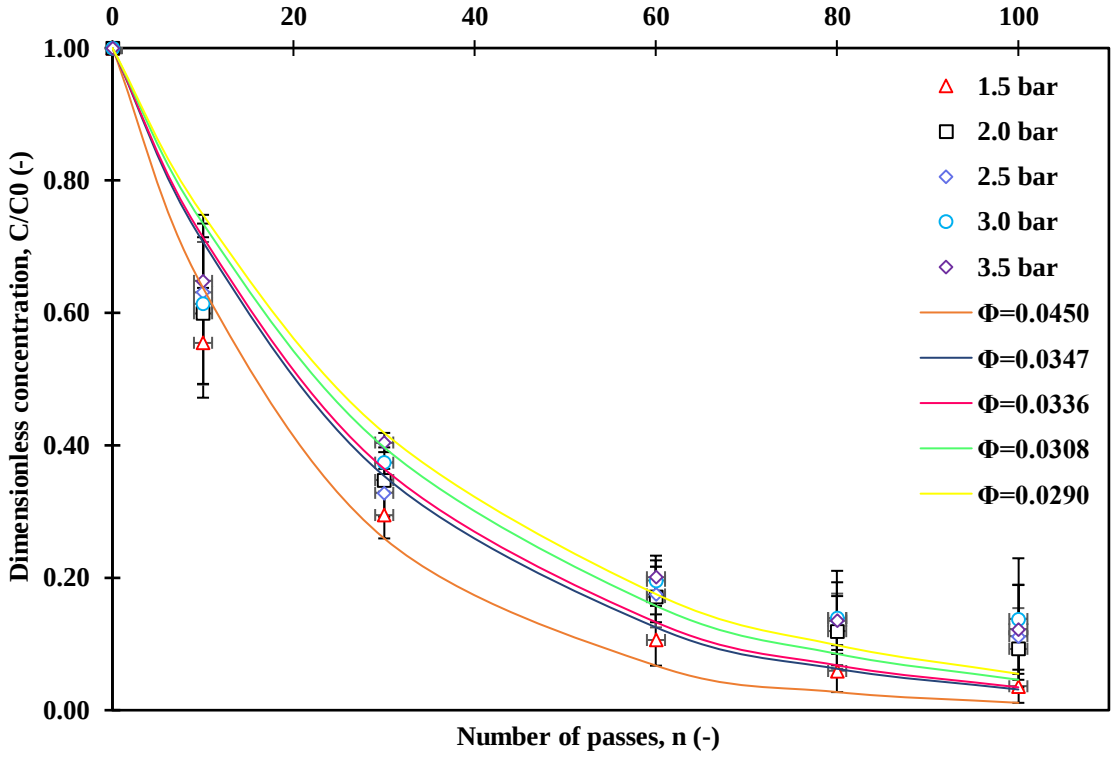

Fig. II.3.1 MO degradation as a function of the number of passes under different inlet pressure conditions; V = 2.5 L, pH = 2, and an initial concentration of 10 ppm.

II.3.2 HC combined with H_2O_2: Synergistic effect

Among the diverse potent oxidation agents, H_2O_2 is extensively utilized in oxidation reactions and has recently been explored for enhancing cavitation processes, particularly in the degradation of persistent organic pollutants **[156, 224, 247]**. The addition of H_2O_2 to the HC process is expected to boost free radical generation, thereby improving pollutant degradation efficiency **[226,248]. Fig. II.3.2** presents the results of the sets of experiments comparing HC alone, a control test with only H_2O_2 in the absence of HC, and various H_2O_2 concentrations combined with HC, evaluated as function of number of passes at the optimal inlet pressure of 1.5 bar. The results indicate that HC alone achieved a maximum MO degradation of 83.3%, whereas the blank MO/H_2O_2 test resulted in a negligible 0.9% degradation after 26 passes (corresponding to 60 min of treatment). When H_2O_2 was combined with HC, the overall degradation efficiency improved significantly, reaching 99.8% at an H_2O_2 concentration of 0.1%. Initially, increasing the H_2O_2 concentration led to a higher degradation rate and extent. Specifically, adding 0.001% v/v H_2O_2 increased the degradation from 83.3% (HC alone) to 89.4% in 26 passes. A concentration of 0.005% H_2O_2 further enhanced degradation to 99.6% within 21 passes, while 0.01% H_2O_2 achieved 99.8% degradation in just 16 passes. However, increasing the H_2O_2 concentration to 0.1% did not further improve degradation and slightly reduced the degradation rate, as the number of passes required to reach 99.8% increased from 16 to 25. At elevated H_2O_2 concentrations, such as 1% v/v, the degradation efficiency decreases due to enhanced radical scavenging. This occurs as a result of recombination reactions, where radical species undergo self-scavenging, thus limiting the presence of hydroxyl radicals (•OH) for pollutant degradation. Additionally, excessive H_2O_2 may act as a radical quencher, reacting with the generated hydroxyl radicals and diminishing their oxidative potential **[249]**. These recombination reactions can be represented as follows **[226]:**

$$OH^{\cdot} + OH^{\cdot} \longrightarrow H_2O_2 \qquad \text{II.8}$$

$$OH^{\cdot} + H_2O_2 \longrightarrow HO_2^{\cdot} + H_2O \qquad \text{II.9}$$

$$OH^{\cdot} + HO_2^{\cdot} \longrightarrow H_2O + O_2 \qquad \text{II.10}$$

As illustrated in **Fig. II.3.2**, The per-pass degradation factor increases at first with rising H_2O_2 concentration, peaking at 0.328 at an optimal concentration of 0.01% v/v. Beyond this point,

the degradation factor declines significantly, dropping to 0.0487 at 1% v/v H_2O_2. Experimental observations across various concentrations suggest that the most effective condition was the addition of 0.01% v/v H_2O_2, which resulted in a 99.8% degradation of MO within just 16 passes, corresponding to a treatment duration of 36 minutes.

Table II.3.1 presents the results of MO degradation, summarizing treatment time, percentage degradation, calculated effective rate constants (k_{eff}), per-pass degradation factor (Φ), synergistic coefficients, and cavitation yield ($Y_{cav,HC}$) for this second set of experiments. The effective rate constants, determined using first-order kinetics (-ln(C/C₀) vs. time), varied between 0.0385 min^{-1} for 0.001% v/v H_2O_2 and 0.0161 min^{-1} for 1% v/v H_2O_2. Additionally, the synergy between HC and H_2O_2 was evaluated using the rate constants obtained from the independent and combined processes. The synergistic coefficient was determined using the appropriate formula as described in the literature **[250]:**

$$\text{Synergistic coefficient} = \frac{k(HC+H2O2)}{kHC + kH2O2} \qquad \text{II.11}$$

The values of the rate constants *k* were extracted from the pseudo-first-order kinetic plots corresponding to each process.

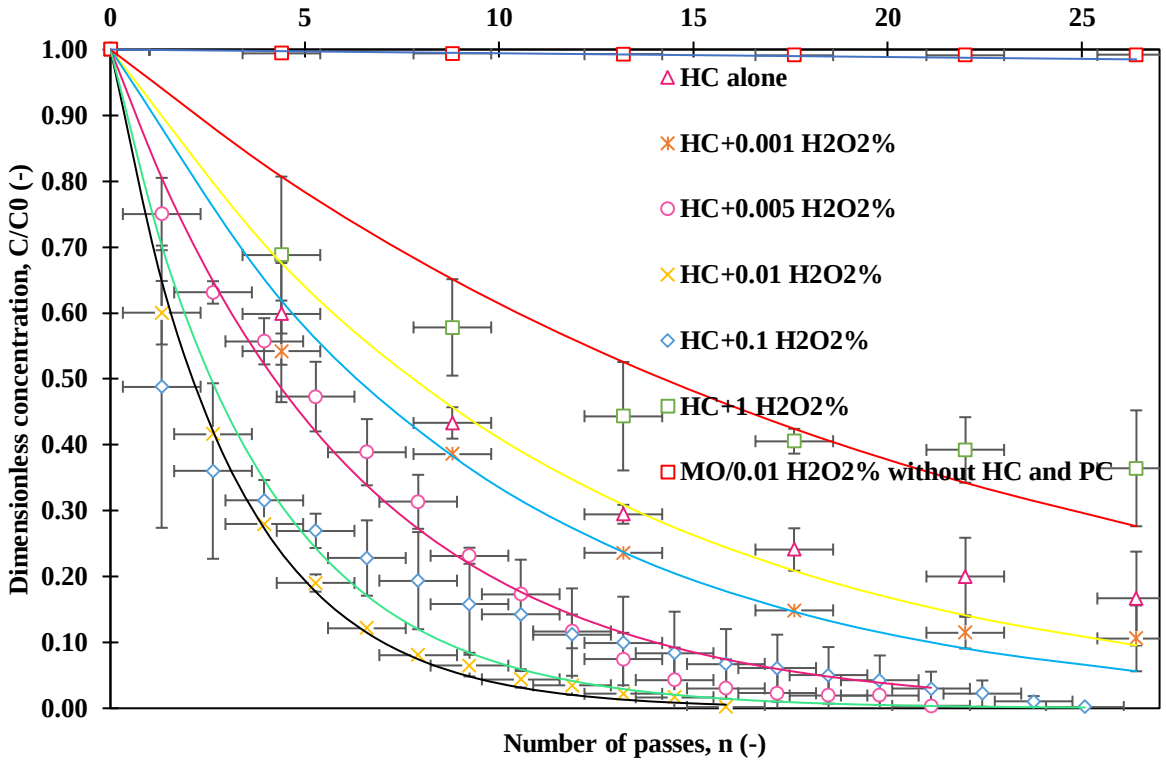

Fig. II.3.2 MO degradation as a function of number of passes for different concentrations of H_2O_2; V= 2.5 L, pH = 2, ΔP= 1.5 bar, and MO initial concentration = 10 ppm

A noticeable synergistic effect was observed in the degradation of MO, as the effective rate constant significantly increased from 0.0001 min^{-1} for the MO/H_2O_2 system alone to 0.14 min^{-1} when HC and H_2O_2 were applied together. The highest synergistic coefficient, calculated for the optimal combination of HC with 0.01% v/v H_2O_2, was 4.78, surpassing those obtained for other conditions (**Table II.3.1**). This enhancement can be attributed to the role of HC in promoting the dissociation of H_2O_2, leading to the generation of additional hydroxyl radicals. These radicals, possessing a stronger oxidation potential, contribute more effectively to pollutant degradation compared to those generated by H_2O_2 or HC alone.

At an inlet pressure drop of 1.5 bar, HC exhibited a cavitation yield of 3.65 mg/kJ, serving as a reference point for assessing the influence of H_2O_2 addition on process efficiency. Introducing a A low concentration of H_2O_2 (0.001% v/v) led to a slight increase in cavitation yield to 3.93 mg/kJ, suggesting a potential synergistic effect between HC and H_2O_2. The highest cavitation yield of 6.77 mg/kJ was achieved at 0.01% v/v H_2O_2, indicating optimal synergy between HC and H_2O_2 at this concentration. However, at higher concentrations (0.1% and 1% v/v H_2O_2), the

cavitation yield declined to 4.4 mg/kJ and 2.67 mg/kJ, respectively. This decrease suggests that excessive H_2O_2 may act as a scavenger, reducing the availability of hydroxyl radicals for MO degradation, which aligns with the previously discussed interpretations.. These findings confirm that coupling HC with H_2O_2 can significantly enhance pollutant degradation under optimized conditions.

Table II.3.1 Summary of MO degradation results.

Operative conditions	Time of degradation [min]	Effective degradation rate constant, $\mathbf{k}_{eff}$ [min^{-1}]	Per pass degradation factor Φ [-]	Degradation [%]	Synergistic **coefficient** [-]	$\boldsymbol{Y}_{cav,HC}$ [mg/kJ]
HC alone (1.5 bar)	60	0.0291	0.0890	83.3	-	3.65
MO/0.01%v/v H_2O_2 alone	60	0.0001	0.0006	0.9	-	-
1.5 bar + 0.001% v/v H_2O_2	60	0.0385	0.1091	89.4	1.32	3.93
1.5 bar + 0.005% v/v H_2O_2	48	0.1051	0.1642	99.6	3.6	5.43
1.5 bar + 0.01% v/v H_2O_2	36	0.1396	0.3279	99.8	4.78	6.77
1.5 bar + 0.1% v/v H_2O_2	57	0.0759	0.2677	99.8	2.6	4.41
1.5 bar + 1% v/v H_2O_2	60	0.0161	0.0487	63.6	0.55	2.68

II.3.3 MO degradation by HC, H_2O_2, and PC coupling

To further enhance the degradation of MO, additional tests were conducted by integrating the optimal pressure drop across the vortex-based HC device and the optimal amount of H_2O_2 with PC utilizing TiO_2-coated GFT. Under UV irradiation, the TiO_2-coated GFT generates electron-hole pairs, which facilitate the breakdown of water molecules via an electron transfer process.

This reaction sequence leads to the formation of hydroxyl radicals, complementing those already produced by the HC/H_2O_2 system **[251].** The combined action of these oxidative species significantly improves the effectiveness of organic contaminant degradation from the aqueous solution.

The degradation of MO using three different treatment approaches namely, HC alone, HC combined with H_2O_2, and the combined system of HC, H_2O_2, and PC, as a function of the number of passes, is illustrated in **Fig. II.3.3**. Each method was evaluated under the optimal operating conditions (a pressure drop of 1.5 bar, and H_2O_2 concentration of 0.01% v/v) at a pH of 2. The results indicate that the combined HC/H_2O_2/PC system achieved a 99.8% degradation rate after just 9 passes (equivalent to 21 minutes). This represents a treatment time nearly three times shorter than HC alone and almost twice as fast as the HC/H_2O_2 system, demonstrating the enhanced efficiency of the integrated approach.

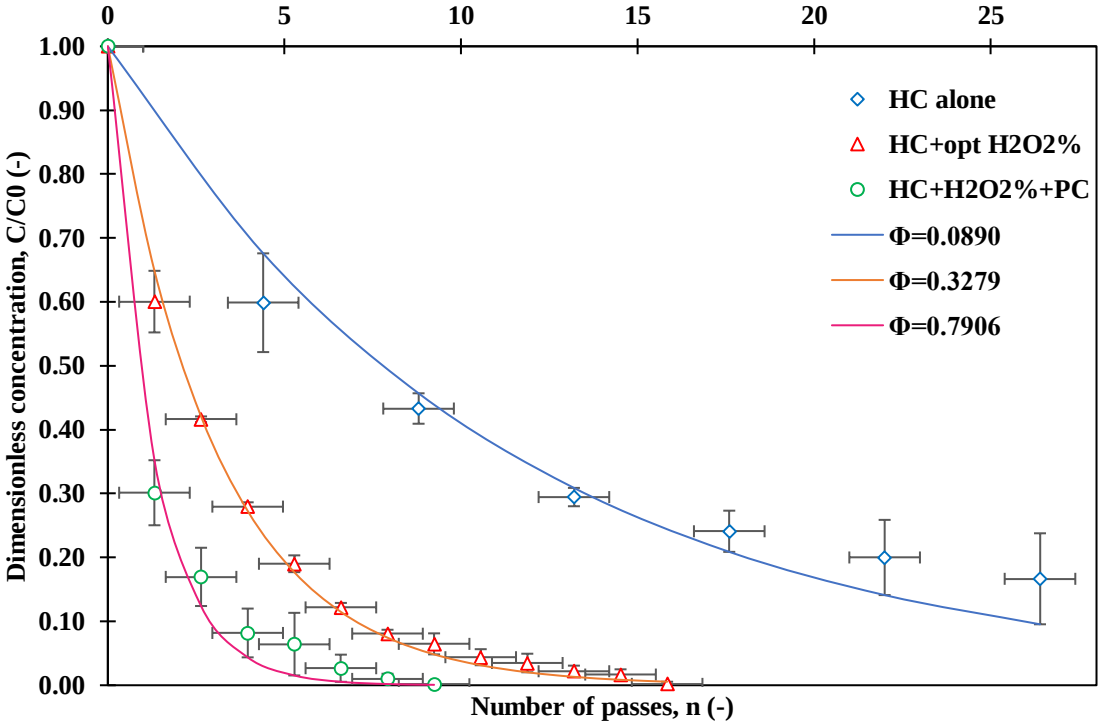

Fig. II.3.3 MO degradation using HC alone, HC/H_2O_2, and HC/H_2O_2/PC under agitation of 200 rpm using TiO2-coated GFT; V= 2.5 L, pH = 2 and MO initial concentration = 10 ppm, ΔP= 1.5 bar, and % H_2O_2 (0.01%v/v)

Table II.3.2 presents the degradation rates, effective rate constant (k_{eff},), per-pass degradation factor, treatment duration, synergistic coefficients, and cavitation yield for the different treatment methods. It was noted that the effective rate constant for MO degradation was 0.029 min^{-1} with HC alone, increasing to 0.14 min^{-1} when HC was combined with H_2O_2. The highest rate constant of 0.27 min^{-1} was observed when HC, H_2O_2, and PC were applied together. Corresponding per-pass degradation factors were 0.089 for HC, 0.328 for HC/H_2O_2, and 0.79 for the combined HC/H_2O_2/PC system, confirming the enhanced generation of hydroxyl radicals. The hybrid approach utilizing all three AOPs proved to be twice as effective as the HC/H_2O_2 system.

A notable synergistic effect was also observed when HC/H_2O_2 was combined with PC, yielding a significant synergistic coefficient of 9.2. This enhancement can be attributed to the hydroxyl radicals generated by HC and H_2O_2, which actively participate in the photocatalytic reaction, further accelerating the degradation process. The obtained synergistic coefficient (9.2) under the optimized conditions in this study is considerably higher than those reported in previous literature.

As reported by Fedorov et al. [252], the HC/H_2O_2/PC process exhibited a synergistic coefficient of 2.5. In this study, the maximum cavitation yield, reaching 11.83 mg/kJ, was observed when HC, H_2O_2, and PC were combined, highlighting the enhanced efficiency of this hybrid approach. The significant improvement in degradation efficiency, coupled with a reduced treatment time of just 21 minutes, underscores the effectiveness of this combined system. These findings suggest promising applications for wastewater treatment, particularly in addressing textile industry effluents.

Table II.3.2 MO degradation rates, effective rate constant k_{eff}, per pass degradation factor Φ and synergistic coefficients using the combination of HC, H_2O_2, and photocatalytic process in different treatment times.

Operative conditions	Time of degradation [min]	Apparent degradation rate constant, $\mathbf{k_{eff}}$ [min^{-1}]	Per pass degradation factor Φ [-]	Degradation [%]	Synergistic coefficient [-]	$\boldsymbol{Y_{cav,HC}}$ [mg/kJ]

HC (1.5 bar)	60	0.0291	0.0890	83.3	-	3.65
HC/H_2O_2 (0.01%v/v)	36	0.1396	0.3279	99.8	4.78	6.77
HC/H_2O_2/PC	21	0.2692	0.7906	99.8	9.22	11.83

II.3.4 Mineralization study

The previously discussed results focused on MO degradation based on its concentration reduction. However, a decrease in MO concentration does not necessarily indicate complete mineralization. Complex molecules like MO typically undergo a series of intermediate transformations when reacting with oxidizing radicals before achieving full mineralization. Therefore, assessing the extent of mineralization is crucial alongside monitoring MO degradation. One extensively utilized approach for evaluating the breakdown of organic carbon in aqueous solutions is the measurement of chemical oxygen demand (COD), which provides a quantitative assessment of organic matter decomposition. In this study, the extent of mineralization was examined under optimal conditions across different systems, including HC alone, H_2O_2 alone, HC/H_2O_2, and the combination of HC/H_2O_2 with a photocatalytic process. The discoloration observed in the MO solution during treatment is a result of the oxidative degradation of its chromophore (-N=N-), which disrupts the two aromatic rings in the parent structure **[253]**. However, the absence of color does not necessarily indicate complete mineralization **[254]**. **Fig. II.3.4** presents the mineralization data obtained across the four different systems. It was noted that COD reduction rates of 0% and 12.4% were observed for H_2O_2 alone and HC alone, respectively, over 26 passes corresponding to 60 minutes of treatment. For the HC/H_2O_2 system, the extent of mineralization increased significantly, more than doubling to 25.7% after 16 passes, equivalent to 36 minutes of treatment. The highest mineralization rate of 50% was achieved with the HC/H_2O_2/PC system, which is twice as high as that observed for the HC/H_2O_2 hybrid system and three times greater than the values for HC and H_2O_2 systems individually, within just 9 passes or 21 minutes of treatment. This increase in mineralization is likely due to the higher generation of OH radicals. It is essential to highlight that the degradation experiments were carried out until over 99.5% degradation was achieved, which corresponded to nearly 50% mineralization. Beyond this point, precise monitoring of the dye concentration became impossible. Additional treatment does not lead to further degradation

of the dye since it is already nearly completely degraded, but mineralization continues to increase. Thus, our approach enhances mineralization, rendering the effluent more suitable for discharge. The reported mineralization outcomes surpass those of previous studies **[255]**. The findings provide valuable insights for designing a hybrid treatment process aimed at achieving the desired mineralization of azo dyes.

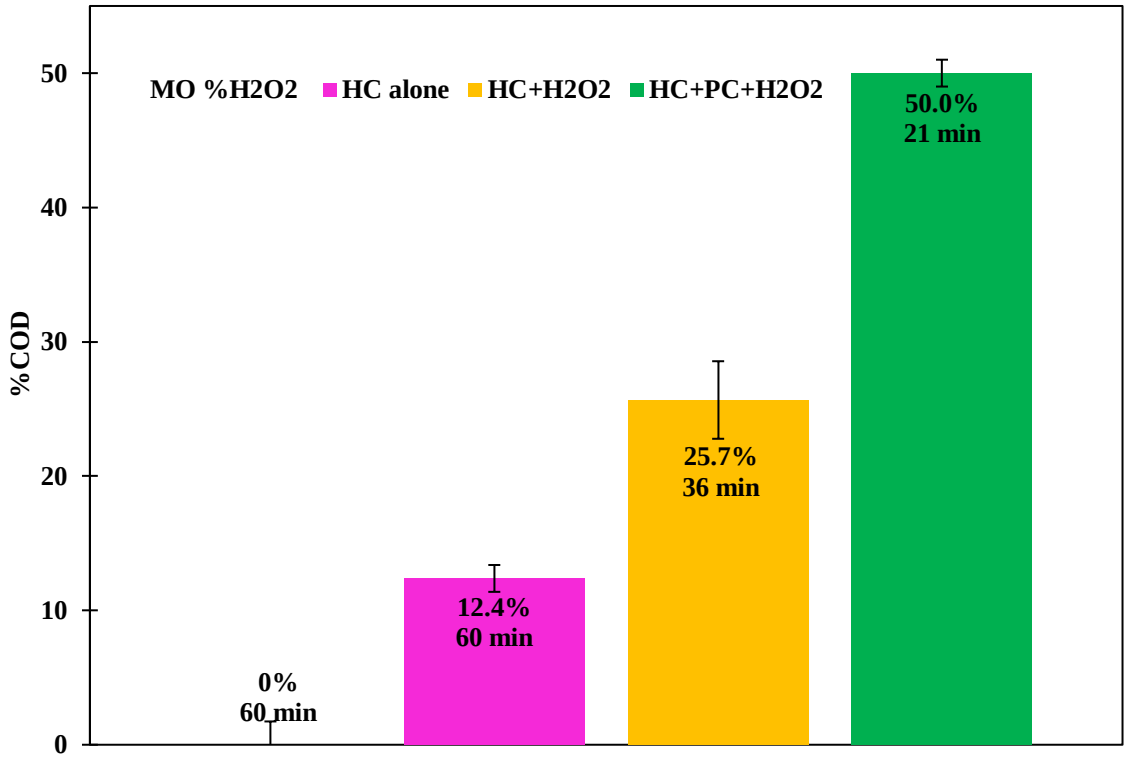

Fig. II.3.4 Effect of HC alone, H_2O_2 alone; HC/ H_2O_2, and HC/ H_2O_2 coupled PC on the degradation of COD in MO solutions.

II.4 Conclusions

In this study, we explored MO degradation utilizing three advanced oxidation processes (AOPs) at the laboratory scale. A vortex-based cavitation device was employed for HC. The outcomes from HC alone were enhanced by combining it with H_2O_2 and H_2O_2 with PC. The main findings from this work are:

- Maximum degradation of MO by HC (with a nominal capacity of 1 LPM) was achieved when the pressure drop across the device was set at 1.5 bar. Increasing the pressure drop

beyond this point resulted in a decrease in the effective per-pass degradation factor. With a pressure drop of 1.5 bar, the degradation of MO reached 96.4% at pH 2, with a mineralization extent of 12.4%.

- When H_2O_2 was added to the MO solution without HC, the degradation effect was minimal, resulting in only a 1% reduction in MO concentration and no significant mineralization.

- The combination of HC and H_2O_2 demonstrated a notable synergistic effect of 4.78 at an optimal H_2O_2 amount of 0.01% v/v, achieving a degradation rate of 99.8%. The cavitation yield for HC alone was 3.65 mg/kJ, while the combination of H_2O_2 and HC resulted in an improved cavitation yield of 6.77 mg/kJ. The mineralization extent increased to 25.7% after 16 passes, corresponding to 36 minutes of treatment, surpassing the results obtained when HC and H_2O_2 were used individually.
- The hybrid system of HC/H_2O_2/PC significantly improved MO degradation, achieving 50% mineralization in 21 minutes (equivalent to 9 passes). This result is three times greater than when using HC alone and twice as high as the combination of HC/H_2O_2. The system exhibited a considerable synergistic effect of 9.2 and a notable cavitation yield of 11.83 mg/kJ.
- The combined treatment of HC, H_2O_2, and PC using TiO2-coated GFT was the most efficient in degrading and mineralizing MO. This hybrid approach led to a significant improvement in cavitation yield compared to individual treatments.

Our study demonstrates that integrating HC with various AOPs (H2O2, PC) presents an effective approach for enhancing MO degradation while also improving cost efficiency through the synergistic interaction of these processes. The findings provide valuable insights for researchers focused on wastewater treatment using the combined HC/H2O2/PC system.

Chapter III: Methyl orange degradation using Ag-doped TiO_2, H_2O_2, and hydrodynamic cavitation

Abstract

This study investigates the photocatalytic degradation of Methyl Orange (MO) using doped photocatalysts, specifically Ag-TiO_2 synthesized via a novel solid-state method, with varying silver concentrations (0%, 0.5%, 1%, 1.5%, 2.5% w/w relative to TiO_2) under different UV light intensities (60 W and 200 W). The photocatalysts were characterized using XRD, SEM-EDS, and BET. The optimal performance was observed with a 0.5% Ag-TiO_2 concentration, achieving a degradation efficiency of 59% under 200 W UV light over 180 min of treatment. The effect of photocatalyst loading was then optimized, followed by the investigation of the synergistic effects of PC coupled with H_2O_2. The highest degradation efficiency of 94% was achieved at 0.01% v/v H_2O_2 with a synergistic coefficient of 24, within 60 min. Further enhancement was observed when combining PC, H_2O_2, and hydrodynamic cavitation, achieving complete degradation of MO in just 3 minutes (1.5 passes) with an extraordinary synergistic coefficient of 42. The degradation process was represented as pseudo-first-order kinetics for PC alone and combined with H_2O_2, and a per-pass degradation model for HC. Finally, The influence of different radical scavengers on the photocatalytic process was examined, highlighting the crucial roles of hydroxyl radicals (•OH), and photo-generated holes (h^+) in the degradation mechanism. This research underscores the importance of optimizing doped photocatalyst composition and operational conditions to maximize pollutant degradation efficiency, demonstrating significant advancements in advanced oxidation processes through synergy.

Keywords: Doped photocatalysts, Advanced oxidation, Per-pass degradation, Synergy

III.1 Introduction

The contamination of water bodies by synthetic dyes poses a significant environmental challenge, as it degrades water quality and endangers aquatic life **[256]**. This issue is exacerbated by the widespread use of these dyes in various industries, including textiles, pharmaceuticals, and food **[257]**. These dyes are often toxic, carcinogenic, and resistant to natural biodegradation processes, posing significant risks to aquatic ecosystems and human health **[10, 258, 259]**.

Conventional wastewater treatment methods often fail to completely degrade or mineralize these dyes, allowing them completely or partially to remain in treated water **[260]**. Therefore, effective degradation methods are essential to mitigate these environmental impacts **[261]**.

In this work, we aim to develop such effective degradation methods. MO is used in this work as a model pollutant for evaluating the efficiency of new treatment technologies. MO's complex aromatic structure makes it resistant to conventional degradation methods, offering a reliable benchmark for advanced techniques. Furthermore, MO represents a broader class of azo dyes that are commonly found in industrial effluents, making research on its degradation highly relevant for real-world applications **[262]**.

Various traditional methods have been utilized for the degradation of MO including adsorption **[263]**, filtration **[264]**, coagulation **[2651**, precipitation **[266]**, and biological methods **[267]**. All of these traditional treatment technologies for removing organic dyes face limitations such as high energy and chemical demands, elevated operating costs, sludge production, and the release of toxic gases, reflect the need for effective treatment technologies **[13]**.

Among these, AOPs have attracted considerable interest wing to their capacity to generate highly reactive species that can effectively degrade complex organic pollutants **[268]**. Photocatalysis, particularly using titanium dioxide (TiO_2), has been extensively studied for MO degradation **[269]**. This method leverages the photocatalytic properties of TiO_2 under UV light to produce reactive oxygen species that break down MO molecules. However, the effectiveness of photocatalysis can be restricted by the fast recombination of electron-hole pairs, diminishing the availability of reactive species **[270]**.

Doped photocatalysts have been recognized as a promising strategy to enhance the efficiency of photocatalytic degradation of organic pollutants like MO **[271]**.

Doping introduces foreign atoms into the crystal lattice of the photocatalyst, improving charge separation by minimizing electron-hole recombination, which enhances the production of reactive species vital for degradation. Furthermore, doping can alter the surface properties of photocatalysts, such as modifying surface area, surface energy, or the availability and arrangement of active sites. All of these may influence interaction of catalyst with dye molecules. This combination of effects significantly boosts photocatalytic performance. Silver

(Ag) doping is commonly used to enhance the photocatalytic performance of TiO_2. Its effectiveness is particularly notable due to the plasmonic effect, which enhances the local electromagnetic field, thus increasing photocatalytic activity. Ag acts as an efficient electron trap, improving charge separation and reducing electron-hole recombination, which enhances the generation of reactive species crucial for the degradation of organic pollutants like MO. Studies have shown that Ag doping significantly improves the photocatalytic efficiency of TiO_2 in degrading MO, even under UV light. These advancements make Ag-doped photocatalysts an important area of research for environmental remediation **[272]**. **Table III.1** summarizes recent studies investigating the use of Ag-doped photocatalysts for the degradation of MO.

Table III.1 Recent studies on Ag-doped photocatalysts for the degradation of MO

Photo-catalyst	Dye	Degradation Efficiency	Conditions	Key Findings	Reference
Ag-ZnO	MO, RhB	MO: 99.3%, RhB: 99.7%	UV light, 35 min	Superior photoactivity and recyclability	**[273]**
Ag-ZnO nanofibers	MB, RhB, MO	MB: ~100% (75 min), RhB: ~66% (120 min), MO: ~51% (120 min)	UV light	Ag doping significantly improved degradation rates	**[274]**
Ag-TiO_2	MO	MO: 95%	UV light, 120 min	Higher efficiency by using Ag-TiO_2 compared to pure TiO_2. Pure TiO_2 data: MO: ~50%.	**[173]**
Ag-TiO_2	MO	MO: ~100%	UV light, 55 min	Complete degradation by using Ag-TiO_2 compared to pure TiO_2. Pure TiO_2 data: MO: ~60%.	**[275]**
Ag-TiO_2	MO	MO: 95%	UV light, 60 min	Ag-TiO_2 achieved 95% degradation, while pure TiO_2 gave about 50%	**[276]**

To further enhance the photocatalytic degradation of pollutants, hydrogen peroxide (H_2O_2) is frequently used in photocatalytic systems due to its capability to generate highly reactive hydroxyl radicals (•OH) upon exposure to UV light, in the presence of the photocatalyst. These

radicals are highly effective in breaking down complex pollutants like dyes. Previous studies have demonstrated the benefits of coupling H_2O_2 with photocatalysts. For example, Shahzad et al. **[277],** demonstrated enhanced degradation of Orange 16 reactive dye using H_2O_2-activated ZnO-Bi_2O_3 heterostructured composites under UV light. Similarly, Wang et al., **[278]** found that a synergistic Ag/g–C_3N_4 and H_2O_2 system significantly improved the photocatalytic degradation of azo dyes under UV light. These studies highlight the effectiveness of combining H_2O_2 with PC to enhance the degradation of various pollutants, maintaining an oxidative environment necessary for continuous pollutant degradation.

In addition, HC has demonstrated effectiveness in enhancing the degradation of organic pollutants, including dyes, in wastewater treatment. HC generates high-temperature and high-pressure conditions within the liquid, producing microbubbles that collapse violently, creating reactive radicals such as hydroxyl radicals (•OH) **[219]**. These highly reactive species can effectively degrade pollutants, complementing other advanced oxidation processes (AOPs) **[279]**. Recent studies have explored HC as a promising technique for wastewater treatment. For example, Merdoud et al. **[280],** have highlighted the synergistic effect of coupling HC with PC and H_2O_2 for optimal pollutant degradation efficiency. Several types of cavitation devices are used for HC, including orifice-based **[281]**, venturi-based **[282]**, and vortex-based devices **[280]**. Vortex-based cavitation devices developed by Ranade and co-workers **[190, 239]**, in particular, have been highlighted for their ability to generate more uniform cavitation fields, making them more efficient for large-scale applications.

The present work investigates the hybrid technology of PC, H_2O_2, and HC, aiming to explore their synergistic effects for enhanced degradation of organic dyes, particularly MO in wastewater treatment. The rationale for hybrid technologies lies in the complementary nature of each AOP. PC generates reactive oxygen species under UV light, initiating the degradation process. H_2O_2 further enhances this by contributing to the generation of hydroxyl radicals, amplifying oxidative degradation. HC complements these mechanisms by producing additional radicals through bubble collapse, creating a synergistic effect that significantly improves pollutant removal efficiency. This work represents the first report showcasing Ag-doped TiO_2 photocatalysts synthesized using a solid-state synthesis method, which has not been previously used for the synthesis of this complex. Furthermore, the coupling of this complex with vortex-

based HC has not been previously reported. The presented results serve as a valuable foundation for the advancement of large-scale dye wastewater treatment.

III.2 Experimental

III.2.1 Experimental set-up

The experimental setup consists of a lab-scale photoreactor designed to study PC both independently and in combination with HC represented schematically in **Fig. III.2.1**. The set-ups photographs are illustrated in the supplementary information (**SI**) as **Fig. S1** and **Fig. S2**. For the photocatalytic processes, a 60 W, 395 nm UV light LED, and a 200 W UV light LED were used as light sources. These lamps were mounted horizontally, one at a time, at the upper section of an aluminum photoreactor with a volume of 64,343 cm^3 (37 cm height × 37 cm length × 47 cm width), positioned 21 cm above the surface of the liquid. During the experiments, a 200 mL solution of MO was placed in a glass beaker and magnetic stirred at 200 rpm. The hybrid system consists of a holding tank with a maximum capacity of 2.5 L. The liquid is pumped from this tank utilizing a centrifugal pump with a power rating of 0.75 kW, featuring integrated manual pressure drop control to ensure liquid circulation through the pipe to a vortex-based cavitation device with a throat diameter of 3 mm. The aluminum cavitation device is designed following the model proposed by Ranade et al. **[238]**. The temperature of the holding tank was monitored but remained uncontrolled throughout the experiment.

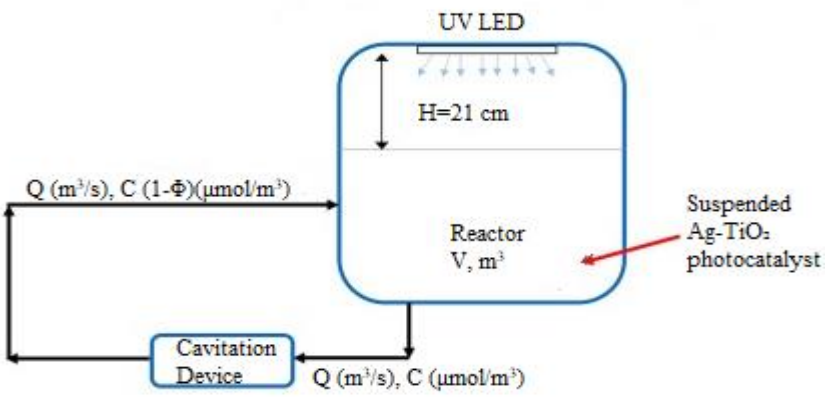

Fig. III.2.1 Schematic of experimental set-up

III.2.2 Preparation and characterization of Ag-TiO_2 NPs

The Ag-doped TiO_2 photocatalysts were synthesized using a solid-state method. Initially, 6 g of powdered TiO_2 was placed in a mortar. Ag_2O was added in varying concentrations (0%, 0.5%, 1%, 1.5%, and 2.5% w/w relative to TiO_2). The mixture underwent mechanical grinding with a pestle, employing alternating circular motions and pressing, for 1 h to ensure thorough homogenization. Subsequently, the resultant powder was sieved through a 40 µm mesh to eliminate agglomeration and achieve uniform particle size distribution. The powders were then subjected to calcination at 600°C for 2 h to facilitate the formation of Ag-TiO_2 photocatalysts. The final products were stored in dark glass containers, which were tightly sealed to maintain their integrity and protect them from light, oxygen, and contamination. Photographs illustrating the process are presented in the SI in **Fig. S3** and **Fig. S4**.

The synthesized photocatalytic materials were characterized using various techniques. X-ray diffraction (XRD) patterns were obtained using an Empyrean diffractometer with Cu Kα radiation at a scan rate of 0.1° 2θ per second, operating under conditions of 45 kV and 40 mA. Scanning electron microscopy (SEM) images were captured with a Hitachi SU-70 microscope at 5 kV, featuring a BSE detector with 3 nm resolution, and equipped with EDS for elemental analysis and mapping. Brunauer–Emmett–Teller (BET) analysis was conducted using a TriStar II Plus (Tristar 3030) analyzer with pure liquid nitrogen at 77.3 K. The samples were degassed at 100°C for 10 hours to accurately determine the photocatalyst's specific surface area.

III.2.3 Experimental methodology

The present work is divided into the following three sets of experiments

Set 1: PC alone

In this set of experiments, all tests were conducted in the same photoreactor with 200 mL of MO solution, with concentrations ranging from 14-15 ppm and a pH adjusted using H_2SO_4 and NaOH to approximately 3, as per previous studies **[283, 284]**. A loading of 1 g/L of photocatalysts was used, and an adsorption time of 60 min was established under magnetic stirring at 200 rpm. To evaluate the initial adsorption behavior, samples were collected before and after the dark equilibration period. The photocatalyst exhibited a limited affinity for dye

molecules under the experimental conditions, with less than 3 % removal attributed to adsorption. Following this, PC was performed under UV LED irradiation for 180 min. Both TiO_2 and Ag-doped TiO_2 were subjected to UV light irradiation using two separate UV LED lamps (60 W and 200 W). Ag-TiO_2 was tested at different doping percentages (0%, 0.5%, 1%, 1.5%, and 2.5% Ag-TiO_2 w/w relative to TiO_2) to determine the optimal light intensity and the best photocatalyst in terms of MO degradation. Samples of 2 mL were collected every 30 min. Using the optimal conditions for photocatalyst type and light intensity, the effect of photocatalyst loading was also investigated. Three loadings were tested: 0.5 g/L, 1 g/L, and 1.5 g/L.

Set 2: PC and H_2O_2

After determining the optimal conditions of photocatalyst type, light intensity, and photocatalyst loading in the first set of experiments, the synergistic effect of PC in combination with varying concentrations of H_2O_2 (30% v/v) was studied. The concentrations tested were 0%, 0.001%, 0.005%, and 0.01% v/v, with 2 mL of samples taken every 10 min over 60 min after switching on the lamp.

Set 3: PC, H_2O_2, and HC

Finally, MO degradation was examined using a hybrid system consisting of PC and H_2O_2, combined with HC in a 2.5 L MO solution under the optimal conditions determined in the first and second sets of experiments. The vortex diode (3 mm) was used at the optimal inlet pressure of 150 kPa, which was determined in our previous work **[280]**. The experiment was conducted for 60 min, with the MO solution kept in the dark and stirred at 200 rpm for 60 min to achieve adsorption-desorption equilibrium before activating the light and starting the PC process. before turning on the light and initiating the PC process. The effect of different scavengers was studied using the optimal conditions for photocatalyst, light intensity, and photocatalyst loading. Throughout all experiments, the photocatalyst was separated from the solution using a PTFE filter (0.2 µm), and the solution was analyzed to determine the dye concentration at λmax 470 nm. The pH of the solutions was monitored and maintained at approximately 2.8-3. All experiments involving dye degradation were conducted in triplicate to ensure accuracy and reliability, with experimental errors found to be less than 5%.

III.2.4 Analysis and processing of data

The collected samples were analyzed using a UV–Vis spectrophotometer (Shimadzu UV1800) to track changes in absorbance over time at a specific wavelength, which varied with the pH of the medium. At pH = 3, the maximum absorbance peak of the MO solution was observed at 470 nm (**Fig. S5**). After each sampling, the reaction system was momentarily suspended to prevent further progression of the process, and the withdrawn aliquot was immediately subjected to UV-Vis spectrophotometric analysis. The MO solution concentrations were determined using a calibration curve, and all concentration values obtained from UV measurements were considered accurate for subsequent calculations. The rate of MO removal was calculated using the following **Equation [114]**:

$$\%MO\ removal = \frac{C_0 - C}{C_0} \times 100 \qquad \text{III.1}$$

Where C_0 is the initial concentration of MO, and C [ppm] is the concentration at time t.

The degradation kinetics of MO were modeled using different approaches depending on the method applied. For PC alone, the experimental data was interpreted using first-order kinetics, represented by **Equation III.2 [285]**:

$$C = C_0 \times e^{-kt} \qquad \text{III.2}$$

where k [min^{-1}] is the first-order rate constant of the reaction and$t$ is time [min].

In our previous work, we discussed that pseudo-first-order kinetics have been widely utilized for pollutant degradation via HC **[226, 286, 287].** Alternatively, per-pass model of Ranade et al. **[217],** can also be used. In this work, the overall behavior of a typical cavitation-based water-treatment setup was modeled using both these approaches as:

$$V\frac{dC}{dt} = Q\Phi C \ or\ V\frac{dC}{dt} = -k_{eff}C \qquad \text{III.3}$$

Where C [ppm] represents the concentration of pollutants, V [L] denotes the working volume (including the holding tank and the volume of piping with the pump), and Q [L/min] is the flow rate through the cavitation device. The apparent degradation rate constant is k_{eff} [min^{-1}], and

Φ [-] is the per-pass degradation factor. Although temperature effects can be considered by accounting for activation energy, this study does not include such considerations. Instead, we report the effective values of the per-pass factor Φ or the effective rate constant k_{eff}, estimated over the range of temperatures applied in the experiments.

III.3 Results and discussion

III.3.1 Characterization of TiO2-based photocatalysts

III.3.1.1 XRD

Fig. III.3.1 represents the XRD pattern of TiO_2 and Ag-TiO_2 at varying doping levels (0.5%, 1%, 1.5%, and 2.5%). It reveals the dominant anatase phase with characteristic peaks at 25.3°, 37.8°, 48.0°, 53.9°, and 55.1° (2θ), corresponding to the (101), (004), (200), (105), and (211) planes, respectively. The stability of these peaks across all doping levels indicates that the anatase structure is preserved despite incorporating silver **[288]**. Additionally, a minor peak at 27.4° (2θ), associated with the rutile phase (110) plane, is present in all samples, but it remains weak, confirming that anatase is the predominant phase **[289]**. Doping with 0.5% Ag notably enhances the intensity of the anatase peak at 25.3°, reflecting improved crystallinity and a reduction in structural imperfections **[290]**.

This enhancement suggests that a lower concentration of silver stabilizes the anatase phase by strengthening the lattice structure and minimizing defects. At this optimal concentration, the incorporation of silver fills oxygen vacancies without significantly distorting the lattice, thereby improving crystallinity **[291]**. Additionally, at 0.5%, the dopant level remains low enough to avoid triggering the anatase-to-rutile transformation, allowing the anatase phase to dominate critical for achieving optimal photocatalytic performance. At higher doping levels, such as 1%, 1.5%, and 2.5%, a marked increase in the intensity of the rutile peak at 27.4° (2θ), corresponding to the (110) plane, is observed. This phenomenon may be due to the cumulative lattice distortions induced by the incorporation of larger amounts of silver atoms **[271]**. Higher dopant concentrations may introduce significant stress within the TiO_2 matrix, destabilizing the anatase phase and lowering the energy barrier for the anatase-to-rutile transformation **[292]**. Furthermore, the increased silver content may generate more structural defects and oxygen vacancies, which act as nucleation sites for the growth of rutile crystallites **[293]**. Thus, while

lower silver concentrations stabilize anatase, higher concentrations destabilize it and promote the rutile phase.

Despite the structural modifications, no distinct peaks corresponding to silver or silver oxide phases are detected. This absence may indicate that silver is either highly dispersed within the TiO_2 lattice or present in amounts below the detection sensitivity of XRD, confirming successful doping without the formation of segregated silver phases **[294]**. The preservation of the anatase structure, even at higher doping levels, demonstrates the robustness of the TiO_2 lattice and the effective incorporation of silver **[295]**.

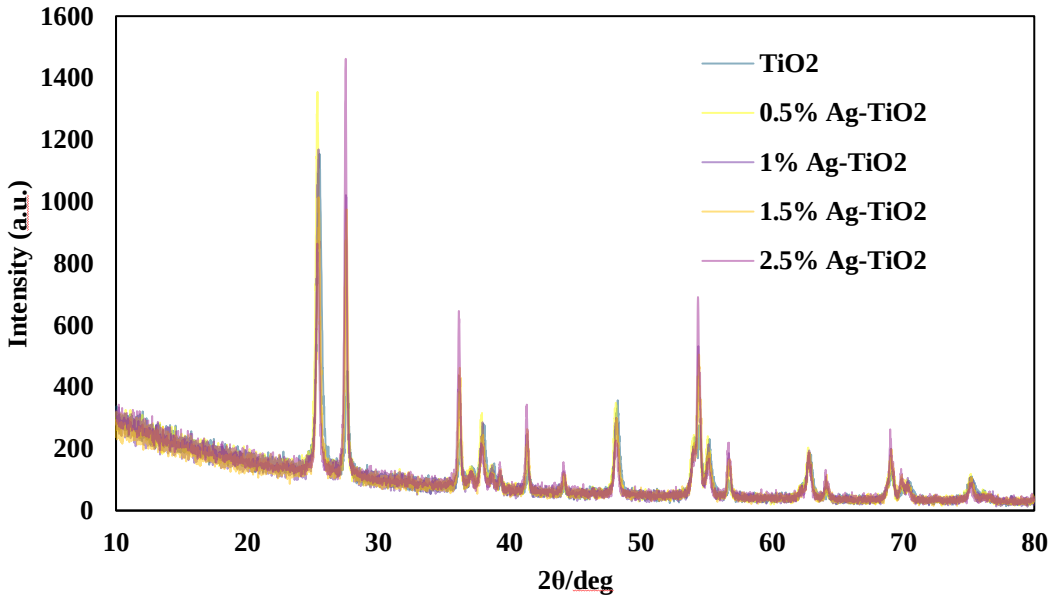

Fig. III.3.1 XRD patterns of undoped TiO_2, and Ag-TiO_2 photocatalysts at different doping levels (0.5%, 1%, 1.5%, and 2.5% w/w relative to TiO_2)

III.3.1.2 SEM-EDS

Fig. III.3.2 represents the SEM-EDS mapping and spectra for undoped TiO_2, and Ag-TiO_2 with different proportions of Ag NPs (0.5%, 1%, 1.5%, and 2.5% w/w relative to TiO_2), highlighting the elemental distribution, structural features, and morphological characteristics of each sample. For the pure TiO_2 sample, the mapping illustrates a uniform distribution of titanium particles across the surface, as depicted by the green spots. This is corroborated by the EDS spectrum, which shows distinct peaks for titanium and oxygen, confirming the high purity and structural

homogeneity of the TiO_2 sample. In the 0.5% Ag-TiO_2 sample, the SEM images reveal the initial incorporation of silver into the TiO_2 matrix, with silver particles appearing as small, evenly distributed red spots. The EDS spectrum shows the presence of silver alongside titanium and oxygen, with a low-intensity Ag peak, reflecting successful doping at a low concentration **[296]**. For the 1%, 1.5%, and 2.5% Ag-TiO_2 samples, the SEM images show an increasing density of red spots, indicating higher silver content. At 1%, the silver particles are well-dispersed, enhancing photocatalytic potential without significant aggregation. At 1.5%, some clustering of silver particles begins to appear, which could slightly reduce the uniformity of the distribution. At 2.5%, the images reveal clear evidence of particle agglomeration, which might hinder photocatalytic efficiency due to reduced active surface area. The EDS spectra for these samples show progressively intensified Ag peaks, confirming the higher silver concentrations.

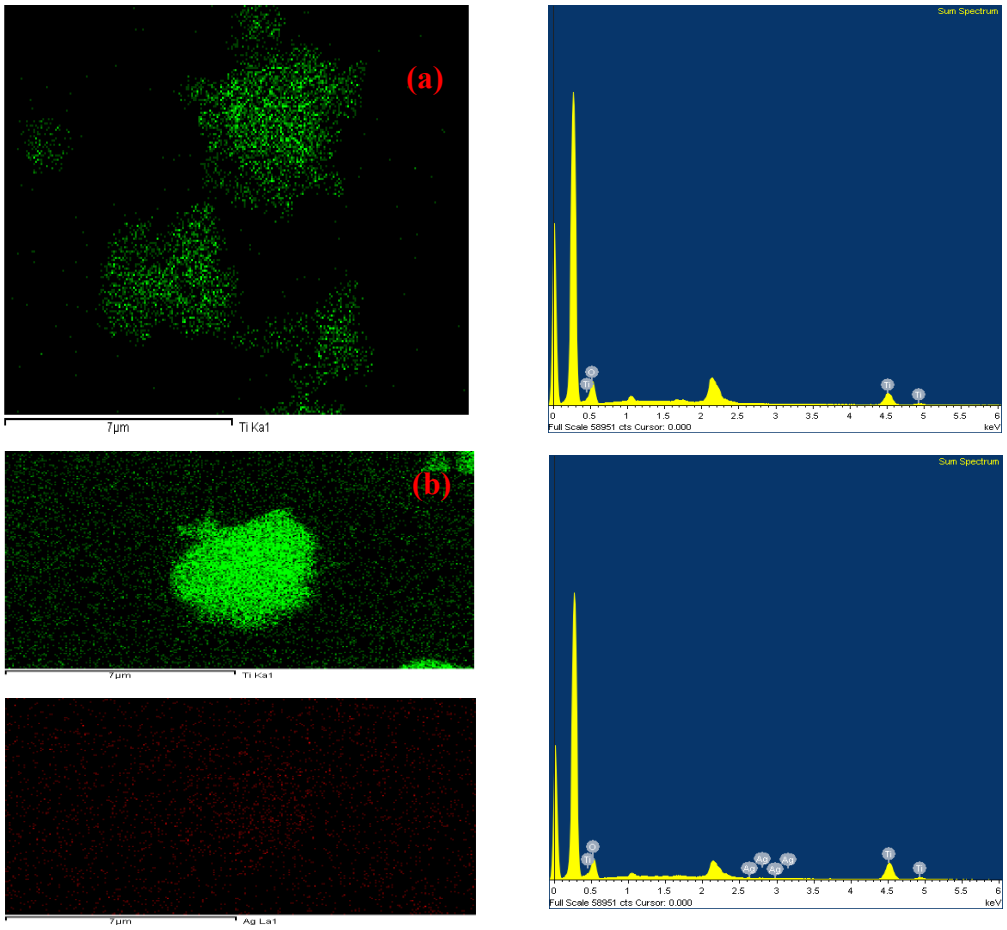

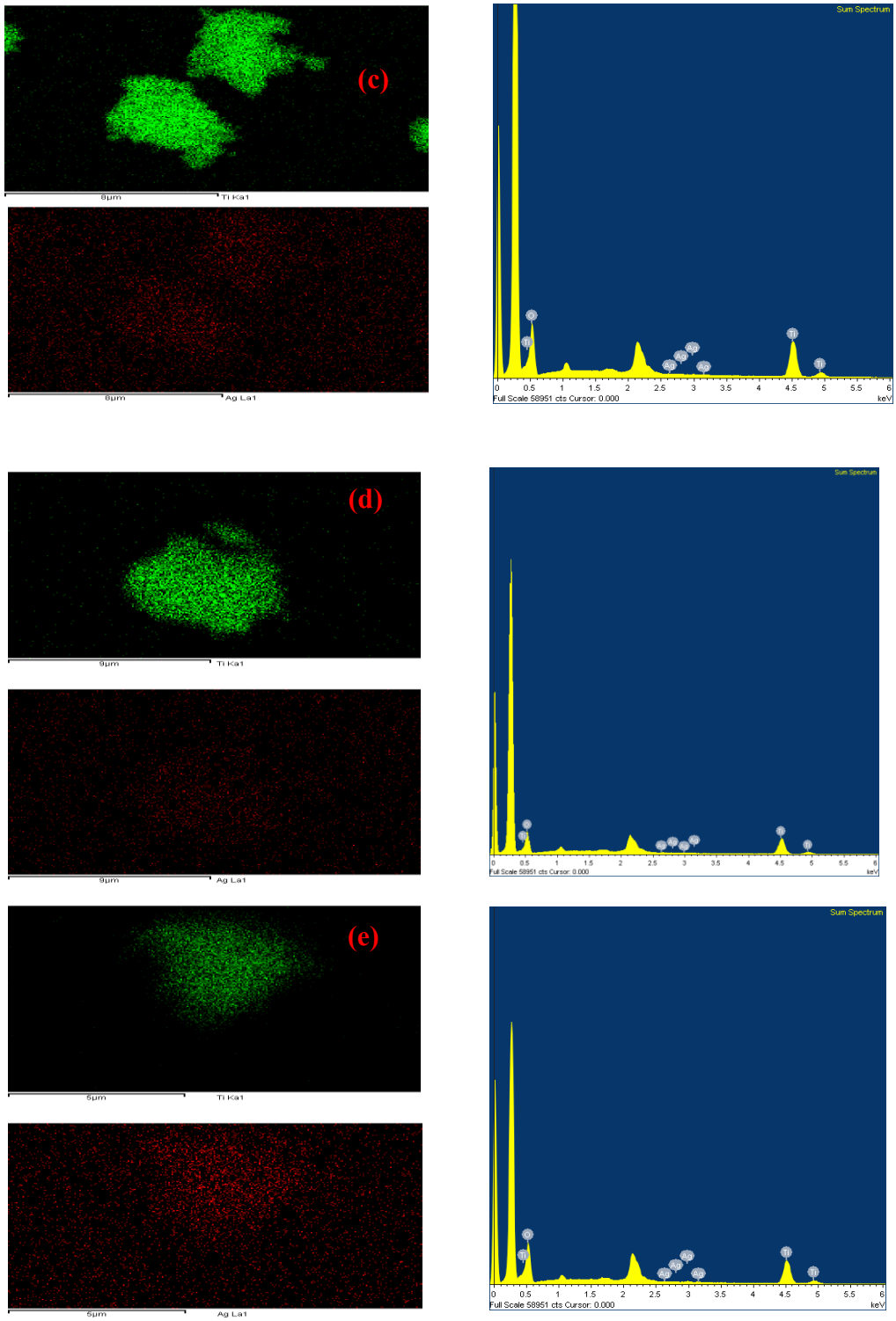

Fig. III.3.2 SEM-EDS mapping analysis and spectra of a) TiO_2, b) 0.5% Ag-TiO_2, c) 1% Ag-TiO_2, d) 1.5% Ag-TiO_2, e) 2.5% Ag-TiO_2 photocatalysts

III.3.1.3 BET Analysis

The BET analysis reveals significant trends in the textural properties of TiO_2 and Ag-doped TiO_2 photocatalysts, which directly correlate with their photocatalytic activity. The pore size of undoped TiO_2 is 118.44 Å, with a surface area of 30.44 m^2/g, providing a baseline mesoporous structure ideal for PC. Upon doping with 0.5% Ag, the pore size (116.95 Å) and surface area (28.86 m^2/g) remain relatively unchanged, maintaining sufficient active sites and reactant accessibility while introducing the plasmonic effect of silver, which enhances light absorption and minimizes charge recombination. This balance results in 0.5% Ag-TiO_2 being the most efficient catalyst for MO degradation. At higher doping levels, structural modifications become more pronounced. The 1% Ag-TiO_2 exhibits a slight increase in pore size (121.37 Å) but a marked decrease in surface area (23.79 m^2/g), suggesting agglomeration of silver particles that begin to obstruct active surface regions. Further increases in Ag content (1.5% and 2.5%) result in significant reductions in both pore size (105.85 Å and 63.66 Å, respectively) and surface area (22.47 m^2/g and 15.22 m^2/g). These reductions indicate excessive silver deposition blocking fine capillaries, diminishing the accessible catalytic surface, and potentially introducing recombination centers for electron-hole pairs, thus undermining photocatalytic efficiency.

Overall, the BET analysis demonstrates that while low levels of silver doping (0.5%) optimize the synergy between enhanced light absorption and maintained structural properties, higher silver concentrations disrupt this balance, leading to diminished photocatalytic performance. **Table III.3.1** summarizes the BET analysis of TiO_2 and Ag-doped TiO_2 photocatalysts. For comparison, Sobana et al., **[297],** reported that the surface area of TiO_2 decreased from 21.53 m^2/g to 17,78 m^2/g with 1.5% Ag doping, and further to 12.39 m^2/g with 2% Ag doping. Similarly, Chuang et al., **[298]**, found that the surface area of TiO_2 decreased from 196.8 m^2/g to 117.8 m^2/g upon Ag doping. These findings align with our observations that silver doping generally leads to a slight decrease in surface area, which can impact photocatalytic efficiency.

Table III.3.1 BET surface area and pore size analysis of TiO_2 and Ag-doped TiO_2 photocatalysts

Photocatalyst	Pore size (Å)	BET surface area (m^2/g)
0% Ag-TiO_2	118.44	30.44
0.5% Ag-TiO_2	116.95	28.86
1% Ag-TiO_2	121.37	23.79
1.5% Ag-TiO_2	105.85	22.47
2.5% Ag-TiO_2	63.66	15.22

III.3.2 Influence of silver concentrations and different lamp intensities on MO degradation

The study investigates the effect of Ag-TiO_2 photocatalysts with different silver concentrations (0%, 1%, 1.5%, 2.5% w/w relative to TiO_2) on MO degradation under different UV Led lamp intensities (60 W and 200 W). From **Fig. III.3.3 (a)**, at a lower lamp intensity of 60 W, the 0.5% Ag-TiO_2 photocatalyst has demonstrated the highest degradation efficiency of 24.6% with a kinetic constant of 0.0016 min^{-1}, indicating faster reaction rates, over 180 min of treatment.

This enhanced performance is attributed to silver's role as an electron trap, capturing photogenerated electrons and reducing the recombination of electron-hole pairs, thereby prolonging the lifespan of reactive species responsible for MO degradation. However, as the silver concentration increases, the degradation efficiency decreases. At 1% Ag-TiO_2, the efficiency drops to 21.7% with a kinetic constant of 0.0014 min^{-1}, indicating slower reaction rates, likely due to partial agglomeration of silver particles, which reduces their dispersion and effectiveness. Further increases to 1.5% and 2.5% Ag-TiO_2 result in even lower efficiencies of 14.3% ($k = 0.0008\ min^{-1}$) and 5.3% ($k = 0.0003\ min^{-1}$), respectively. This decline is attributed to excessive silver coverage hindering light absorption and blocking active sites on the TiO_2 surface, as well as promoting recombination of electron-hole pairs. For pure TiO_2, a degradation efficiency of 19.6% and a kinetic constant of 0.0013 min^{-1} were achieved.

In contrast, From **Fig. III.3.3 (b),** at a higher lamp intensity of 200 W, the photocatalytic performance improves significantly across all silver concentrations. The 0.5% Ag-TiO_2 photocatalyst shows a dramatic increase in degradation efficiency to 58.8% with a kinetic

constant of 0.0048 min^{-1}, highlighting the critical role of higher light intensity in enhancing photocatalytic activity. The increased light intensity generates more photogenerated electron-hole pairs, improving the availability of reactive oxygen species required for MO degradation. Even pure TiO_2 sees a performance boost, achieving a degradation efficiency of 35.7% and a kinetic constant of 0.0024 min^{-1}. However, similar to the 60 W intensity, increasing the silver concentration beyond 0.5% leads to diminished performance. At 1% Ag-TiO_2, the degradation efficiency reduces to 29.6% ($k = 0.0023\ min^{-1}$), and further declines to 25% ($k = 0.002\ min^{-1}$) and 9.8% ($k = 0.0007\ min^{-1}$) at 1.5% and 2.5% Ag-TiO_2, respectively. The consistent trend of declining efficiency with higher silver concentrations is due to agglomeration, light blocking, and increased recombination of charges. Lines in **Fig. III.3.3** are as per **Equation III.2** with rate constants listed in **Table III.3.2.**

While higher light intensity (200 W) significantly enhances the degradation rates and reaction kinetics, the optimal silver concentration remains at 0.5% Ag-TiO_2. This concentration balances charge separation and maintains an accessible TiO_2 surface for photocatalytic reactions. Excessive silver doping, regardless of light intensity, leads to agglomeration and recombination issues that negate the benefits of increased lamp power. **Table III.3.2** summarizes the intensity and silver concentration effect on MO degradation.

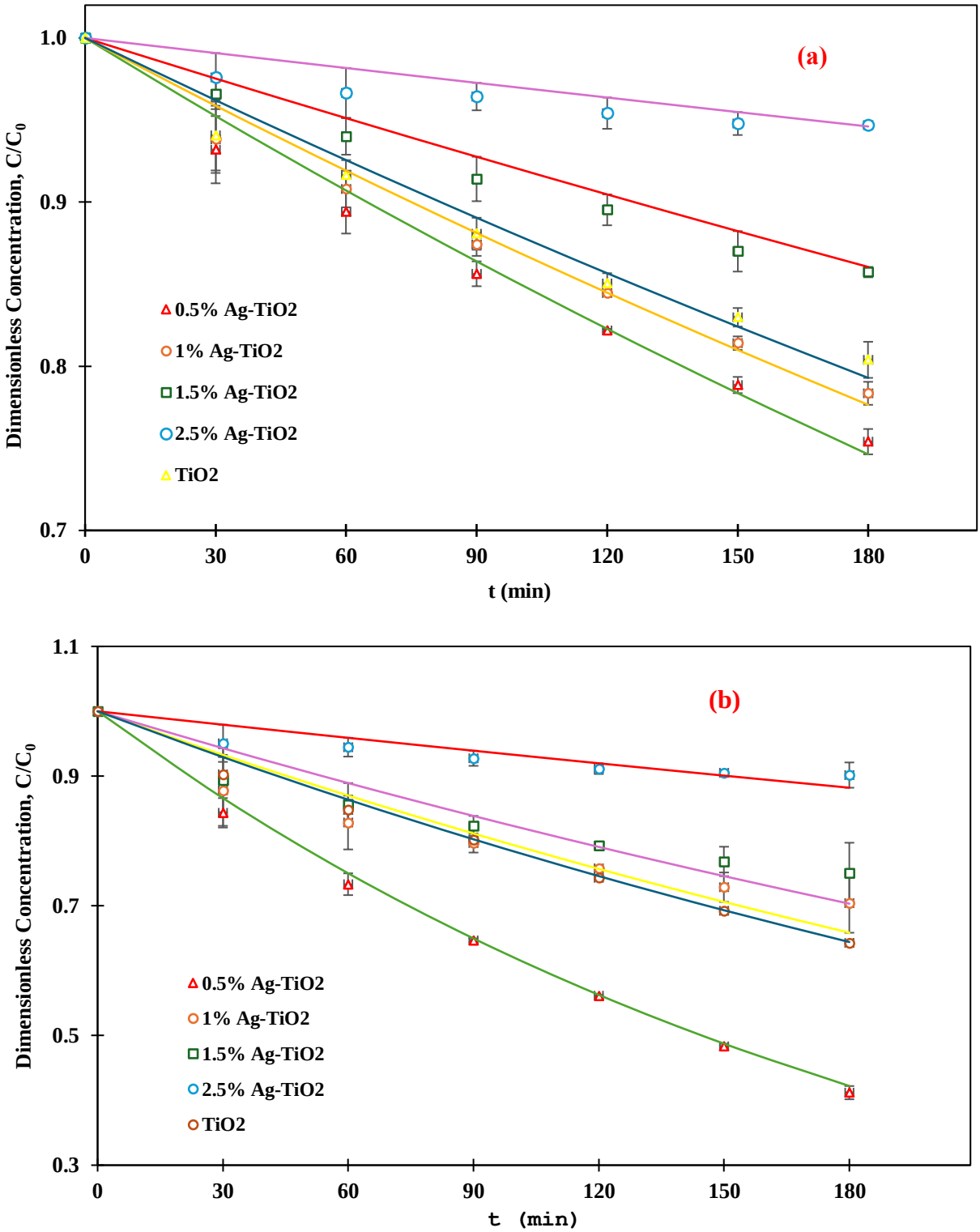

Fig. III.3.3 MO dye degradation versus time for different photocatalysts under different UV-irradiation intensities: a) 60 W and b) 200 W; photocatalysts dose = 1 g/L, pH = 3, and MO initial concentration = 15 ppm

Table III.3.2 Kinetic parameters and degradation rates at varying UV intensities

Photocatalyst	UV intensity [W]	Time of degradation [min]	k [min^{-1}]	Degradation rate [%]
0% Ag-TiO_2	60	180	0.0013	19.6
0.5% Ag-TiO_2			0.0016	24.6
1% Ag-TiO_2			0.0014	21.7
1.5% Ag-TiO_2			0.0008	14.3
2.5% Ag-TiO_2			0.0003	5.3
0% Ag-TiO_2	200	180	0.0024	35.7
0.5% Ag-TiO_2			0.0048	58.8
1% Ag-TiO_2			0.0023	29.6
1.5% Ag-TiO_2			0.0020	25.0
2.5% Ag-TiO_2			0.0007	9.8

III.3.3 Effect of photocatalyst loading on MO degradation

Fig. III.3.4 represents the influence of different photocatalyst concentrations (0.5 g/L, 1 g/L, and 1.5 g/L) on the photocatalytic degradation of MO using the optimum photocatalyst (0.5% Ag-TiO_2) under optimum UV LED light source (200 W). At 0.5 g/L, a degradation efficiency of 25.7% was obtained, with a rate constant (k) of 0.0019 min^{-1}. The slower degradation rate can be attributed to the insufficient photocatalyst concentration, which provided a limited number of active sites for the photocatalytic reaction. As a result, fewer pollutant molecules interacted with the photocatalyst, leading to lower removal efficiency. At 1 g/L, the degradation efficiency improved significantly to 58.8%, with a higher rate constant (k) of 0.0047 min^{-1}, indicating optimal conditions. At this loading, the photoatalyst provided an adequate number of active sites and maintained good dispersion in the solution. The higher availability of active sites allowed efficient interaction between the pollutant molecules, the photocatalyst, and the light source, leading to enhanced degradation. However, at 1.5 g/L, the degradation efficiency decreased to 38.2%, with a lower rate constant (k) of 0.0028 min^{-1}. Despite the higher photocatalyst concentration, the degradation rate dropped due to particle agglomeration, which reduced the effective surface area and the number of accessible active sites. Additionally, the

excessive photocatalyst may have blocked light penetration, limiting the activation of photocatalytic sites and thereby reducing efficiency. Thus, the optimal performance was observed at 1 g/L, where the 0.5% Ag-TiO_2 photocatalyst achieved the best combination of sufficient active sites and efficient light utilization. Lines in **Fig. III.3.4** are as per **Equation III.2** with rate constants listed in **Table III.3.3**. **Table III.3.3** summarizes the impact of photocatalyst dosages on MO degradation.

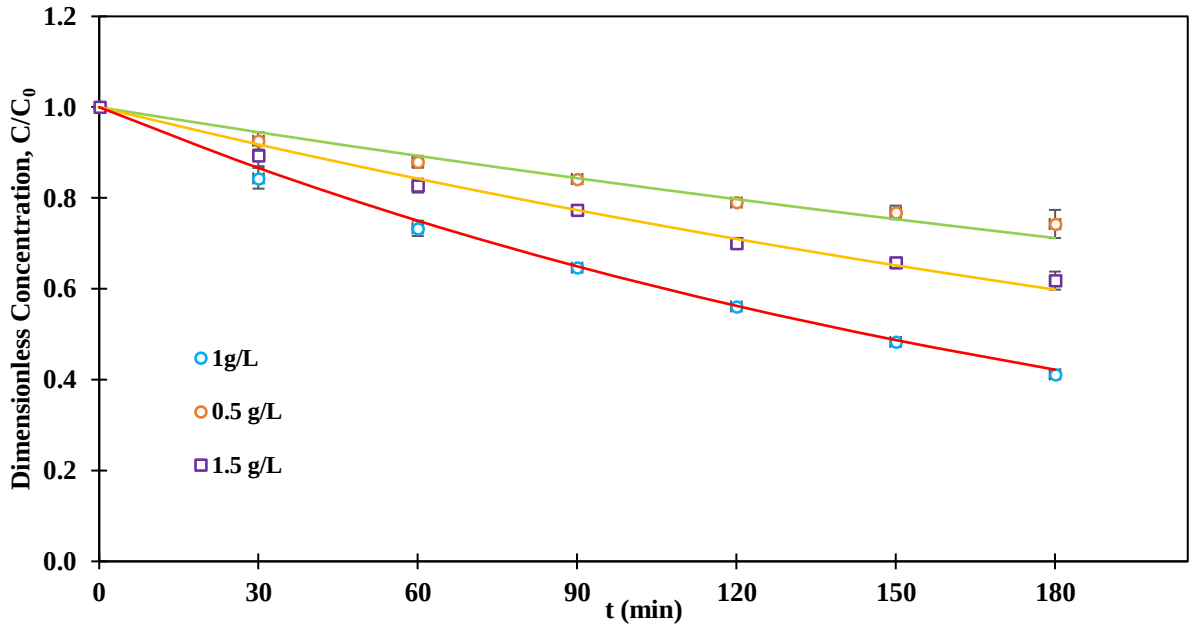

Fig. III.3.4 MO dye degradation versus time for different photocatalyst dosages; 0.5% Ag-TiO_2, 200 W UV-irradiation, pH = 3, and MO initial concentration = 15 ppm.

Table III.3.3 MO degradation, and rate constant k in different photocatalyst dosages.

Photocatalyst dosage [g/L]	Photocatalyst	Time of degradation [min]	Rate constant k [min^{-1}]	Degradation rate [%]
0.5	0.5% Ag-TiO_2	180	0.0019	25.7
1			0.0047	58.8
1.5			0.0028	38.2

III.3.4 Synergy effect of H_2O_2 in PC

The graphs in **Fig. III.3.5** explore the synergy effect of H_2O_2 in combination with PC for the degradation of MO under 200 W UV light, using a 0.5% Ag-TiO_2 photocatalyst concentration of 1 g/L. The synergy coefficient (γ_1) quantifies the enhancement in degradation efficiency due to the combined effect of PC and H_2O_2 compared to their individual contributions. It is calculated using the following Equation **[250]**:

$$\gamma_1 = \frac{k_{PC+H_2O_2}}{k_{PC}+k_{H_2O_2}} \qquad \text{III.4}$$

Where $k_{PC+H_2O_2}$ is the rate constant of PC with H_2O_2, $k_{PC}$is the rate constant of PC without H_2O_2, and $k_{H_2O_2}$ is the rate constant of MO with H_2O_2 without the photocatalyst. The values of the rate constants *k* were extracted from the pseudo-first-order kinetic plots of each process.

When photolysis was performed with 0.01% v/v H_2O_2 in the absence of the photocatalyst, the efficiency of degradation was minimal at 1.6%, with a low-rate constant of 0.003 min^{-1}. This indicates that UV light alone, even in the presence of H_2O_2, is insufficient to generate a significant number of ROSs such as hydroxyl radicals (•OH), which are key to the oxidative degradation process for effective degradation. The reliance on photolysis without the photocatalytic activation of H_2O_2 limits its performance. The PC alone, without the addition of H_2O_2, results in a modest degradation efficiency of 13.9% over 60 min of treatment, with a slightly lower rate constant of 0.0024 min^{-1}. Here, the activity is driven by the photo-induced electron-hole pairs generated by Ag-TiO_2 under UV light. However, the absence of H_2O_2 means that the production of ROSs is limited, and the recombination of electron-hole pairs further reduces the overall degradation efficiency.

In contrast, the addition of small concentrations of H_2O_2 has significantly improved the photocatalytic performance. At 0.001% v/v H_2O_2, the degradation efficiency has increased to 31.2%, with a rate constant of 0.0079 min^{-1}. The presence of H_2O_2 enhances ROSs production by interacting with photo-generated electrons, forming hydroxyl radicals that contribute to the oxidative degradation of MO molecules. The γ_1 for this concentration was 2.93. As the concentration of H_2O_2 was increased to 0.005%, v/v, the degradation efficiency was raised sharply to 67.6%, with a higher rate constant of 0.0247 min^{-1}. This improvement reflects the more effective generation of ROSs, as H_2O_2 not only

supplies hydroxyl radicals but also acts as an electron scavenger, reducing recombination. The γ_1 for this concentration was 9.15. The highest degradation efficiency of 93.8% was achieved with 0.01% v/v H_2O_2, corresponding to a rate constant of 0.066 min^{-1}. At this concentration, H_2O_2 plays a dual role by both suppressing electron-hole recombination and serving as a continuous source of hydroxyl radicals. The system's performance reaches its peak under these optimized conditions, demonstrating the powerful synergy effect between H_2O_2 and PC. The γ_1 for this concentration is 24.44, which has not been achieved before for MO using Ag-TiO_2. Lines in **Fig. III.3.5** are as per **Equation III.2** with rate constants listed in **Table III.3.4**. **Table III.3.4** summarizes the rate constant k, the degradation rate of MO degradation, and the synergy coefficient for different H_2O_2 concentrations.

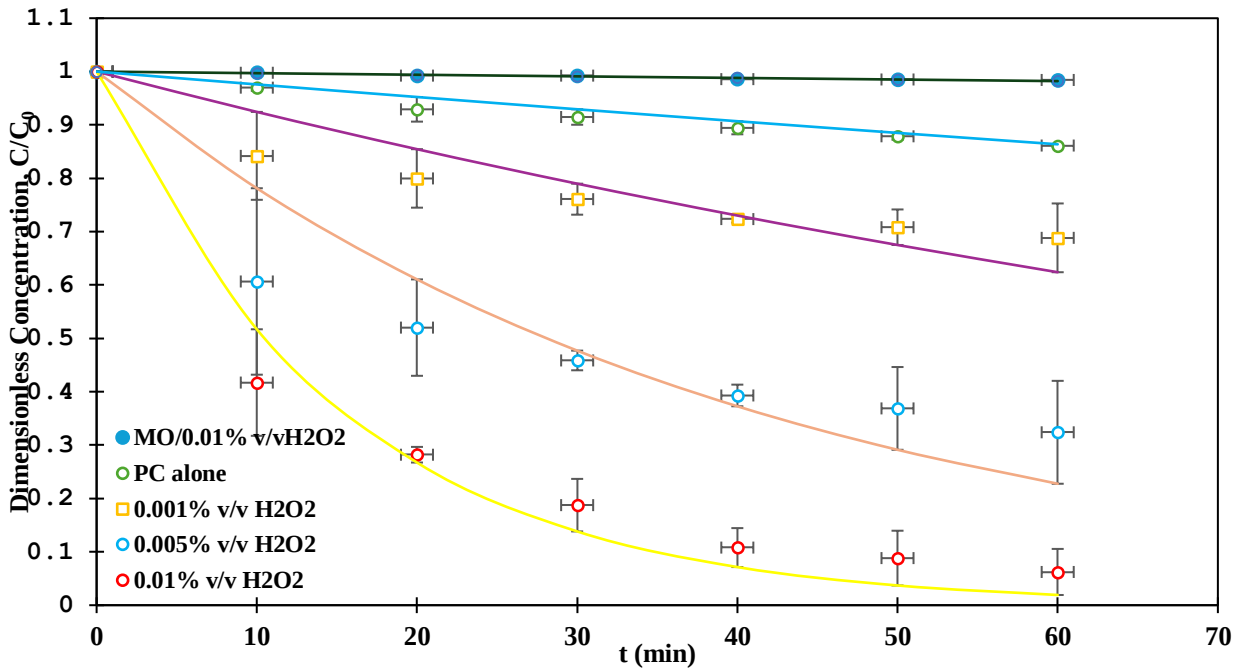

Fig. III.3.5 MO dye degradation versus time for different H_2O_2 concentrations; 0.5% Ag-TiO_2, 200 W UV-irradiation, photocatalyst dosage= 1 g/L, pH = 3, and MO initial concentration = 15 ppm.

Table III.3.4 Synergistic effect of H_2O_2 on photocatalytic degradation of MO

Operative conditions	Time of degradation [min]	Rate constant k [min^{-1}]	Degradation rate [%]	γ_1 [-]

PC alone	60	0.0024	13.9	-
MO/0.01% v/v H_2O_2 alone	60	0.0003	1.6	-
PC+0.001% v/v H_2O_2	60	0.0079	31.2	2.93
PC+0.005% v/v H_2O_2	60	0.0247	67.6	9.15
PC+0.01% v/v H_2O_2	60	0.0660	93.8	24.44

III.3.5 MO degradation by PC, H_2O_2, and HC coupling

The study evaluates the efficiency of a hybrid system combining PC, hydrogen peroxide, and HC, for the degradation of MO. **Fig. III.3.6** illustrates the remarkable performance of this approach under various operational conditions. PC alone, using 0.5% Ag-TiO_2, achieved a modest degradation efficiency of 13.9% over 60 min, while HC alone, at optimum pressure of 1.5 bar, resulted in a significantly higher degradation efficiency of 83.3% over the same duration, as investigated in our previous study **[280],** with a k_{eff} *of* 0.0445 (see Section S1 of the supporting information for more details on calculation of k_{eff}).

At an optimal H_2O_2 concentration of 0.01% and in combination with HC, the system achieved complete degradation of MO in just 3 min (1.5 passes), corresponding to a k_{eff} of 1.9746 min^{-1}. This improvement is attributed to HC, which creates intense turbulence and localized high-energy zones, enhancing the interaction between MO, the photocatalyst, and reactive radicals. The calculated synergy coefficient (γ_2) for this condition was calculated as per **Equation III.5**, demonstrating the advantage of combining these processes.

$$\gamma_2 = \frac{k_{PC+H_2O_2+HC}}{k_{PC}+k_{H2O2}+k_{HC}} \quad \text{III.5}$$

This condition yielded an extraordinary γ_2 of 42, indicating a highly efficient interaction between the advanced oxidation processes. For comparison, a similar study conducted by Merdoud et al., **[280]**, using TiO_2 supported on glass fiber tissue reported a γ_2 of 9.22, underscoring the exceptional performance of the 0.5% Ag-TiO_2 photocatalyst in the present

work. To the best of our knowledge, the synergy coefficient achieved in this study represents an unprecedented efficiency in the literature, emphasizing the system's potential for rapid and effective pollutant degradation. Lines in **Fig. III.3.6** are as per **Equation (III.2, and III.3)** with rate constants listed in **Table III.3.5.**

Table III.3.5 summarizes the rate constant k, the degradation rate of MO degradation, and the synergy coefficient for different H_2O_2 concentrations using PC/H_2O_2/HC.

Table III.3.5 Degradation kinetics and synergistic effects of PC with H_2O_2 and HC

Operative conditions	Time of degradation [min]	Effective degradation rate constant k_{eff} [min^{-1}]	Degradation rate [%]	γ_2 [-]
PC alone	60	0.0024	13.9	-
HC alone	60	0.0445	83.3	-
PC+0.01% v/v H_2O_2/HC	03	1.9746	100	42

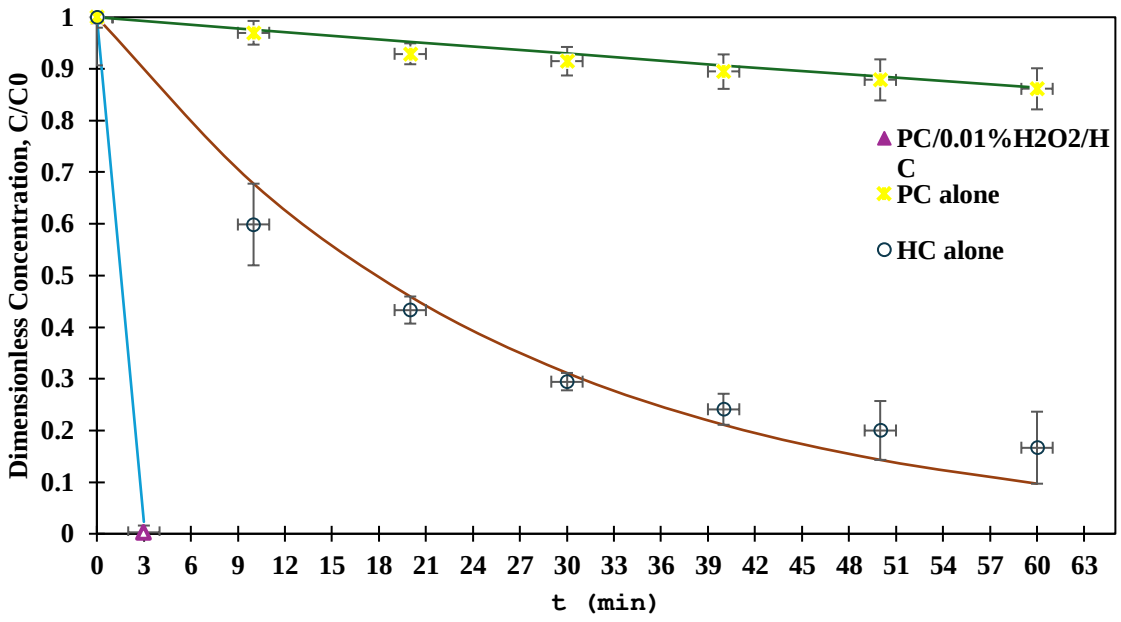

Fig. III.3.6 MO dye degradation versus time using PC combined H2O2 coupled HC; 0.5% Ag-TiO_2, 200 W UV-irradiation, photocatalyst dosage= 1 g/L, pH = 3, and MO initial concentration = 15 ppm.

III.3.6 Scavenger effect

Fig. III.3.7 demonstrates the impact of different scavengers on the photocatalytic degradation process using 0.5% Ag-TiO_2 as a photocatalyst. The degradation efficiencies are compared to a control system operating without any scavenger. The highest degradation efficiency, 58.8%, is observed in the absence of scavengers, indicating the optimal performance of the Ag-TiO_2 photocatalytic system under scavenger-free conditions. This suggests that reactive species, such as hydroxyl radicals (•OH) and superoxide radicals (O_2^{-}•), are actively involved in the degradation process when they are not hindered by scavengers **[299]**. The addition of isopropanol significantly reduces the degradation efficiency to 19.7%. Isopropanol, a well-known scavenger for hydroxyl radicals (•OH), causes this marked decrease, highlighting the dominant role of these radicals in the photocatalytic activity facilitated by Ag-TiO_2. Zhou et al. **[300],** also observed that (•OH) plays a crucial role in the photocatalytic processes involving TiO_2, further supporting these findings. Similarly, the introduction of EDTA lowers the efficiency to 27.9%. As EDTA primarily scavenges photo-generated holes (h^+), this result emphasizes the importance of these holes in the degradation mechanism. Methanol, which acts as a scavenger for superoxide radicals (O_2^{-}•), leads to a reduction in efficiency to 31.3%. This result underscores the critical role of superoxide radicals in the degradation process. The lowest degradation efficiency, 14.5%, is observed with KI, which acts as a scavenger for both hydroxyl radicals and photo-generated holes. This result indicates that both reactive species are essential for achieving effective photocatalytic degradation using Ag-TiO_2. A summary of the main reaction mechanisms involved in each scavenging process is presented in **Table III.3**, outlining the specific reactive species targeted by each scavenger.

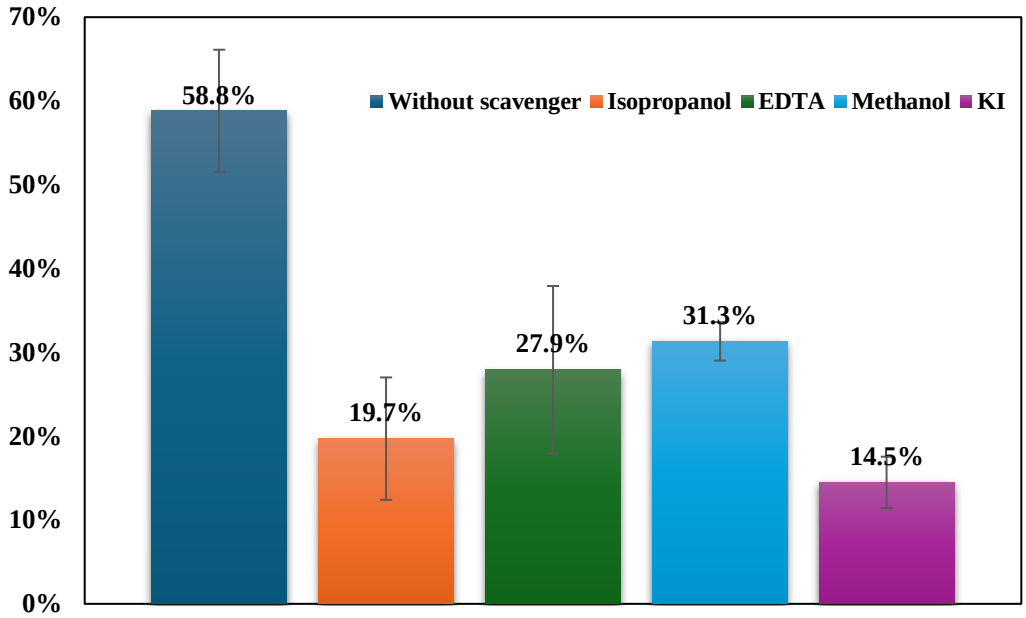

Fig. III.3.7 MO dye degradation with and without scavengers; 0.5% Ag-TiO_2, 200 W UV-irradiation, photocatalyst dosage= 1 g/L, pH = 3, and MO initial concentration = 15 ppm.

Table III.3.6 Reactive species trapping by different scavengers and associated reaction mechanisms

Scavenger	Target Reactive Species	Reaction Mechanisms
Isopropanol $(CH_3)_2CHOH$	Hydroxyl radicals (•OH)	$\cdot OH + (CH_3)_2CHOH \rightarrow (CH_3)_2 \cdot COH + H_2O$
EDTA (Ethylenediaminetetraacetic acid)	Photogenerated holes (h^+)	$EDTA^{4-} + h^+ \rightarrow EDTA^{3-}$
Methanol CH_3OH	Superoxide radicals (O_2^-•)	$\cdot O_2^- + CH_3OH \rightarrow$ less reactive products
KI (Potassium iodide)	Photogenerated holes (h^+) & Hydroxyl radic als (•OH)	$I^- + h^+ \rightarrow \cdot I$ $I^- + \cdot OH \rightarrow \cdot I + OH^-$ $2 \cdot I \rightarrow I_2$

III.4 Conclusion

In this work, the degradation of MO dye solution was investigated using a combination of AOPs at laboratory scale. The study focused on the use of Ag-doped TiO_2 photocatalysts, H_2O_2, and vortex-based HC for MO degradation. Ag-doped TiO_2 photocatalysts were successfully synthesized using a solid-state method, confirmed through various characterization techniques, including XRD, SEM-EDS, and BET. The key conclusions from this study are:

- The optimal concentration of Ag-TiO_2 was found to be 0.5%. This concentration achieved the highest degradation efficiency under both 60 W (24.6%) and 200 W (58.8%) UV lamp intensities.
- The photocatalyst loading of 1 g/L was found to be optimal loading for achieving the best degradation efficiency.
- The combination of PC with 0.01% v/v H_2O_2 significantly improved degradation efficiency, achieving 93.87% degradation within 60 min and yielding a synergy coefficient of 24.44.
- The hybrid system combining PC, H_2O_2, and HC showed remarkable improvements in degradation efficiency. Complete degradation of MO was achieved in just 3 min (1.5 passes) with a synergy coefficient of 42, indicating a highly efficient interaction between the advanced oxidation processes.
- The presence of scavengers like isopropanol, EDTA, methanol, and KI significantly reduced degradation efficiency, underscoring the roles of these reactive species.

Our study demonstrates that the integration of Ag-TiO_2 with various AOPs such as H_2O_2 and HC significantly enhances the degradation of MO. This synergistic effect among the processes provides a promising approach for improving effluent treatment. The findings will benefit researchers focused on the combined application of photocatalysis, H_2O_2, and HC in wastewater management.

General conclusion

This thesis was supported by the Direction Générale de la Recherche Scientifique et du Développement Technologique (DGRSDT), Algeria, and the Erasmus+ Exchange Program. The work was carried out at the University of Bouira, Laboratory of Materials and Durable Development (LMDD), LGVRNAQ, and the Bernal Institute at the University of Limerick, Ireland. The primary objective of this study was to develop advanced photocatalytic materials to improve the effectiveness of wastewater treatment processes, thereby contributing to the advancement of sustainable and effective remediation strategies.

The first enhancement strategy focused on using immobilized TiO_2 on GFT, a cost-effective and efficient support to facilitate the degradation of MO in water, thereby mitigating the challenges associated with the use of powdered TiO_2, such as catalyst recovery and aggregation. This supported photocatalyst was then integrated into an advanced hybrid process combining HC, whose operational parameters were systematically optimized, with the controlled addition of H_2O_2 to enhance oxidative degradation. Subsequently, the system was coupled with PC, leading to a significant improvement in MO degradation efficiency of 99.8% over 21 min with 50% COD mineralization under UV light. This synergistic interaction exhibited a unique enhancement mechanism, not previously reported in the literature for TiO_2-based systems with a synergy coefficient of 9.2. A key innovation of this work lies in the coupling of vortex-induced hydrodynamic cavitation with TiO_2 immobilized on GFT, a novel approach for the degradation of organic contaminants in aqueous environments, demonstrating enhanced performance and practical applicability.

The second enhancement strategy involved doping TiO_2 with a metallic element, specifically silver, using a more environmentally friendly, cost-effective, and straightforward synthesis method: a solid-state method. The photocatalytic process was systematically optimized by evaluating key parameters, including the silver doping percentage, light intensity, photocatalyst loading, and H_2O_2 concentration. Once the optimal conditions were established, the system was further integrated with HC, resulting in a complete degradation of MO within 3 min of treatment under UV light, and a unique synergistic effect that has not been documented in prior studies with a synergy coefficient of 42. To gain deeper insights into the reaction mechanisms, the scavenger effect was employed to identify the dominant reactive species responsible for pollutant

degradation, thereby elucidating the underlying pathways governing the enhanced photocatalytic activity.

In conclusion, this thesis successfully developed and optimized both the photocatalyst performance and the photocatalysis process for wastewater treatment. The integration of TiO_2 immobilized on glass fiber tissue with vortex-induced hydrodynamic cavitation and the doping of TiO_2 with silver using an environmentally friendly solid-state method have led to significant improvements in the degradation of organic pollutants, particularly the methyl orange. The synergistic effects observed in both strategies, with exceptional synergy coefficients, demonstrate the potential of these innovative approaches for practical, sustainable wastewater treatment solutions.

In the future, the prospects of this work lie in expanding the photocatalytic system to treat real textile wastewater, where we plan to conduct further tests to assess its efficiency under more complex and realistic conditions. Additionally, we aim to further develop the doping strategies to optimize the photocatalysts, with a focus on shifting their activation to sunlight, enhancing their potential for large-scale, sustainable applications. This advancement will open the door to more energy-efficient photocatalytic processes, providing a promising solution for the treatment of wastewater in industrial settings while reducing reliance on UV light. Moreover, we will explore the integration of these systems with other emerging technologies to further enhance performance and sustainability.

References

[1] Long, X., Zhang, Y., Ye, Y., Ye, Y., Xu, T., & Li, T. (2022). Spatiotemporal water quality variations in the urbanizing Chongqing reach of Jialing River, China. *Water Supply*, *22*(5), 5603-5617.

[2] Baracho, R. O., Najberg, E., & Scalize, P. S. (2023). Factors That Impact the Implementation of Water Safety Plans—A Case Study of Brazil. *Water*, *15*(4), 678.

[3] Benavides-Muñoz, H. M., Lapo-Pauta, M., Martínez-Solano, F. J., Quiñones-Cuenca, M., & Quiñones-Cuenca, S. (2024). Global Events and Surge in Residential Water Demand: Exploring Possible Hydraulic Scenarios. *Water*, *16*(7), 956.

[4] Devi, O. R., & Devi, L. J. (2024). Water Consumption and Microfibers: The Biggest Threat. In *Climate Action Through Eco-Friendly Textiles* (pp. 73-90). Singapore: Springer Nature Singapore

[5] Chakraborty, R., & Ahmad, F. (2022). Economical use of water in cotton knit dyeing industries of Bangladesh. *Journal of Cleaner Production*, 340, 130825. https://doi.org/10.1016/j.jclepro.2022.130825

[6] Khan, W. U., Ahmed, S., Dhoble, Y., & Madhav, S. (2023). A critical review of hazardous waste generation from textile industries and associated ecological impacts. *Journal of the Indian Chemical Society*, *100*(1), 100829

[7] Watari, T., Hata, Y., Hirakata, Y., Nguyet, P. N., Nguyen, T. H., Maki, S., ... & Yamaguch, T. (2021). Performance evaluation of down-flow hanging sponge reactor for direct treatment of actual textile wastewater; Effect of effluent recirculation to performance and microbial community. *Journal of Water Process Engineering*, *39*, 101724.

[8] Uddin, F. (2021). Environmental hazard in textile dyeing wastewater from local textile industry. *Cellulose*, *28*(17), 10715-10739

[9] Kumar, A. (2022). Impact of textile wastewater on water quality. *Central Asian Journal of Medical and Natural Science*, *3*(3), 449-459

[10] Islam, T., Repon, M. R., Islam, T., Sarwar, Z., & Rahman, M. M. (2023). Impact of textile dyes on health and ecosystem: A review of structure, causes, and potential solutions. *Environmental Science and Pollution Research*, *30*(4), 9207-9242

[11] Periyasamy, A. P. (2024). Recent advances in the remediation of textile-dye-containing wastewater: prioritizing human health and sustainable wastewater treatment. *Sustainability*, *16*(2), 495

[12] Sangamnere, R., Misra, T., Bherwani, H., Kapley, A., & Kumar, R. (2023). A critical review of conventional and emerging wastewater treatment technologies. *Sustainable Water Resources Management*, *9*(2), 58

[13] Al-Tohamy, R., Ali, S. S., Li, F., Okasha, K. M., Mahmoud, Y. A. G., Elsamahy, T., ... & Sun, J. (2022). A critical review on the treatment of dye-containing wastewater: Ecotoxicological and health concerns of textile dyes and possible remediation approaches for environmental safety. *Ecotoxicology and Environmental Safety*, *231*, 113160.

[14] Stone, C., Windsor, F. M., Munday, M., & Durance, I. (2020). Natural or synthetic—How global trends in textile usage threaten freshwater environments. *Science of the Total Environment*, 718, 134689. https://doi.org/10.1016/j.scitotenv.2019.1346

[15] Feijoo, S., Yu, X., Kamali, M., Appels, L., & Dewil, R. (2023). Generation of oxidative radicals by advanced oxidation processes (AOPs) in wastewater treatment: a mechanistic, environmental and economic review. *Reviews in Environmental Science and Bio/Technology*, *22*(1), 205-248

[16] Priyadarshini, M., Das, I., Ghangrekar, M. M., & Blaney, L. (2022). Advanced oxidation processes: Performance, advantages, and scale-up of emerging technologies. *Journal of environmental management*, *316*, 115295

[17] Jackulin, F., Kumar, P. S., & Rangasamy, G. (2024). Degradation of tartrazine dye using advanced oxidation process: Application of response surface methodology for optimization. *Desalination and Water Treatment*, *317*, 100066.

[18] Nouren, S., Bibi, I., Kausar, A., Sultan, M., Bhatti, H. N., Safa, Y., ... & Iqbal, M. (2024). Green synthesis of CuO nanoparticles using Jasmin sambac extract: Conditions optimization and photocatalytic degradation of Methylene Blue dye. *Journal of King Saud University-Science*, *36*(3), 103089.

[19] Deveoglu, M., Deveoglu, O., & Karadag, R. (2022). Historical, economic and agricultural dimensions of madder (Rubia tinctorum L.) plant. *Research Journal of Agriculture and Forestry Sciences ISSN*, *2320*, 6063.

[20] M. Taylor, (2017). The role of animal-based dyes in cultural heritage, in: Cultural HeritageConservation and Environmental Impact Assessment by Non-destructive Testing and Micro-analysis, Springer, pp. 207–225

[21] Pujazon Patron, E. C., & Domingo Elias, J. (2024). The conspicuous colour blue-'Lapis Lazuli'-in the history of art. *Idealogy Journal*, *9*(1), 113-130.

[22] Haridevamuthu, B., Murugan, R., Seenivasan, B., Meenatchi, R., Pachaiappan, R., Almutairi, B. O., ... & Arockiaraj, J. (2024). Synthetic azo-dye, Tartrazine induces

neurodevelopmental toxicity via mitochondria-mediated apoptosis in zebrafish embryos. *Journal of Hazardous Materials*, *461*, 132524.

[23] Millbern, Z., Trettin, A., Wu, R., Demmler, M., & Vinueza, N. R. (2024). Synthetic dyes: A mass spectrometry approach and applications. *Mass Spectrometry Reviews*, *43*(2), 327-344.

[24] Siddiqui, B., Husain, A., Nasibullah, M., & Ahmad, N. (2025). Challenges of Using Natural Dyes in the Global Market. In *Advances in Natural Dyes for Environmental Protection* (pp. 215-228). Apple Academic Press.

[25] Nagendrappa, G. (2010). Sir William Henry Perkin: the man and his 'mauve'. *Resonance*, *15*(9), 779-793.

[26] Tamburini, D., Sabatini, F., Berbers, S., van Bommel, M. R., & Degano, I. (2024). An introduction and recent advances in the analytical study of early synthetic dyes and organic pigments in cultural heritage. *Heritage*, *7*(4), 1969-2010.

[27] Do, K. L., Mushtaq, A., Zhao, F., & Su, M. (2024). Alizarin old and new: Extraction techniques for coloration, advances in detection methods for historical textiles and novel applications as a functional dye. *Coloration Technology*, *140*(1), 5-29.

[28] Hartmann, H. (2024). On the discovery of the first synthetic dyes prepared from phenolic tar ingredients. *Journal of Chemical Research*, *48*(4), 17475198241262008

[29] Alegbe, E. O., & Uthman, T. O. (2024). A review of history, properties, classification, applications and challenges of natural and synthetic dyes. *Heliyon*

[30] Ciccola, A., McClure, K. R., Serafini, I., Vincenti, F., Montesano, C., Gentili, A., ... & Postorino, P. (2024). The 20th century and its new colours: Investigating the molecular structures of historical synthetic dyes using Raman spectroscopy. *Journal of Raman Spectroscopy*, *55*(3), 324-335.

[31] Kusumlata, Ambade, B., Kumar, A., & Gautam, S. (2024). Sustainable Solutions: Reviewing the Future of Textile Dye Contaminant Removal with Emerging Biological Treatments. *Limnological Review*, *24*(2), 126-149.

[32] Palianskikh, A. I., Sychik, S. I., Leschev, S. M., Pliashak, Y. M., Fiodarava, T. A., & Belyshava, L. L. (2022). Development and validation of the HPLC-DAD method for the quantification of 16 synthetic dyes in various foods and the use of liquid anion exchange extraction for qualitative expression determination. *Food Chemistry*, *369*, 130947.

[33] Kumelachew, D. M., Wagaye, B. T., & Adamu, B. F. (2023). Digital textile printing innovations and the future. *Digital Textile Printing: Science, Technology and Markets*, 241.

[34] Kumar, A., Dixit, U., Singh, K., Gupta, S. P., & Beg, M. S. J. (2021). Structure and properties of dyes and pigments. *Dyes and pigments-novel applications and waste treatment*, *131*.

[35] Sharma, J., Sharma, S., & Soni, V. (2021). Classification and impact of synthetic textile dyes on Aquatic Flora: A review. *Regional Studies in Marine Science*, *45*, 101802.

[36] Benkhaya, S., M'rabet, S., Lgaz, H., El Bachiri, A., & El Harfi, A. (2022). Dyes: classification, pollution, and environmental effects. *Dye biodegradation, mechanisms and techniques: Recent advances*, 1-50.

[37] Benkhaya, S., M'rabet, S., & El Harfi, A. (2020). A review on classifications, recent synthesis and applications of textile dyes. *Inorganic Chemistry Communications*, *115*, 107891

[38] Ali, A. E., Chowdhury, Z. Z., Devnath, R., Ahmed, M. M., Rahman, M. M., Khalid, K., ... & Mitra, A. (2023). Removal of Azo Dyes from Aqueous Effluent Using Bio-Based Activated Carbons: Toxicity Aspects and Environmental Impact. *Separations*, *10*(9), 506.

[39] Poronik, Y. M., Sadowski, B., Szychta, K., Quina, F. H., Vullev, V. I., & Gryko, D. T. (2022). Revisiting the non-fluorescence of nitroaromatics: presumption versus reality. *Journal of Materials Chemistry C*, *10*(8), 2870-2904.

[40] Sen, S., Raut, S., & Raut, S. (2023). Mycoremediation of anthraquinone dyes from textile industries: a mini-review. *BioTechnologia*, *104*(1), 85-91.

[41] El Aggadi, S., & El Hourch, A. (2021). Removal of reactive blue 21 (RB21) phthalocyanine dye from aqueous solution by adsorption process: a review. *Polish J Environ Stud*, *30*(4), 3425-32.

[42] Karunarathne, K., Kee, T. R., Jeon, H., Cazzaro, S., Gamage, Y. I., Pan, J., ... & Muschol, M. (2024). Crystal Violet Selectively Detects Aβ Oligomers but Not Fibrils In Vitro and in Alzheimer's Disease Brain Tissue. *Biomolecules*, *14*(6), 615.

[43] Wu, J., Shi, Z., Zhu, L., Li, J., Han, X., Xu, M., ... & Huang, W. (2022). The design and bioimaging applications of NIR fluorescent organic dyes with high brightness. *Advanced Optical Materials*, *10*(8), 2102514.

[44] Manzoor, J., & Sharma, M. (2020). Impact of textile dyes on human health and environment. In *Impact of textile dyes on public health and the environment* (pp. 162-169). IGI Global.

[45] Durazzo, A., Carocho, M., Heleno, S., Barros, L., Souto, E. B., Santini, A., & Lucarini, M. (2022). Food dyes and health: Literature quantitative research analysis. *Measurement: Food*, *7*, 100050.

[46] Hassaan, M. A., El Nemr, A., & Hassaan, A. (2017). Health and environmental impacts of dyes: mini review. *American Journal of Environmental Science and Engineering*, *1*(3), 64-67

[47] Bopape, D. A., Ntsendwana, B., & Mabasa, F. D. (2024). Photocatalysis as a pre-discharge treatment to improve the effect of textile dyes on human health: A critical review. *Heliyon*

[48] Sahu, A., & Poler, J. C. (2024). Removal and degradation of dyes from textile industry wastewater: Benchmarking recent advancements, toxicity assessment and cost analysis of treatment processes. *Journal of Environmental Chemical Engineering*, 113754.

[49] Singha, K., Pandit, P., Maity, S., & Sharma, S. R. (2021). Harmful environmental effects for textile chemical dyeing practice. In *Green chemistry for sustainable textiles* (pp. 153-164). Woodhead Publishing.

[50] Zahuri, A. A., Abdul Patah, M. F., Kamarulzaman, Y., Hashim, N. H., Thirumoorthi, T., Wan Mohtar, W. H. M., Mohd Hanafiah, Z., Amir, Z., & Wan-Mohtar, W. A. A. Q. I. (2023). Decolourisation of Real Industrial and Synthetic Textile Dye Wastewater Using Activated Dolomite. *Water*, *15*(6), 1172. https://doi.org/10.3390/w15061172

[51] Bildirici, M., Türkkahraman, I., & Ersin, Ö. Ö. (2024). Unraveling the Environmental Impacts of the Fashion Industry: A Fourier-Based Analysis of Pollution Dynamics and Causality Across Five Countries. *Sustainability*, *17*(1), 69.

[52] Dutta, S., Adhikary, S., Bhattacharya, S., Roy, D., Chatterjee, S., Chakraborty, A., ... & Rajak, P. (2024). Contamination of textile dyes in aquatic environment: Adverse impacts on aquatic ecosystem and human health, and its management using bioremediation. *Journal of Environmental Management*, *353*, 120103.

[53] Tomei, M. C., Pascual, J. S., & Angelucci, D. M. (2016). Analysing performance of real textile wastewater bio-decolourization under different reaction environments. *Journal of Cleaner Production*, *129*, 468-477.

[54] Bu H, Wan J, Zhang Y, Meng W (2013) Spatial characteristics of surface water quality in the Haicheng river (Liao river basin) in Northeast China. Environ Earth Sci 70:2865–2872. https://doi. org/10.1007/s12665-013-2348-5

[55] Siddiqui, Z. H., Wattal, R. K., Batchu, H., & Abbas, Z. K. (2020). Assessment of cytotoxic and genotoxic effects of Yamuna river water pollutants in an urban metropolis, Delhi (India). *Water Supply*, *20*(7), 2682-2697.

[56] Elgarahy, A. M., Elwakeel, K. Z., Mohammad, S. H., & Elshoubaky, G. A. (2021). A critical review of biosorption of dyes, heavy metals and metalloids from wastewater as an efficient and green process. *Cleaner Engineering and Technology*, *4*, 100209.

[57] Parmar, A. I., & Shah, A. I. (2021). Acute toxicity, behavioural response and haematological alterations of Catla catla exposed to Reactive Red 120 textile dye. *Indian Journal of Experimental Biology (IJEB)*, *59*(04), 275-279.

[58] Ramamurthy, K., Madesh, S., Priya, P. S., Ayub, R., Aljawdah, H. M., Arokiyaraj, S., ... & Arockiaraj, J. (2024). Textile azo dye, Sudan Black B, inducing hepatotoxicity demonstrated in in vivo zebrafish larval model. *Fish Physiology and Biochemistry*, *50*(4), 1811-1829.

[59] To, K. T., St. Mary, L., Wooley, A. H., Wilbanks, M. S., Bednar, A. J., Perkins, E. J., ... & Garcia-Reyero, N. (2021). Morphological and behavioral effects in zebrafish embryos after exposure to smoke dyes. *Toxics*, *9*(1), 9.

[60] Hussain, B., Sajad, M., Usman, H., Al-Ghanim, K. A., Riaz, M. N., Berenjian, A., ... & Show, P. L. (2022). Assessment of hepatotoxicity and nephrotoxicity in Cirrhinus mrigala induced by trypan blue-An azo dye. *Environmental Research*, *215*, 114120.

[61] Moorthy, A. K., Rathi, B. G., Shukla, S. P., Kumar, K., & Bharti, V. S. (2021). Acute toxicity of textile dye Methylene blue on growth and metabolism of selected freshwater microalgae. *Environmental Toxicology and Pharmacology*, *82*, 103552.

[62] Wang, C., Gu, W., Zhang, S., Li, L., Kong, J., Zhi, H., ... & Tang, S. (2024). Multigenerational effects of disperse blue 79 at environmentally relevant concentrations on zebrafish (Danio rerio) fecundity: An integrated approach. *Journal of Hazardous Materials*, *478*, 135442.

[63] Miller, M. D., Steinmaus, C., Golub, M. S., Castorina, R., Thilakartne, R., Bradman, A., & Marty, M. A. (2022). Potential impacts of synthetic food dyes on activity and attention in children: a review of the human and animal evidence. *Environmental Health*, *21*(1), 45.

[64] Khan, S., & Malik, A. (2018). Toxicity evaluation of textile effluents and role of native soil bacterium in biodegradation of a textile dye. *Environmental Science and Pollution Research*, *25*, 4446-4458.

[65] Amchova, P., Siska, F., & Ruda-Kucerova, J. (2024). Food safety and health concerns of synthetic food colors: an update. *Toxics*, *12*(7), 466.

[66] Ambroziewicz, Z. M., Siemiątkowski, R., Łata, M., Dowgiert, S., Sikorska, M., Kamiński, J., ... & Mąsior, G. (2024). Long-Term Health Effects of Artificially Colored Foods in Adults and Children: A Review of Scientific Literature on Attention Deficits, Carcinogenicity, and Allergy Risks. *Journal of Education, Health and Sport*, *76*, 56522-56522.

[67] Akintunde, M., Golub, M., Marty, M., Miller, M., Oham, N., & Steinmaus, C. (2021). Health Effects Assessment: Potential Neurobehavioral Effects of Synthetic Food Dyes in Children.

[68] Rafi, I. K. (2024). Different Food Color Used in Food Samples: A Chemical Analysis Study in Kishoreganj District, Bangladesh. iraetc med. bull; 2 (2) 32-39. *This work is licensed under a Creative Commons Attribution-NonCommercial*, *4*.

[69] Alnuqaydan, A. M. (2024). The dark side of beauty: an in-depth analysis of the health hazards and toxicological impact of synthetic cosmetics and personal care products. *Frontiers in Public Health*, *12*, 1439027.

[70] Gore, A. C., La Merrill, M. A., Patisaul, H., & Sargis, R. M. (2024). Endocrine Disrupting Chemicals: Threats to Human Health. *The Endocrine Society and IPEN. February*.

[71] Siddiqui, S. I., Allehyani, E. S., Al-Harbi, S. A., Hasan, Z., Abomuti, M. A., Rajor, H. K., & Oh, S. (2023). Investigation of Congo red toxicity towards different living organisms: a review. Processes, 11(3), 807.

[72] Khan, I., Saeed, K., Zekker, I., Zhang, B., Hendi, A. H., Ahmad, A., ... & Khan, I. (2022). Review on methylene blue: Its properties, uses, toxicity and photodegradation. Water, 14(2), 242.

[73] BANC, R., FILIP, L., COZMA-PETRUȚ, A., CIOBÂRCĂ, D., & MIERE, D. (2024). Yellow and red synthetic food dyes and potential health hazards: A Mini review. Bull. Univ. Agric. Sci. Vet. Med. Cluj-Napoca. Food Sci. Technol, 81, 1-17.

[74] Fernandes, F. H., Bustos-Obregon, E., & Salvadori, D. M. F. (2015). Disperse Red 1 (textile dye) induces cytotoxic and genotoxic effects in mouse germ cells. *Reproductive Toxicology*, *53*, 75-81.

[75] Mani, S., & Bharagava, R. N. (2016). Exposure to crystal violet, its toxic, genotoxic and carcinogenic effects on environment and its degradation and detoxification for environmental safety. *Reviews of Environmental Contamination and Toxicology Volume 237*, 71-104.

[76] Duggireddy, R. P., & Pisharody, L. (2024). Traditional methods of water purification in rural areas. In *Water Resources Management for Rural Development* (pp. 55-64). Elsevier.

[77] Zhou, Y., Lu, J., Zhou, Y., & Liu, Y. (2019). Recent advances for dyes removal using novel adsorbents: a review. *Environmental pollution*, *252*, 352-365.

[78] Sonal, S., & Mishra, B. K. (2021). Role of coagulation/flocculation technology for the treatment of dye wastewater: trend and future aspects. *Water pollution and management practices*, 303-331.

[79] Cevallos-Mendoza, J., Amorim, C. G., Rodríguez-Díaz, J. M., & Montenegro, M. D. C. B. (2022). Removal of contaminants from water by membrane filtration: a review. *Membranes*, *12*(6), 570.

[80] Hendaoui, K., Trabelsi-Ayadi, M., & Ayari, F. (2021). Optimization and mechanisms analysis of indigo dye removal using continuous electrocoagulation. *Chinese Journal of Chemical Engineering*, *29*, 242-252.

[81] Bhatia, D., Sharma, N. R., Singh, J., & Kanwar, R. S. (2017). Biological methods for textile dye removal from wastewater: A review. *Critical Reviews in Environmental Science and Technology*, *47*(19), 1836-1876.

[82] Riaz, A., Ibrar, B. S., Bibi, K., Habib, Z., Ikram, S., Shahzad, H. M. A., ... & Zahra, Z. (2024). Degradation of Methyl Orange from Aqueous Solution Using Fe-Ni-Co-Based Trimetallic Nanocomposites: Optimization by Response Surface Methodology. *Sustainability*, *16*(16), 6958.

[83] Fito, J., Abewaa, M., Mengistu, A., Angassa, K., Ambaye, A. D., Moyo, W., & Nkambule, T. (2023). Adsorption of methylene blue from textile industrial wastewater using activated carbon developed from Rumex abyssinicus plant. *Scientific Reports*, *13*(1), 5427.

[84] Wei, Y., Ding, A., & Chen, Y. (2022). Removal of refractory dyes by a novel chlorine-free coagulant of polyferric-silicate-acetate (PFSA): Characterization and performance evaluation. *Journal of Environmental Chemical Engineering*, *10*(5), 108524.

[85] Mohammed Ali, A. T., & Salman, R. H. (2024). Enhancing the Removal of Methyl Orange Dye by Electrocoagulation System with Nickel Foam Electrode-Optimization with Surface Response Methodology. *Journal of Ecological Engineering*, *25*(12).

[86] El-Sayed, G. O., Hazaa, M. M., & El-Komy, A. M. (2018). Biotreatment of water polluted with methyl orange dye by using different forms of yeast. *Journal of Basic and Environmental Sciences*, *5*, 217-221.

[87] Homem NC, de Camargo Lima Beluci N, Amorim S, et al (2019) Surface modifcation of a polyethersulfone microfltration membrane with graphene oxide for reactive dyes removal. Appl Surf Sci 486:499–507. https://doi.org/10.1016/j.apsusc.2019.04.276

[88] Middea, A., Spinelli, L. S., Junior, F. G. S., Neumann, R., da FM Gomes, O., Fernandes, T. L., ... & de Carvalho, F. V. (2015). Synthesis and characterization of magnetic palygorskite nanoparticles and their application on methylene blue remotion from water. *Applied Surface Science*, *346*, 232-239.

[89] Gedda, G., Balakrishnan, K., Devi, R. U., Shah, K. J., Gandhi, V., Gandh, V., & Shah, K. (2021). Introduction to conventional wastewater treatment technologies: limitations and recent advances. *Mater. Res. Found*, *91*, 1-36

[90] Srivastava, A., Gupta, B., Majumder, A., Gupta, A. K., & Nimbhorkar, S. K. (2021). A comprehensive review on the synthesis, performance, modifications, and regeneration of

activated carbon for the adsorptive removal of various water pollutants. *Journal of Environmental Chemical Engineering*, *9*(5), 106177.

[91] Msemwa, G. G., Nasr, M., Abdelhaleem, A., Fujii, M., & Ibrahim, M. G. (2025). Coagulation-Flocculation/Pyrolysis Integrated System for Dye-Laden Wastewater Treatment: A Techno-Economic and Sustainable Approach. *Water, Air, & Soil Pollution*, *236*(1), 1-21.

[92] Payami Shabestar, M., Alavi Moghaddam, M. R., & Karamati-Niaragh, E. (2021). Evaluation of energy and electrode consumption of Acid Red 18 removal using electrocoagulation process through RSM: alternating and direct current. *Environmental Science and Pollution Research*, *28*, 67214-67223.

[93] Perera, R. S. M., & Kalpage, C. S. (2024, March). Textile Dye Removal from Wastewater by Biological Methods: A Review. In *International Conference on Sustainable Development* (pp. 357-369). Singapore: Springer Nature Singapore.

[94] Chauhan, P., Sharma, M., Nehra, S., Sharma, R., & Kumar, D. (2023). Dye Removal from Industrial Water Using Nanofiltration Membrane. In *Nanofiltration Membrane for Water Purification* (pp. 83-117). Singapore: Springer Nature Singapore.

[95] Abu-Rayyan, A., & Al-Bagawi, A. H. (2024). The Feasibility Application of the Fenton Oxidation Technique for Removal of Textile Dye from Wastewater: Batch, Kinetics, and Real Application. *Arabian Journal for Science and Engineering*, *49*(1), 665-672.

[96] Kumari, H., Sonia, Suman, Ranga, R., Chahal, S., Devi, S., ... & Parmar, R. (2023). A review on photocatalysis used for wastewater treatment: dye degradation. *Water, Air, & Soil Pollution*, *234*(6), 349.

[97] Abumelha, H. M., Sari, A. A., Ibarhiam, S. F., Alzahrani, S. O., Alhasani, M., Alaysuy, O., ... & El-Metwaly, N. M. (2024). SnO2QDs: Photophysical properties, photocatalytic activity, mineralization financial cost and recycling process during industrial effluent treatment. *Journal of Water Process Engineering*, *67*, 106213.

[98] Matos, J. (2016). Eco-friendly heterogeneous photocatalysis on biochar-based materials under solar irradiation. *Topics in catalysis*, *59*(2), 394-402.

[99] Chakravorty, A., & Roy, S. (2024). A Review of-Photocatalysis, basic principles, processes, and materials. *Sustainable Chemistry for the Environment*, 100155.

[100] Wu, H., Li, L., Wang, S., Zhu, N., Li, Z., Zhao, L., & Wang, Y. (2023). Recent advances of semiconductor photocatalysis for water pollutant treatment: mechanisms, materials and applications. *Physical Chemistry Chemical Physics*, *25*(38), 25899-25924.

[101] Thennarasu, G., Rajendran, S., Kalairaj, A., Rathore, H. S., Panda, R. C., & Senthilvelan, T. (2024). A comprehensive review on the application of semiconductor nanometal oxides

photocatalyst for the treatment of wastewater. *Clean Technologies and Environmental Policy*, 1-22.

[102] Simončič, B., & Glažar, D. (2023). TiO2 and ZnO as Advanced Photocatalysts for Effective Dye Degradation in Textile Wastewater. *Tekstilec*, 178-198.

[103] Khan, Y., Khan, M. N., Salam, A., Sadia, H., Ullah, M. F., Khan, M. I., ... & Ismail, E. A. (2024). Photocatalytic treatment of organic dyes using metal oxides and nanocomposites: A quantitative study. *Open Chemistry*, *22*(1), 20240026.

[104] Abbasi, S. (2025) Evaluating the efficiency of environmentally friendly magnetic photocatalyst for the treatment of industrial effluents containing dye pollutants. *Appl Water Sci* 15, 36. https://doi.org/10.1007/s13201-025-02369-6

[105] Hassaan, M. A., El-Nemr, M. A., Elkatory, M. R., Ragab, S., Niculescu, V. C., & El Nemr, A. (2023). Principles of photocatalysts and their different applications: a review. *Topics in Current Chemistry*, *381*(6), 31.

[106] Tolosana-Moranchel, A., Pecharromán, C., Faraldos, M., & Bahamonde, A. (2021). Strong effect of light scattering by distribution of TiO2 particle aggregates on photocatalytic efficiency in aqueous suspensions. *Chemical Engineering Journal*, *403*, 126186.

[107] Djurišić, A. B., He, Y., & Ng, A. (2020). Visible-light photocatalysts: Prospects and challenges. *Apl Materials*, *8*(3).

[108] Mamaghani, A. H., Haghighat, F., & Lee, C. S. (2020). Role of titanium dioxide (TiO2) structural design/morphology in photocatalytic air purification. *Applied Catalysis B: Environmental*, *269*, 118735.

[109] Dutta, L., Sethi, G. K., & Dey, S. (2024). A Comprehensive and Critical Assessment on the Efficiency of Natural and Synthetic Adsorbents for the Removal of Recalcitrant Malachite Green from Water: Present Level and Future Perspectives. *Korean Journal of Chemical Engineering*, *41*(3), 589-607

[110] Ghosh, S., Sen, K., Debnath, P., Mondal, A., & Mondal, N. K. (2023). Enhanced photocatalytic activity of methylene blue using heterojunction Ag@ TiO2 nanocomposite: Mechanistic and optimization study. *Chinese Journal of Chemical Engineering*, *64*, 49-63

[111] Zare, E. N., Iftekhar, S., Park, Y., Joseph, J., Srivastava, V., Khan, M. A., ... & Varma, R. S. (2021). An overview on non-spherical semiconductors for heterogeneous photocatalytic degradation of organic water contaminants. *Chemosphere*, *280*, 130907

[112] Rafiq, A., Ikram, M., Ali, S., Niaz, F., Khan, M., Khan, Q., & Maqbool, M. (2021). Photocatalytic degradation of dyes using semiconductor photocatalysts to clean industrial water pollution. *Journal of Industrial and Engineering Chemistry*, *97*, 111-128

[113] Suhan, M. B. K., Al-Mamun, M. R., Farzana, N., Aishee, S. M., Islam, M. S., Marwani, H. M., ... & Awual, M. R. (2023). Sustainable pollutant removal and wastewater remediation using TiO2-based nanocomposites: A critical review. *Nano-Structures & Nano-Objects*, *36*, 101050

[114] Al-Mamun, M. R., Karim, M. N., Nitun, N. A., Kader, S., Islam, M. S., & Khan, M. Z. H. (2021). Photocatalytic performance assessment of GO and Ag co-synthesized TiO2 nanocomposite for the removal of methyl orange dye under solar irradiation. *Environmental Technology & Innovation*, *22*, 101537

[115] Chen, Y. W., & Hsu, Y. H. (2021). Effects of reaction temperature on the photocatalytic activity of TiO2 with Pd and Cu cocatalysts. *Catalysts*, *11*(8), 966

[116] Velardi, L., Scrimieri, L., Serra, A., Manno, D., & Calcagnile, L. (2020). Effect of temperature on the physical, optical and photocatalytic properties of TiO 2 nanoparticles. *SN Applied Sciences*, *2*, 1-6

[117] Kumar, A., & Pandey, G. (2017). A review on the factors affecting the photocatalytic degradation of hazardous materials. *Mater. Sci. Eng. Int. J*, *1*(3), 1-10.

[118] Tanos, F., Razzouk, A., Lesage, G., Cretin, M., & Bechelany, M. (2024). A comprehensive review on modification of titanium dioxide-based catalysts in advanced oxidation processes for water treatment. *ChemSusChem*, *17*(6), e202301139.

[119] Li, C., & Tang, M. (2024). The toxicological effects of nano titanium dioxide on target organs and mechanisms of toxicity. *Journal of applied toxicology*, *44*(2), 152-164.

[120] Yang, X., Zhao, R., Zhan, H., Zhao, H., Duan, Y., & Shen, Z. (2024). Modified Titanium dioxide-based photocatalysts for water treatment: Mini review. *Environmental Functional Materials*.

[121] Arun, J., Nachiappan, S., Rangarajan, G., Alagappan, R. P., Gopinath, K. P., & Lichtfouse, E. (2023). Synthesis and application of titanium dioxide photocatalysis for energy, decontamination and viral disinfection: A review. *Environmental Chemistry Letters*, *21*(1), 339-362.

[122] Farooq, N., Kallem, P., ur Rehman, Z., Khan, M. I., Gupta, R. K., Tahseen, T., ... & Shanableh, A. (2024). Recent trends of titania (TiO2) based materials: A review on synthetic approaches and potential applications. *Journal of King Saud University-Science*, 103210.

[123] Eddy, D. R., Permana, M. D., Sakti, L. K., Sheha, G. A. N., Solihudin, Hidayat, S., ... & Rahayu, I. (2023). Heterophase polymorph of TiO2 (Anatase, Rutile, Brookite, TiO2 (B)) for efficient photocatalyst: fabrication and activity. *Nanomaterials*, *13*(4), 704.

[124] Das, U. D., Ahamed, J. U., Razzaq, M. E. A., Dewanjee, S., & Jisu, R. N. (2022). Synthesis and characterization of TiO2 and ZnO nanoparticles.

[125] Marcelis, E. J., ten Elshof, J. E., & Morales-Masis, M. (2024). Titanium Dioxide: A Versatile Earth-Abundant Optical Material for Photovoltaics. *Advanced Optical Materials*, *12*(36), 2401423.

[126] Zhang, W., Al Samarai, M., Zhao, H., Liu, D., Kiuchi, H., Ugalino, R., ... & Harada, Y. (2025). Facet-dependent photocatalytic performance and electronic structure of single-crystalline anatase TiO 2 particles revealed by X-ray photoelectron spectromicroscopy. *Journal of Materials Chemistry C*, *13*(1), 61-67.

[127] Wang, J., Peng, Z., Huang, J., Zhang, Y., Zhang, X., Wang, Y., ... & Chen, K. (2023). Enhanced charge generation and transfer properties on anatase nanodendrite array photo-electrodes for high-efficiency quantum dot sensitized solar cells. *Solar Energy Materials and Solar Cells*, *257*, 112348.

[128] Byrne, C., Moran, L., Hermosilla, D., Merayo, N., Blanco, Á., Rhatigan, S., ... & Pillai, S. C. (2019). Effect of Cu doping on the anatase-to-rutile phase transition in TiO2 photocatalysts: theory and experiments. *Applied Catalysis B: Environmental*, *246*, 266-276.

[129] Lemraski, A. H., Hossein Zadeh, A. S. A., Naghizadeh, R., & Majidian, H. (2024). Investigation of the Effect of Titanium Dioxide and Aluminum Titanate on Physical, Mechanical, and Microstructural Properties of Synthesized Cordierite. *Iranian Journal of Materials Science & Engineering*, *21*(4).

[130] O'Byrne, M., Kerzabi, B., Abbarchi, M., Lifschitz, A., Zamora, T., Malgras, V., ... & Putero, M. (2024). Investigation of the anatase-to-rutile transition for TiO2 sol-gel coatings with refractive index up to 2.7. *Thin Solid Films*, *790*, 140193.

[131] Broll, S., Pöttgen, R., & Strassert, C. A. (2022). 1.4 Inorganic pigments. *From Construction Materials to Technical Gases; Walter de Gruyter: Berlin, Germany*, 47.

[132] Thakur, N., Thakur, N., Kumar, A., Thakur, V. K., Kalia, S., Arya, V., ... & Kyzas, G. Z. (2024). A critical review on the recent trends of photocatalytic, antibacterial, antioxidant and nanohybrid applications of anatase and rutile TiO2 nanoparticles. *Science of The Total Environment*, 169815.

[133] Komaraiah, D., Madhukar, P., Vijayakumar, Y., Reddy, M. R., & Sayanna, R. (2016). Photocatalytic degradation study of methylene blue by brookite TiO2 thin film under visible light irradiation. *Materials Today: Proceedings*, *3*(10), 3770-3778.

[134] Mamakhel, A., Yu, J., Søndergaard-Pedersen, F., Hald, P., & Iversen, B. B. (2020). Facile synthesis of brookite TiO 2 nanoparticles. *Chemical Communications*, *56*(95), 15084-15087.

[135] Manzoli, M., Freyria, F. S., Blangetti, N., & Bonelli, B. (2022). Brookite, a sometimes under evaluated TiO 2 polymorph. *RSC Advances*, *12*(6), 3322-3334.

[136] Szołdra, P., Frąc, M., Lach, R., Zych, Ł., Radecka, M., Trenczek-Zając, A., & Pichór, W. (2023). Effect of brookite on the photocatalytic properties of mixed-phase TiO2 obtained at a higher temperature. *Materials Science and Engineering: B*, *287*, 116104.

[137] Momma, K., & Izumi, F. (2011). VESTA 3 for three-dimensional visualization of crystal, volumetric and morphology data. *Journal of applied crystallography*, *44*(6), 1272-1276.

[138] Armaković, S. J., Savanović, M. M., & Armaković, S. (2022). Titanium dioxide as the most used photocatalyst for water purification: An overview. *Catalysts*, *13*(1), 26.

[139] Somogyi Škoc, M., Macan, J., Jakovljević, S., & Rezić, I. (2024). Synthesis and characterization of ZnO and TiO2 hybrid coatings for textile UV anti-aging protection. *Polymers*, *16*(14), 2001.

[140] Weir, A., Westerhoff, P., Fabricius, L., Hristovski, K., & Von Goetz, N. (2012). Titanium dioxide nanoparticles in food and personal care products. *Environmental science & technology*, *46*(4), 2242-2250.

[141] Ziental, D., Czarczynska-Goslinska, B., Mlynarczyk, D. T., Glowacka-Sobotta, A., Stanisz, B., Goslinski, T., & Sobotta, L. (2020). Titanium dioxide nanoparticles: prospects and applications in medicine. *Nanomaterials*, *10*(2), 387.

[142] Amorello, D., Ferrara, M., & Orecchio, S. (2024). Titanium dioxide in face powders and eyeshadows: Developing an analytical methodology for accessing customer safety. *Journal of Cosmetic Dermatology*

[143] Lana, G. M., Bello, I. T., Adedokun, O. M., Adenigba, V. O., Jubu, P. R., Adedokun, O., ... & Awodugba, A. O. (2024). One-Dimensional TiO2 Nanocomposite-based Photoanode for Dye-Sensitized solar Cells: A review. *Solar Energy*, *279*, 112850

[144] Chen, M. C., Koh, P. W., Ponnusamy, V. K., & Lee, S. L. (2022). Titanium dioxide and other nanomaterials based antimicrobial additives in functional paints and coatings. *Progress in Organic Coatings*, *163*, 106660.

[145] Aronne, A., Fantauzzi, M., Imparato, C., Atzei, D., De Stefano, L., D'Errico, G., ... & Rossi, A. (2017). Electronic properties of TiO 2-based materials characterized by high Ti 3+ self-doping and low recombination rate of electron–hole pairs. *RSC advances*, *7*(4), 2373-2381.

[146] Li, G. Z., Zhang, S., Tian, D., Liu, G., Wang, W., Chen, G., ... & Han, R. (2024). Improving the Visible Light Absorption and Photocatalytic Degradation Activity of TiO2 Particles Towards MB by Organic Sensitizer Decoration. *Catalysis Letters*, 1-15.

[147] Balakrishnan, A., Appunni, S., Chinthala, M., & Vo, D. V. N. (2022). Biopolymer-supported TiO2 as a sustainable photocatalyst for wastewater treatment: a review. *Environmental Chemistry Letters*, *20*(5), 3071-3098.

[148] Huayna, G., Laura, A., Churata, R., Lazo, L., Guzmán, R., Ramos, P. G., & Rodriguez, J. M. (2024). Synthesis and Characterization of a Photocatalytic Material from TiO2 Nanoparticles Supported on Zeolite Obtained from Ignimbrite Residue Used in Decolorization of Methyl Orange. *Applied Sciences*, *14*(8), 3146

[149] Liu, N., Qi, R., Sun, X., Kawazoe, N., Chen, G., & Yang, Y. (2022). Synthesis and characterization of 3D-zeolite–modified TiO2-based photocatalyst with synergistic effect for elimination of organic pollutant in wastewater treatment. *Frontiers in Environmental Science*, *10*, 1009045.

[150] Prakoso, M. I., Maharani, K. Y., Ariq, M. R., Indah, A. N., Apriansyah, A., Iryani, A., ... & Syahputri, Y. (2024). Photodegradation Of Methyl Orange (MO) Using TiO2/Zeolite From Coal Fly Ash Waste Under Acidic Conditions and H2O2 Addition. *Helium: Journal of Science and Applied Chemistry*, *4*(1), 01-07.

[151] Sriramoju, J. B., Muniyappa, M., Marilingaiah, N. R., Sabbanahalli, C., Shetty, M., Mudike, R., ... & Rangappa, D. (2021). Carbon-based TiO2-x heterostructure nanocomposites for enhanced photocatalytic degradation of dye molecules. *Ceramics International*, *47*(7), 10314-10321.

[152] Badoni, A., Thakur, S., Vijayan, N., Swart, H. C., Bechelany, M., Chen, Z., ... & Prakash, J. (2025). Recent progress in understanding the role of graphene oxide, TiO2 and graphene oxide-TiO2 nanocomposites as multidisciplinary photocatalysts in energy and environmental applications. *Catalysis Science & Technology*.

[153] Gomes, J., Maniezo, B., Alves, P., Ferreira, P., & Martins, R. C. (2022). Immobilization of TiO2 onto a polymeric support for photocatalytic oxidation of a paraben's mixture. *Journal of Water Process Engineering*, *46*, 102458.

[154] Wang, Y., Feng, G., Lin, N., Lan, H., Li, Q., Yao, D., & Tang, J. (2023). A review of degradation and life prediction of polyethylene. *Applied Sciences*, *13*(5), 3045

[155] Islam, S., & Akyildiz, H. I. (2022). Atomic layer deposition of TiO2 thin films on glass fibers for enhanced photocatalytic activity. *Journal of Materials Science: Materials in Electronics*, *33*(22), 18002-18013.

[156] Yu, H., Lee, S. C., Yu, J., & Ao, C. H. (2006). Photocatalytic activity of dispersed TiO2 particles deposited on glass fibers. *Journal of Molecular Catalysis A: Chemical*, *246*(1-2), 206-211.

[157] Liu, Y., Yuan, X., & Wang, Y. (2019). Crystallization of Nano-TiO2 Films based on Glass Fiber Fabric Substrate and Its Impact on Catalytic Performance. *Open Physics*, *17*(1), 345-351.

[158] Wang, Y., Meng, F., Han, L., Liu, X., Guo, F., Lu, H., ... & Wang, W. (2023). Constructing a highly tough, durable, and renewable flexible filter by epitaxial growth of a glass fiber fabric for high flux and superefficient oil-water separation. *Journal of Hazardous Materials*, *448*, 130807.

[159] Tsioptsias, C., Fardis, D., Ntampou, X., Tsivintzelis, I., & Panayiotou, C. (2023). Thermal behavior of poly (vinyl alcohol) in the form of physically crosslinked film. *Polymers*, *15*(8), 1843.

[160] Babaghayou, M. I., Mourad, A. H. I., Ochoa, A., Beltrán, F., & Cherupurakal, N. (2021). Study on the thermal stability of stabilized and unstabilized low-density polyethylene films. *Polymer Bulletin*, *78*(9), 5225-5241.

[161] Ching, Y. C., Gunathilake, T. U., Ching, K. Y., Chuah, C. H., Sandu, V., Singh, R., & Liou, N. S. (2019). Effects of high temperature and ultraviolet radiation on polymer composites. In *Durability and life prediction in biocomposites, fibre-reinforced composites and hybrid composites* (pp. 407-426). Woodhead Publishing

[162] Rahman, R. O. A., El-Kamash, A. M., & Hung, Y. T. (2022). Applications of nano-zeolite in wastewater treatment: an overview. Water, 14(2), 137.

[163] Mahdavi Far, R., Van der Bruggen, B., Verliefde, A., & Cornelissen, E. (2022). A review of zeolite materials used in membranes for water purification: History, applications, challenges and future trends. Journal of Chemical Technology & Biotechnology, 97(3), 575-596.

[164] Dubey, R., Dutta, D., Sarkar, A., & Chattopadhyay, P. (2021). Functionalized carbon nanotubes: Synthesis, properties and applications in water purification, drug delivery, and material and biomedical sciences. *Nanoscale Advances*, *3*(20), 5722-5744.

[165] Meng, S. H., Liu, J. F., Kong, X. T., & Du, S. G. (2020). Preparation of TiO2/CNTs nanocomposite and its catalytic performance on the thermal decomposition of ammonium perchlorate. *Transition Metal Chemistry*, *45*(8), 545-551.

[166] Lu, B. J., Lin, K. T., Kuo, Y. M., & Tsai, C. H. (2021). Preparation of high-transparency, superhydrophilic visible photo-induced photocatalytic film via a rapid plasma-modification process. *Coatings*, *11*(7), 784.

[167] Najafidoust, A., Allahyari, S., Rahemi, N., & Tasbihi, M. (2020). Uniform coating of TiO2 nanoparticles using biotemplates for photocatalytic wastewater treatment. *Ceramics International*, *46*(4), 4707-4719.

[168] Manna, S., Adak, D., Manna, S., Maity, S., Jana, S., Bhattacharya, R., & Medda, S. K. (2023). Antireflection cum photocatalytic with superhydrophilic based durable single layer mesoporous TiO2-ZrO2 coating surface for efficient solar photovoltaic application. *Sustainable Energy Technologies and Assessments*, *57*, 103236.

[169] Ohya, Y., Mishina, J., Matsuda, T., Ban, T., & Takahashi, Y. (1999). Crystallization and Microstructure Development of Sol–Gel-Derived Titanium Dioxide Thin Films with Single and Multiple Layers. *Journal of the American Ceramic Society*, *82*(10), 2601-2606.

[170] Ao, C. H., Lee, S. C., & Jimmy, C. Y. (2003). Photocatalyst TiO2 supported on glass fiber for indoor air purification: effect of NO on the photodegradation of CO and NO2. *Journal of Photochemistry and photobiology A: Chemistry*, *156*(1-3), 171-177

[171] Tian, S., Feng, Y., Zheng, Z., & He, Z. (2023). TiO2-Based photocatalytic coatings on glass substrates for environmental applications. *Coatings*, *13*(8), 1472.

[172] Adamek, E., Baran, W., Ziemiańska-Błaszczyk, J., & Sobczak, A. (2019). Immobilisation of TiO2-P25 on a glass fibre mat: Preparation, photocatalytic activity and stability. *Solar Energy*, *188*, 1232-1242.

[173] Estrada-Vázquez, R., Vaca-Mier, M., Bustos-Terrones, V., Rangel-Peraza, J. G., Loaiza, J. G., & Bustos-Terrones, Y. A. (2024). Assessment of TiO2 and Ag/TiO2 photocatalysts for domestic wastewater treatment: synthesis, characterization, and degradation kinetics analysis. *Reaction Kinetics, Mechanisms and Catalysis*, *137*(2), 1085-1104.

[174] Sharma, R. K., Yadav, S., Dutta, S., Kale, H. B., Warkad, I. R., Zbořil, R., ... & Gawande, M. B. (2021). Silver nanomaterials: synthesis and (electro/photo) catalytic applications. *Chemical Society Reviews*, *50*(20), 11293-11380.

[175] Nguyen, C. H., Van Tran, T. T., Tran, M. L., & Juang, R. S. (2023). Facile synthesis of reusable Ag/TiO2 composites for efficient removal of antibiotic oxytetracycline under UV and solar light irradiation. *Journal of the Taiwan Institute of Chemical Engineers*, *145*, 104825.

[176] Chakhtouna, H., Benzeid, H., Zari, N., Qaiss, A. E. K., & Bouhfid, R. (2021). Recent progress on Ag/TiO 2 photocatalysts: Photocatalytic and bactericidal behaviors. *Environmental Science and Pollution Research*, *28*, 44638-44666.

[177] Kanakaraju, D., anak Kutiang, F. D., Lim, Y. C., & Goh, P. S. (2022). Recent progress of Ag/TiO2 photocatalyst for wastewater treatment: Doping, co-doping, and green materials functionalization. *Applied Materials Today*, *27*, 101500.

[178] Adenuga, D. O., Tichapondwa, S. M., & Chirwa, E. M. (2020). Facile synthesis of a Ag/AgCl/BiOCl composite photocatalyst for visible–light–driven pollutant removal. *Journal of Photochemistry and Photobiology A: Chemistry*, *401*, 112747.

[179] Chawhan, S. S., Barai, D. P., & Bhanvase, B. A. (2021). Investigation on thermophysical properties, convective heat transfer and performance evaluation of ultrasonically synthesized Ag-doped TiO2 hybrid nanoparticles based highly stable nanofluid in a minichannel. *Thermal Science and Engineering Progress*, *25*, 100928.

[180] Amrani, R., Lekoui, F., Garoudja, E., Zenati, Y., Hamri, A., Filali, W., ... & Hassani, S. (2024). Structural and optical properties of highly Ag-doped TiO2 thin films prepared by flash thermal evaporation. *Physica Scripta*, *99*(6), 065914.

[181] Chakhtouna, H., Benzeid, H., Zari, N., Qaiss, A. E. K., & Bouhfid, R. (2021). Recent progress on Ag/TiO 2 photocatalysts: Photocatalytic and bactericidal behaviors. *Environmental Science and Pollution Research*, *28*, 44638-44666.

[182] Nyankson, E., Yeboah, N., Jnr, S. O., Onaja, S., Mensah, T., & Efavi, J. K. (2022). The effect of synthesis route on the photocatalytic performance of Ag-TiO2 using rhodamine b dyes, pesticides, and pharmaceutical waste as model pollutants. *Materials Research Express*, *9*(9), 094001.

[183] Ratshiedana, R., Fakayode, O. J., Mishra, A. K., & Kuvarega, A. T. (2021). Visible-light photocatalytic degradation of tartrazine using hydrothermal synthesized Ag-doped TiO2 nanoparticles. *Journal of Water Process Engineering*, *44*, 102372.

[184] Nasr, M., Soussan, L., Viter, R., Eid, C., Habchi, R., Miele, P., & Bechelany, M. (2018). High photodegradation and antibacterial activity of BN–Ag/TiO 2 composite nanofibers under visible light. *New Journal of Chemistry*, *42*(2), 1250-1259.

[185] Halim, W., Eddahbi, A., Mouna, S. I., Kassiba, A., & Ouaskit, S. (2024). Synthesis of perfect TiO2 nanospheres decorated by silver shell nanoparticles for photocatalytic applications. *Journal of Cluster Science*, 1-10.

[186] Wu, Z., Guo, K., Cao, S., Yao, W., & Piao, L. (2020). Synergetic catalysis enhancement between H 2 O 2 and TiO 2 with single-electron-trapped oxygen vacancy. *Nano Research*, *13*, 551-556.

[187] Zhang, J., Wang, Y., Peng, B., Wen, S., & Zhang, Q. (2024). Light-induced degradation of organic pollutants under high salinity conditions using titanium dioxide/ferrocene polymer nanocomposites as photocatalyst and H 2 O 2 activator simultaneously. *Environmental Science: Nano*, *11*(1), 431-440.

[188] Ambrosio, E., Lucca, D. L., Garcia, M. H., de Souza, M. T., Freitas, T. K. D. S., de Souza, R. P., ... & Garcia, J. C. (2017). Optimization of photocatalytic degradation of biodiesel using TiO2/H2O2 by experimental design. *Science of the Total Environment*, *581*, 1-9.

[189] Zhang, B., Li, X., Ma, Y., Jiang, T., Zhu, Y., & Ren, H. (2022). Visible-light photoelectrocatalysis/H 2 O 2 synergistic degradation of organic pollutants by a magnetic Fe 3 O 4@ SiO 2@ mesoporous TiO 2 catalyst-loaded photoelectrode. *RSC advances*, *12*(47), 30577-30587.

[190] Ranade, V. V., Bhandari, V. M., Nagarajan, S., Sarvothaman, V. P., & Simpson, A. T. (2022). *Hydrodynamic Cavitation: Devices, Design and Applications*. John Wiley & Sons.

[191] Thaker, A. H., & Ranade, V. V. (2022). Emulsions using a vortex-based cavitation device: influence of number of passes, pressure drop, and device scale on droplet size distributions. *Industrial & Engineering Chemistry Research*, *62*(45), 18837-18851.

[192] Sarvothaman, V. P., Nagarajan, S., & Ranade, V. V. (2018). Treatment of solvent-contaminated water using vortex-based cavitation: influence of operating pressure drop, temperature, aeration, and reactor scale. *Industrial & Engineering Chemistry Research*, *57*(28), 9292-9304

[193] Sun, X., Liu, J., Ji, L., Wang, G., Zhao, S., Yoon, J. Y., & Chen, S. (2020). A review on hydrodynamic cavitation disinfection: The current state of knowledge. *Science of the Total Environment*, *737*, 139606.

[194] Sarvothaman, V. P. (2020). *Hydrodynamic Cavitation for Effluent Treatment: Using Vortex-based Cavitation Devices* (Doctoral dissertation, Queen's University Belfast)

[195] Zhao, Z., Wang, L., Fan, J., Song, Y., Chu, G., & Shao, L. (2020). Degradation of indigo carmine by coupling Fe (II)-activated sodium persulfate and ozone in a rotor-stator reactor. *Chemical Engineering and Processing-Process Intensification*, *148*, 107791.

[196] Petkovšek, M., Mlakar, M., Levstek, M., Stražar, M., Širok, B., & Dular, M. (2015). A novel rotation generator of hydrodynamic cavitation for waste-activated sludge disintegration. *Ultrasonics sonochemistry*, *26*, 408-414.

[197] Garlicka, A., Zubrowska-Sudol, M., Umiejewska, K., Roubinek, O., Palige, J., & Chmielewski, A. (2020). Effects of thickened excess sludge pre-treatment using hydrodynamic cavitation for anaerobic digestion. *Energies*, *13*(10), 2483.

[198] Bimestre, T. A., Júnior, J. A. M., Canettieri, E. V., & Tuna, C. E. (2022). Hydrodynamic cavitation for lignocellulosic biomass pretreatment: a review of recent developments and future perspectives. *Bioresources and Bioprocessing*, *9*(1), 7.

[199] Kulkarni, A. A., Ranade, V. V., Rajeev, R., & Koganti, S. B. (2009). Pressure drop across vortex diodes: Experiments and design guidelines. *Chemical Engineering Science*, *64*(6), 1285-1292.

[200] Das, S., Bhat, A. P., & Gogate, P. R. (2021). Degradation of dyes using hydrodynamic cavitation: Process overview and cost estimation. *Journal of Water Process Engineering*, *42*, 102126.

[201] Yadav, M., Sharma, J., Yadav, R. K., & Gole, V. L. (2021). Microbial disinfection of water using hydrodynamic cavitational reactors. *Journal of Water Process Engineering*, *41*, 102097.

[202] Sun, X., Liu, S., Zhang, X., Tao, Y., Boczkaj, G., Yoon, J. Y., & Xuan, X. (2022). Recent advances in hydrodynamic cavitation-based pretreatments of lignocellulosic biomass for valorization. *Bioresource technology*, *345*, 126251.

[203] Chandanshive, V., Kadam, S., Rane, N., Jeon, B.H., Jadhav, J., Govindwar, S., 2020. In situ textile wastewater treatment in high rate transpiration system furrows planted with aquatic macrophytes and floating phytobeds. Chemosphere 252, 126513.

[204] Batra, V., Kaur, I., Pathania, D., & Chaudhary, V. (2022). Efficient dye degradation strategies using green synthesized ZnO-based nanoplatforms: A review. Applied Surface Science Advances, 11, 100314.

[205] Soni, V., Keswani, K., Bhatt, U., Kumar, D., Singh, H., (2021). In vitro propagation and analysis of mixotrophic potential to improve survival rate of Dolichandra unguiscati under ex vitro conditions. Heliyon 7 (2), e06101.

[206] Tounsadi, H., Metarfi, Y., Taleb, M., El Rhazi, K., Rais, Z., (2020). Impact of chemical substances used in textile industry on the employee's health: epidemiological study. Ecotoxicol. Environ. Saf. 197, 110594.

[207] Patil, R., Zahid, M., Govindwar, S., Khandare, R., Vyavahare, G., Gurav, R., Desai, N., Pandit, S., Jadhav, J., (2022). Constructed wetland: a promising technology for the treatment of hazardous textile dyes and effluent. Development in Wastewater Treatment Research and Processes. Elsevier, pp. 173–198.

[208] Bhat, S., Uthappa, U., Sadhasivam, T., Altalhi, T., Soo Han, S., & Kurkuri, M. D. (2023). Abundant cilantro derived high surface area activated carbon (AC) for superior adsorption performances of cationic/anio nic dyes and supercapacitor application. *Chemical Engineering Journal*, *459*, 141577. https://doi.org/10.1016/j.cej.2023.141577.

[209] Punzi, M., Anbalagan, A., Aragão Börner, R., Svensson, B., Jonstrup, M., & Mattiasson, B. (2015). Degradation of a textile azo dye using biological treatment followed by photo-Fenton oxidation: Evaluation of toxicity and microbial community structure. *Chemical Engineering Journal*, *270*, 290-299. https://doi.org/10.1016/j.cej.2015.02.042

[210] Mcyotto, F., Wei, Q., Macharia, D. K., Huang, M., Shen, C., & Chow, C. W. (2021). Effect of dye structure on color removal efficiency by coagulation. *Chemical Engineering Journal*, *405*, 126674. https://doi.org/10.1016/j.cej.2020.126674.

[211] Karmakar, S., Roy, D., & De, S. (2021). Multicomponent transport model-based scaling up of long-term adsorptive filtration of MOF incorporated mixed matrix hollow fiber membrane: Treatment of textile effluent. *Chemical Engineering Journal*, *403*, 125103. https://doi.org/10.1016/j.cej.2020.125103

[212] Adachi, A., Ouadrhiri, F. E., Kara, M., El Manssouri, I., Assouguem, A., Almutairi, M. H., ... & Lahkimi, A. (2022). Decolorization and degradation of methyl orange azo dye in aqueous solution by the electro fenton process: Application of optimization. *Catalysts*, *12*(6), 665.

[213] Ge, D., Zeng, Z., Arowo, M., Zou, H., Chen, J., & Shao, L. (2016). Degradation of methyl orange by ozone in the presence of ferrous and persulfate ions in a rotating packed bed. *Chemosphere*, *146*, 413-418. https://doi.org/10.1016/j.chemosphere.2015.12.058.

[214] Hamlaoui, M., Sahraoui, A., Boulebd, H., & Zertal, A. (2023). Kinetics of three commercial textile dyes decomposition by UV/H2O2 and UV/acetone processes: An experimental comparative study and DFT calculations. *Journal of Molecular Liquids*, *383*, 122212. https://doi.org/10.1016/j.molliq.2023.122212

[215] Cheng, L., Zhang, Y., Fan, W., & Ji, Y. (2022). Synergistic adsorption-photocatalysis for dyes removal by a novel biochar–based Z-scheme heterojunction BC/2ZIS/WO3: Mechanistic investigation and degradation pathways. *Chemical Engineering Journal*, *445*, 136677. https://doi.org/10.1016/j.cej.2022.136677.

[216] Asghar, A., Raman, A. A. A., & Daud, W. M. A. W. (2015). Advanced oxidation processes for in-situ production of hydrogen peroxide/hydroxyl radical for textile wastewater treatment: a review. *Journal of cleaner production*, *87*, 826-838.

[217] Ranade, V. V., Prasad Sarvothaman, V., Simpson, A., & Nagarajan, S. (2021). Scale-up of vortex based hydrodynamic cavitation devices: A case of degradation of di-chloro aniline in water. *Ultrasonics Sonochemistry*, *70*, 105295. https://doi.org/10.1016/j.ultsonch.2020.105295.

[218] Wang, B., Su, H., & Zhang, B. (2021). Hydrodynamic cavitation as a promising route for wastewater treatment – A review. *Chemical Engineering Journal*, *412*, 128685. https://doi.org/10.1016/j.cej.2021.128685

[219] Ranade, V. V. (2022). Modeling of hydrodynamic cavitation reactors: Reflections on present status and path forward. *ACS Engineering Au*, *2*(6), 461-476.

[220] Warade, A., Shinde, G., Gaikwad, R., Hakke, V. S., Sonawane, S. H., & Lingayat, A. (2023). Intensification of pharmaceutical wastewater treatment using hydrodynamic cavitation process. *Materials Today: Proceedings*, *77*, 692-697. https://doi.org/10.1016/j.matpr.2022.11.355

[221] Raut-Jadhav, S., Badve, M. P., Pinjari, D. V., Saini, D. R., Sonawane, S. H., & Pandit, A. B. (2016). Treatment of the pesticide industry effluent using hydrodynamic cavitation and its combination with process intensifying additives (H2O2 and ozone). *Chemical Engineering Journal*, *295*, 326-335. https://doi.org/10.1016/j.cej.2016.03.019.

[222] Deggelmann, M., Nöpel, J., Rüdiger, F., Paustian, D., & Braeutigam, P. (2022). Hydrodynamic cavitation for micropollutant degradation in water – Correlation of bisphenol A degradation with fluid mechanical properties. Ultrasonics Sonochemistry, 83, 105950. https://doi.org/10.1016/j.ultsonch.2022.10595

[223] Wang, S., Zhao, L., Ruan, Y., Qin, J., Yi, L., Zhang, Z., Wang, J., & Fang, D. (2023). Investigation on series-wound orifice plate hydrodynamic cavitation (HC) degradation of Rhodamine B (RhB) assisted by several by-pass line orifice plates. *Journal of Water Process Engineering*, *51*, 103404. https://doi.org/10.1016/j.jwpe.2022.103404

[224] Patil, P. B., Thanekar, P., & Bhandari, V. M. (2022). A strategy for complete degradation of metformin using vortex-based hydrodynamic cavitation. *Industrial & Engineering Chemistry Research*, *62*(45), 19262-19273.

[225] Dhanke, P. B., & Wagh, S. M. (2020). Intensification of the degradation of Acid RED-18 using hydrodynamic cavitation. *Emerging Contaminants*, *6*, 20-32.

[226] Innocenzi, V., Prisciandaro, M., Centofanti, M., & Vegliò, F. (2019). Comparison of performances of hydrodynamic cavitation in combined treatments based on hybrid induced advanced Fenton process for degradation of azo-dyes. *Journal of environmental chemical engineering*, *7*(3), 103171.

[227] Saxena, S., Saharan, V. K., & George, S. (2018). Enhanced synergistic degradation efficiency using hybrid hydrodynamic cavitation for treatment of tannery waste effluent. *Journal of Cleaner Production*, *198*, 1406-1421.

[228] Li, G., Yi, L., Wang, J., & Song, Y. (2020). Hydrodynamic cavitation degradation of Rhodamine B assisted by Fe3+-doped TiO2: Mechanisms, geometric and operation parameters. *Ultrasonics sonochemistry*, *60*, 104806.

[229] Khajeh, M., Amin, M. M., Taheri, E., Fatehizadeh, A., & McKay, G. (2020). Influence of co-existing cations and anions on removal of direct red 89 dye from synthetic wastewater by

hydrodynamic cavitation process: An empirical modeling. *Ultrasonics Sonochemistry*, *67*, 105133.

[230] Qin, T., Nie, S., Ji, H., & Xie, Z. (2023). Synergistic degradation and degradation pathways of methylene blue by plasma process combined with cavitation impinging stream reactor based on hydrodynamic cavitation. *Journal of Environmental Chemical Engineering*, *11*(5), 110356. https://doi.org/10.1016/j.jece.2023.110356

[231] Chen, M., Zhuang, K., Sui, J., Sun, C., Song, Y., & Jin, N. (2023). Hydrodynamic cavitation-enhanced photocatalytic activity of P-doped TiO2 for degradation of ciprofloxacin: Synergetic effect and mechanism. *Ultrasonics sonochemistry*, *92*, 106265.

[232] Azizollahi, N., Taheri, E., Mehdi Amin, M., Rahimi, A., Fatehizadeh, A., Sun, X., & Manickam, S. (2023). Hydrodynamic cavitation coupled with zero-valent iron produces radical sulfate radicals by sulfite activation to degrade direct red 83. *Ultrasonics Sonochemistry*, *95*, 106350. https://doi.org/10.1016/j.ultsonch.2023.106350

[233] Askarniya, Z., Baradaran, S., Sonawane, S. H., & Boczkaj, G. (2022). A comparative study on the decolorization of Tartrazine, Ponceau 4R, and Coomassie Brilliant Blue using persulfate and hydrogen peroxide based Advanced Oxidation Processes combined with Hydrodynamic Cavitation. *Chemical Engineering and Processing - Process Intensification*, *181*, 109160. https://doi.org/10.1016/j.cep.2022.109160

[234] Wang, B., Wang, T., & Su, H. (2022). A dye-methylene blue (MB)-degraded by hydrodynamic cavitation (HC) and combined with other oxidants. *Journal of Environmental Chemical Engineering*, *10*(3), 107877. https://doi.org/10.1016/j.jece.2022.107877

[235] Kumar, M. S., Sonawane, S., Bhanvase, B., & Bethi, B. (2018). Treatment of ternary dye wastewater by hydrodynamic cavitation combined with other advanced oxidation processes (AOP's). *Journal of Water Process Engineering*, *23*, 250-256. https://doi.org/10.1016/j.jwpe.2018.04.004

[236] Innocenzi, V., Colangeli, A., & Prisciandaro, M. (2022). Methyl orange decolourization through hydrodynamic cavitation in high salinity solutions. *Chemical Engineering and Processing - Process Intensification*, *179*, 109050. https://doi.org/10.1016/j.cep.2022.109050

[237] Mitra, S., Mukherjee, T., & Kaparaju, P. (2021). Prediction of methyl orange removal by iron decorated activated carbon using an artificial neural network. *Environmental Technology*, *42*(21), 3288-3303.

[238] Thaker, A. H., & Ranade, V. V. (2023). Drop breakage in a single-pass through vortex-based cavitation device: Experiments and modeling. *AIChE Journal*, *69*(1), e17512.

[239] Ranade, V. V., Kulkarni, A. A., & Bhandari, V. M. (2016). *U.S. Patent No. 9,422,952*. Washington, DC: U.S. Patent and Trademark Office.

[240] Suryawanshi, P. G., Bhandari, V. M., Sorokhaibam, L. G., Ruparelia, J. P., & Ranade, V. V. (2018). Solvent degradation studies using hydrodynamic cavitation. *Environmental Progress & Sustainable Energy*, *37*(1), 295-304.

[241] Liu, S., Lim, M., & Amal, R. (2014). TiO2-coated natural zeolite: rapid humic acid adsorption and effective photocatalytic regeneration. *Chemical engineering science*, *105*, 46-52.

[242] Maxime, G., Aymen Amine, A., Abdelkrim, B., & Dominique, W. (2014). Removal of gas-phase ammonia and hydrogen sulfide using photocatalysis, nonthermal plasma, and combined plasma and photocatalysis at pilot scale. *Environmental Science and Pollution Research*, *21*, 13127-13137.

[243] Innocenzi, V., Prisciandaro, M., Tortora, F., & Vegliò, F. (2018). Optimization of hydrodynamic cavitation process of azo dye reduction in the presence of metal ions. *Journal of Environmental Chemical Engineering*, *6*(6), 6787-6796. https://doi.org/10.1016/j.jece.2018.10.046.

[244] Gode, A., Madane, K., & Ranade, V. V. (2023). Design of vortex-based cavitation devices/reactors: Influence of aspect ratio, number of inlets and shape. *Ultrasonics Sonochemistry*, *101*, 106695.

[245] Liyanaarachchi, H., Thambiliyagodage, C., Liyanaarachchi, C., & Samarakoon, U. (2023). Efficient photocatalysis of Cu doped TiO2/g-C3N4 for the photodegradation of methylene blue. *Arabian Journal of Chemistry*, *16*(6), 104749. https://doi.org/10.1016/j.arabjc.2023.104749

[246] Patil, P. B., Bhandari, V. M., & Ranade, V. V. (2021). Wastewater treatment and process intensification for degradation of solvents using hydrodynamic cavitation. *Chemical Engineering and Processing - Process Intensification*, *166*, 108485. https://doi.org/10.1016/j.cep.2021.108485.

[247] Fukugaichi, S. (2019). Fixation of titanium dioxide nanoparticles on glass fiber cloths for photocatalytic degradation of organic dyes. *ACS omega*, *4*(12), 15175-15180.

[248] Wang, J., & Wang, S. (2020). Reactive species in advanced oxidation processes: Formation, identification and reaction mechanism. *Chemical Engineering Journal*, *401*, 126158.

[249] Wang, K., Jin, R.-Y., Qiao, Y.-N., He, Z.-D., Wang, Y., & Wang, X.-J. (2019). The removal of Rhodamine B by H2O2 or ClO2 combined with hydrodynamic cavitation. Water Science and Technology, 80(8), 1571–1580.

[250] Rajoriya, S., Bargole, S., & Saharan, V. K. (2017). Degradation of a cationic dye (Rhodamine 6G) using hydrodynamic cavitation coupled with other oxidative agents: Reaction mechanism and pathway. *Ultrasonics sonochemistry*, *34*, 183-194.

[251] Khan, S., Han, C., Khan, H. M., Boccelli, D. L., Nadagouda, M. N., & Dionysiou, D. D. (2017). Efficient degradation of lindane by visible and simulated solar light-assisted S-TiO2/peroxymonosulfate process: Kinetics and mechanistic investigations. Molecular Catalysis, 428, 9–16.

[252] Fedorov, K., Dinesh, K., Sun, X., Darvishi Cheshmeh Soltani, R., Wang, Z., Sonawane, S., & Boczkaj, G. (2022). Synergistic effects of hybrid advanced oxidation processes (AOPs) based on hydrodynamic cavitation phenomenon – A review. *Chemical Engineering Journal*, *432*, 134191. https://doi.org/10.1016/j.cej.2021.134191

[253] Pandiselvi, K., & Thambidurai, S. (2016). Synthesis of adsorption cum photocatalytic nature of polyaniline-ZnO/chitosan composite for removal of textile dyes. *Desalination and water treatment*, *57*(18), 8343-8357.

[254] Bahrudin, N. N., & Nawi, M. A. (2018). Immobilized titanium dioxide/powdered activated carbon system for the photocatalytic adsorptive removal of phenol. *Korean Journal of Chemical Engineering*, *35*, 1532-1541.

[255] Márquez, A. A., Sirés, I., Brillas, E., & Nava, J. L. (2020). Mineralization of Methyl Orange azo dye by processes based on H2O2 electrogeneration at a 3D-like air-diffusion cathode. *Chemosphere*, *259*, 127466.

[256] Ramamurthy, K., Priya, P. S., Murugan, R., & Arockiaraj, J. (2024). Hues of risk: investigating genotoxicity and environmental impacts of azo textile dyes. *Environmental Science and Pollution research,* 1-22.

[257] Ben Slama, H., et al. (2021). Diversity of Synthetic Dyes from Textile Industries, Discharge Impacts and Treatment Methods. *Applied Sciences, 11*(14), 6255. https://doi.org/10.3390/app11146255

[258] Upadhyay, D., Jindal, T., Tripathi, A., Joshi, K. D., & Shukla, K. (2023). Impact of Synthetic Food Colouring Agents on Aquatic Ecosystems and Human Health. *UTTAR PRADESH JOURNAL OF ZOOLOGY*, *44*(13), 17-37

[259] Kolya, H., & Kang, C. W. (2024). Toxicity of Metal Oxides, Dyes, and Dissolved Organic Matter in Water: Implications for the Environment and Human Health. *Toxics*, *12*(2), 111.

[260] Kallawar, G. A., & Bhanvase, B. A. (2024). A review on existing and emerging approaches for textile wastewater treatments: challenges and future perspectives. *Environmental Science and Pollution Research*, *31*(2), 1748-1789.

[261] Kumari, S., Singh, R., Jahangeer, J., & Garg, M. C. (2024). Innovative Strategies for Dye Removal from Textile Wastewater: A Comprehensive Review of Treatment Approaches and Challenges. *Water, Air, & Soil Pollution*, *235*(11), 720

[262] Moussout, H., Daou, I., Franco, D. S., Dehmani, Y., Georgin, J., Ahlafi, H., ... & Abouarnadasse, S. (2024). Towards a profound understanding of methyl orange removal from industrial wastewater using a raw walnut shell: Kinetics, equilibrium, thermodynamics, and statistical physics calculations. *Journal of Molecular Liquids*, *410*, 125606.

[263] Bahadi, S. A., Iddrisu, M., Al-Sakkaf, M. K., Elgzoly, M. A., Drmosh, Q. A., Al-Amrani, W. A., ... & Onaizi, S. A. (2024). Optimization of methyl orange adsorption on MgFeAl-LTH through the manipulation of solution chemistry and synthesis conditions. *Emergent Materials*, *7*(3), 959-971

[264] Semiz, L. (2020). Membrane Filtration of Methyl Orange. *Journal of the Institute of Science and Technology*, *10*(1), 328-337.

[265] Abbas, S. H., Younis, Y. M., Rashid, K. H., & Khadom, A. A. (2022). Removal of methyl orange dye from simulated wastewater by electrocoagulation technique using Taguchi method: kinetics and optimization approaches. *Reaction Kinetics, Mechanisms and Catalysis*, *135*(5), 2663-2679.

[266] Najafidoust, A., Haghighi, M., Asl, E. A., & Bananifard, H. (2024). Sono-precipitation dispersion of CuO-doped ZnO nanostructures over SiO2-aerogel for photo-removal of methylene blue, congo red and methyl orange from wastewater. *Journal of Industrial and Engineering Chemistry*, *131*, 346-359.

[267] Ibrahim, A., El-Fakharany, E. M., Abu-Serie, M. M., ElKady, M. F., & Eltarahony, M. (2022). Methyl orange biodegradation by immobilized consortium microspheres: experimental design approach, toxicity study and bioaugmentation potential. *Biology*, *11*(1), 76.

[268] Khan, Q., Sayed, M., Khan, J. A., Rehman, F., Noreen, S., Sohni, S., & Gul, I. (2024). Advanced oxidation/reduction processes (AO/RPs) for wastewater treatment, current challenges, and future perspectives: a review. *Environmental Science and Pollution Research*, *31*(2), 1863-1889

[269] Wang, W., Pan, X., Zhang, X., Wang, M., Wang, Z., Feng, L., ... & Zhao, K. (2024). Adsorption and photocatalytic degradation performances of methyl orange-imprinted polysiloxane particles using TiO2 as matrix. *Frontiers of Materials Science*, *18*(3), 1-12.

[270] Zhao, D., Tang, X., Liu, P., Huang, Q., Li, T., & Ju, L. (2024). Recent Progress of Ion-Modified TiO2 for Enhanced Photocatalytic Hydrogen Production. *Molecules*, *29*(10), 2347.

[271] Sukrey, N. A., Bushroa, A. R., & Rizwan, M. (2024). Dopant incorporation into TiO2 semiconductor materials for optical, electronic, and physical property enhancement: doping strategy and trend analysis. *Journal of the Australian Ceramic Society*, *60*(2), 563-589.

[272] Long, X. A., Yu, D., Han, J., Huang, Z., Xiao, J., Feng, G., ... & Yang, K. (2024). High-performance Ag-TiO2 nanoparticle composite catalyst synthesized by pulsed laser ablation in liquid: properties, mechanism and preparation studies. *Optics Express*, *32*(12), 21304-21326

[273] Lim, H., Yusuf, M., Song, S., Park, S., & Park, K. H. (2021). Efficient photocatalytic degradation of dyes using photo-deposited Ag nanoparticles on ZnO structures: simple morphological control of ZnO. *RSC advances*, *11*(15), 8709-8717.

[274] Ersöz, E., & Altintas Yildirim, O. (2022). Green synthesis and characterization of Ag-doped ZnO nanofibers for photodegradation of MB, RhB and MO dye molecules. Journal of the Korean Ceramic Society, 59(5), 655-670

[275] Sun, L., Que, Z., Ruan, T., Yuan, Z., Gong, W., Mei, S., ... & Liu, Y. (2024). The Synthesis of Ag/TiO2 via the DC Magnetron Sputtering Method and Its Application in the Photocatalytic Degradation of Methyl Orange in Na2SO4 Solution. Applied Sciences, 14(10), 4014

[276] Cheng, Z., Zhao, S., Han, Z., Zhang, Y., Zhao, X., & Kang, L. (2016). A novel preparation of Ag@ TiO 2 tubes and their potent photocatalytic degradation efficiency. CrystEngComm, 18(45), 8756-8761

[277] Shahzad, R., Muneer, M., Khalid, R., & Amin, H. M. (2023). ZnO-Bi2O3 heterostructured composite for the photocatalytic degradation of orange 16 reactive dye: Synergistic effect of UV irradiation and hydrogen peroxide. *Catalysts*, *13*(10), 1328

[278] Wang, Y., Yang, W., & Ding, K. (2024). Synergistic Ag/g–C3N4 H2O2 System for Photocatalytic Degradation of Azo Dyes. *Molecules*, *29*(16), 3871.

[279] De-Nasri, S. J., Sarvothaman, V. P., Kelly, C., Nagarajan, S., Manesiotis, P., Robertson, P. K., & Ranade, V. V. (2023). Hydrodynamic cavitation and photocatalysis for effluent treatment: Key operating parameters and synergistic effects. *Chemical Engineering Journal*, *473*, 145241

[280] Merdoud, R., Aoudjit, F., Mouni, L., & Ranade, V. V. (2024). Degradation of methyl orange using hydrodynamic Cavitation, H2O2, and photo-catalysis with TiO2-Coated glass Fibers: Key operating parameters and synergistic effects. *Ultrasonics Sonochemistry*, *103*, 106772.

[281] Gajbhiye, P., Shah, V. U., Mehta, J. P., Panchal, H., & Metre, A. V. (2024). Utilizing Hydrodynamic Cavitation with Variable Orifice Patterns for Textile Wastewater Treatment. *Tikrit Journal of Engineering Sciences*, *31*(1), 33-42.

[282] Sekar, M., Raja, G. G., Salmen, S. H., Chinnathambi, A., Gavurova, B., & Praveenkumar, T. R. (2024). Hydrodynamic cavitation phenomena and flow instabilities in wastewater treatment: A multiphase VOF study with a venturi cavitator. *Journal of the Taiwan Institute of Chemical Engineers*, 105355.

[283] Kader, S., Al-Mamun, M. R., Suhan, M. B. K., Shuchi, S. B., & Islam, M. S. (2022). Enhanced photodegradation of methyl orange dye under UV irradiation using MoO3 and Ag doped TiO2 photocatalysts. *Environmental Technology & Innovation*, *27*, 102476.

[284] Shan, R., Lu, L., Gu, J., Zhang, Y., Yuan, H., Chen, Y., & Luo, B. (2020). Photocatalytic degradation of methyl orange by Ag/TiO2/biochar composite catalysts in aqueous solutions. *Materials Science in Semiconductor Processing*, *114*, 105088.

[285] Islam, M. S., McPhedran, K. N., Messele, S. A., Liu, Y., & El-Din, M. G. (2018). Isotherm and kinetic studies on adsorption of oil sands process-affected water organic compounds using granular activated carbon. *Chemosphere*, *202*, 716-725.

[286] Azizollahi, N., Taheri, E., Amin, M. M., Rahimi, A., Fatehizadeh, A., Sun, X., & Manickam, S. (2023). Hydrodynamic cavitation coupled with zero-valent iron produces radical sulfate radicals by sulfite activation to degrade direct red 83. *Ultrasonics Sonochemistry*, *95*, 106350.

[287] Wang, B., Wang, T., & Su, H. (2022). A dye-methylene blue (MB)-degraded by hydrodynamic cavitation (HC) and combined with other oxidants. *Journal of Environmental Chemical Engineering*, *10*(3), 107877.

[288] Estephane, G. C., & El Jamal, M. M. (2019). EFFECT OF DOPING OF TiO 2 NANOPARTICLES WITH SILVER ON THEIR PHOTOCATALYTIC ACTIVITIES TOWARD DEGRADATION OF E 131 VF. *Journal of Chemical Technology & Metallurgy*, *54*(5).

[289] Dey, B., & Srivastava, S. K. (2022). Crystal structure, microstructure, optical, dielectric, and magnetic properties of TiO2 nanoparticles. *Journal of Materials Science: Materials in Electronics*, *33*(30), 23506-23514

[290] Sharma, H., Singhal, R., Siva Kumar, V. V., & Asokan, K. (2016). Structural, optical and electronic properties of Ag–TiO 2 nanocomposite thin film. *Applied Physics A*, *122*, 1-9.

[291] Muniraj, K. (2022). Synthesis of silver doped Tio2 nanoparticles (Ag-Tio2) photocatalytic degradation of methyl red under sunlight.

[292] AL-Jawad, S. M., RASHEED, M., & Abbas, Z. Y. (2024). Effect of doping on the structural, optical and electrical properties of TiO2 thin films for gas sensor. *Journal of Optics*, 1-22.

[293] Bhattacharyya, K., Modak, B., Nayak, C., Nair, R. G., Bhattacharyya, D., Jha, S. N., & Tripathi, A. K. (2020). The formation and effect of O-vacancies in doped TiO 2. *New Journal of Chemistry*, *44*(20), 8559-8571.

[294] Duan, X. P., Chen, T., Chen, T., Huang, L., Ye, L., Lo, B. T., ... & Tsang, S. C. E. (2021). Intercalating lithium into the lattice of silver nanoparticles boosts catalytic hydrogenation of carbon–oxygen bonds. *Chemical science*, *12*(25), 8791-8802.

[295] Ahmed, T. Y., Abdullah, O. G., Mamand, S. M., & Aziz, S. B. (2024). Band structure study of pure and doped anatase titanium dioxide (TiO2) using first-principle-calculations: Role of atomic mass of transition metal elements (TME) on band gap reduction. *Optical and Quantum Electronics*, *56*(7), 1249.

[296] Jing, Z., Liu, X., Du, Y., He, Y., Yan, T., Wang, W., & Li, W. (2020). Synthesis, characterization, antibacterial and photocatalytic performance of Ag/AgI/TiO 2 hollow sphere composites. *Frontiers of Materials Science*, *14*, 1-13.

[297] Sobana, N., Muruganadham, M., & Swaminathan, M. J. J. O. M. (2006). Nano-Ag particles doped TiO2 for efficient photodegradation of direct azo dyes. Journal of Molecular Catalysis A: Chemical, 258(1-2), 124-132.

[298] Chuang, H. Y., & Chen, D. H. (2009). Fabrication and photocatalytic activities in visible and UV light regions of Ag@ TiO2 and NiAg@ TiO2 nanoparticles. *Nanotechnology*, *20*(10), 105704.

[299] Ahmadian, A., Ahmadi, S., & Goharrizi, B. A. (2023). Roles of reactive species in photocatalysis: effect of scavengers and inorganic ions on dye removal from wastewater. *International Journal of Environmental Science and Technology*, *20*(6), 6433-6448.

[300] Zhou, P., Shen, Y., Zhao, S., Bai, J., Han, C., Liu, W., & Wei, D. (2021). Facile synthesis of clinoptilolite-supported Ag/TiO2 nanocomposites for visible-light degradation of xanthates. *Journal of the Taiwan Institute of Chemical Engineers*, *122*, 231-240.

Annex

Supplementary information

Degradation of methyl orange using hydrodynamic cavitation, H_2O_2 and photocatalysis: key operating parameters and synergistic effects

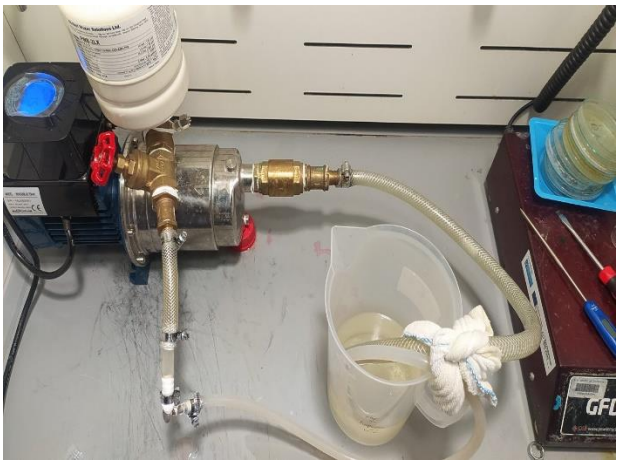

Fig.S1. Experimental setup of HC

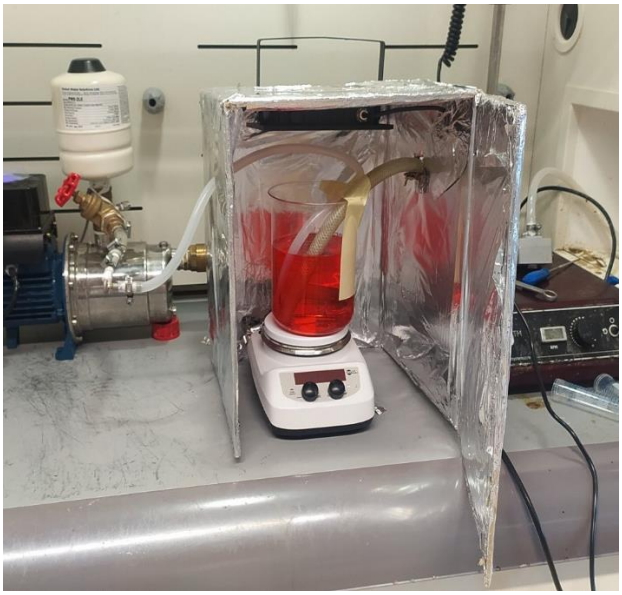

Fig.S2. Experimental setup of HC/PC

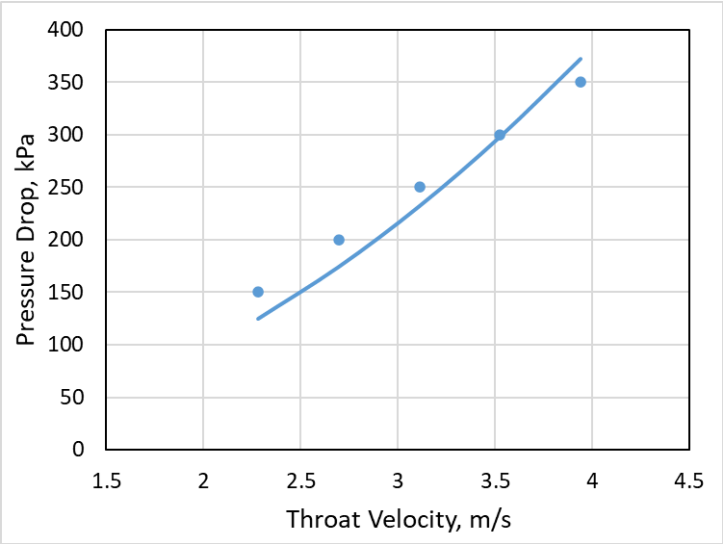

Fig.S3. Pressure drop and flow relationships for vortex based cavitation devices (Continuous line, Eu=48)

Fig. S4. TiO2 coated GFT (25 cm^2)

Fig. S5. UV spectrophotometer (Shimadzu UV1800)

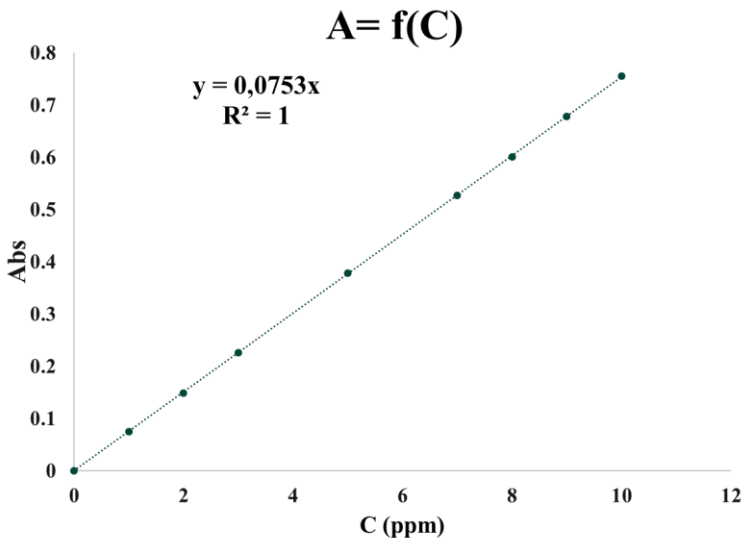

Fig. S6. MO calibration curve at pH= 4.5, λ= 430 nm

Fig. S7. DR 1900 spectrophotometer (Hach)

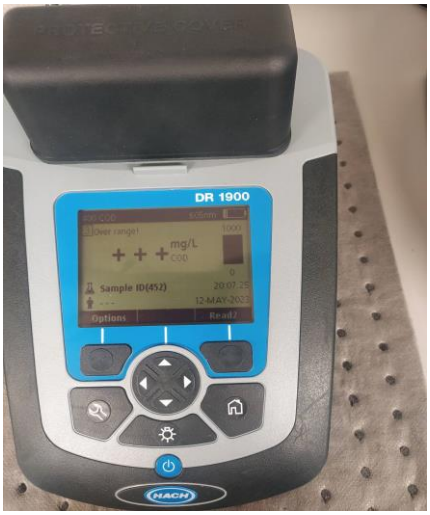

Fig. S8 LT 200 digester (Hach Lange, Germany)

S1. Characteristic of the photocatalyst

S1.1 XRD analysis

Fig.S9 illustrates the XRD diffraction pattern of GFT coated with a TiO_2 photocatalyst. The diffractogram obtained from TiO_2 on the GFT revealed the presence of intense peaks at 2θ = 25.42°, others less intense at 37.07°, 48.19°, and 54.85°, which are typical of the anatase form's crystalline structure of TiO_2, no rutile phase was found. **[1].** On the other hand, the diffractogram shows a broad peak due to the amorphous structure of the GFT. The average crystallite size of the TiO_2, is a vital parameter that influences photo-reactivity because it affects

several physical properties of the nanoparticles such as surface area, surface energy, light absorptivity, and lattice distortion **[2].** Based on this characterization, the average crystallite size was estimated to be 6 nm using the Scherrer equation (**Eq. S1**) **[3],** which was found to be similar as reported by Yu et al. **[4]**. Interestingly, there are a lot of reports indicating that the optimum crystallite size for various photocatalytic reactions is in the range of 7–15 nm **[5].** However, it has been demonstrated that a reduced crystallite size leads to a higher surface area, which enhances the adsorption of reactants and, consequently, photo-reactivity **[6]**. Furthermore, it has been noted that the photogenerated radicals' energy increases as crystallite size is reduced due to the quantum confinement effect, which enhances photocatalyst performance **[7].**

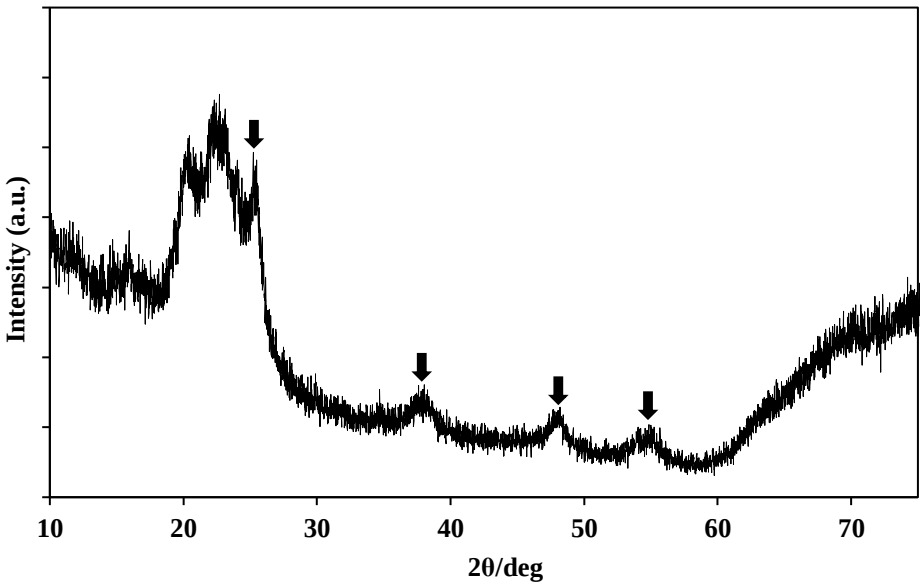

Fig.S9. XRD diffractogram of GFT coated with TiO2.

S1.2 Scanning electron microscopy

SEM is the best method for evaluating the homogeneity, degree of dispersion, degree of aggregation, and purity of nanoparticles. **[8,9]**. **Fig.S10** shows SEM images of the surface morphology of the photocatalyst. It clearly depicts the support's fibrous structure (glass fibers) as well as the heterogeneous dispersion of the TiO2 nanoparticles, with different sizes, as thin films, on its surface (**Fig. 2a and 2b**) as reported by Satoru et al. **[10]**. By zooming in on the fiber surface, the TiO2 clusters are visible (**Fig. 2c**), which were used in the photocatalysis process to degrade MO present in synthetic solution.

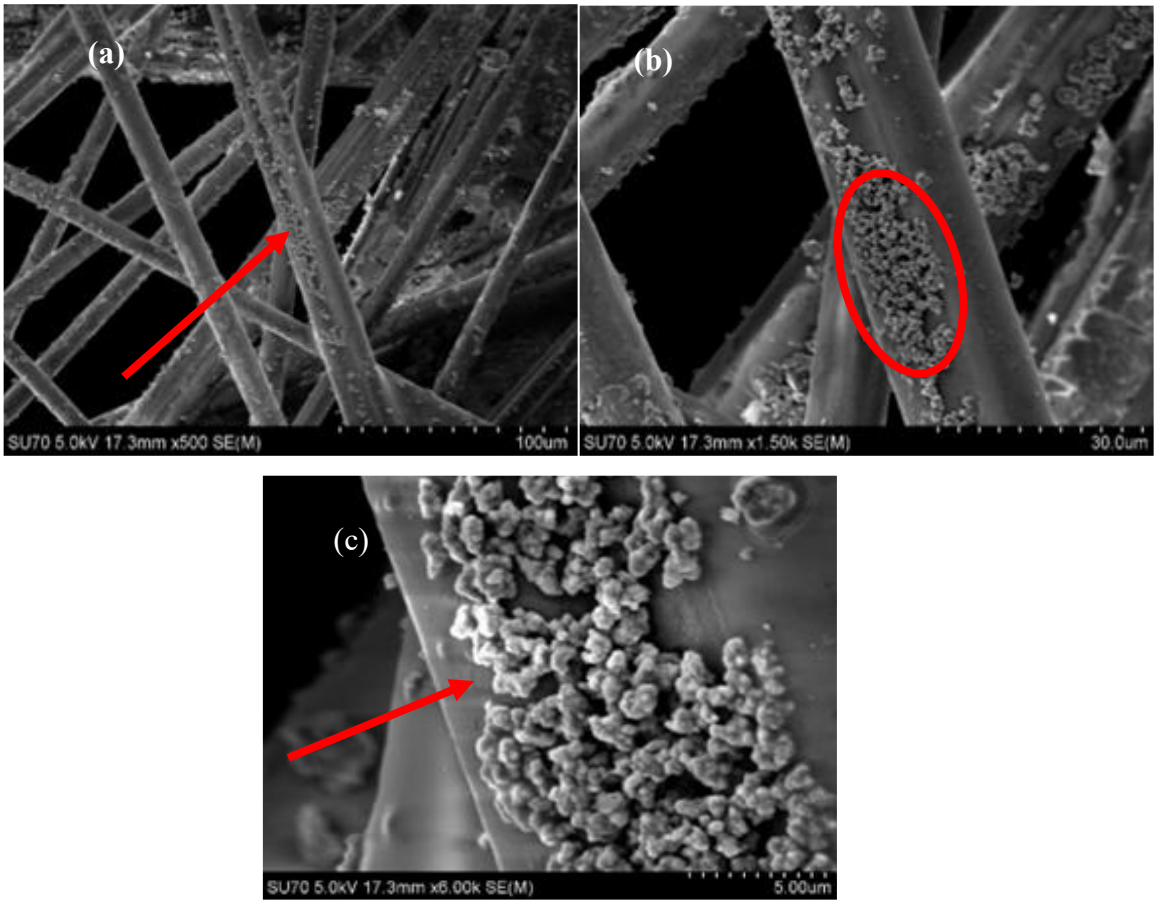

Fig.S10. SEM images of TiO2 coated on GFT×500 (a) ×1.5K (b) ×6.00K (c)

- **The crystallite size calculated using the Scherrer equation:**

$$D = \frac{0.9\lambda}{(\beta\cos\theta)} \quad \textbf{(S1)}$$

Where D (nm) is crystallite size, K is Scherrer constant, λ (0.15406 nm) is the the wavelength of the X-ray sources, β (radians) is the Full width at half maximum (FWHM), and θ (radians) is the peak position.

θ (radians)	β (FWHM)	D (nm)	D average (nm)
25.29264	1.58753	5.13	5.97
37.91085	2.96098	2.84	-
48.07368	1.88648	4.61	-
54.16614	0.78976	11.3	-

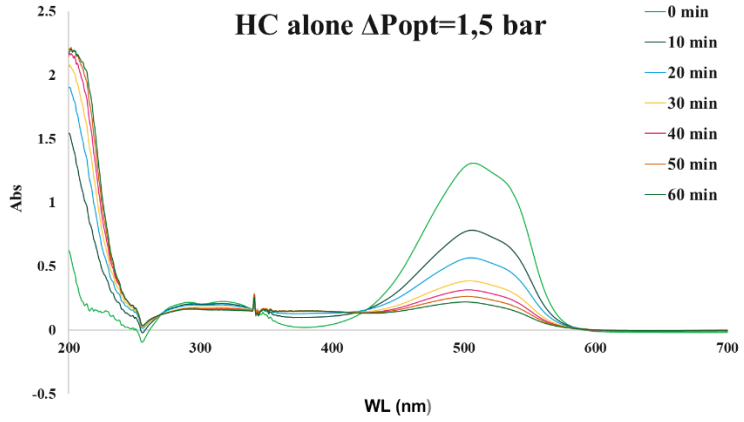

Fig. S11. MO UV spectrum at optimum pressure drop of 1.5 bar; pH=2, and initial concentration = 10 ppm

References

[1] N . Belkessa, Y . Serhane , A . Bouzaza , L . Khezami , A . A . Assadi, Gaseous ethylbenzene removal by photocatalytic TiO2 nanoparticles immobilized on glass fiber tissue under real conditions: evaluation of reactive oxygen species contribution to the photocatalytic process, Environ Sci Pollut Res Int. 30 (13) (2023 Mar) 3574 5 –3575 6 https://doi.org/10.1007/s11356 -02 2 -2463 6 - 8 , Epub 2022 Dec 20 PMID : 36538222 .

[2] M . A . Henderson , A surface science perspective on TiO2 photocatalysis, Surf. Sci. Rep. 66 (6 – 7) (2011) 18 5 –29 7.

[3] M . Music , M . Gotic , M . Ivanda, S . Popovi c , A . Turkovic , R . Trojko , A . Sekuli c , K . Furi c , Mat. Sci. Eng. b: Soli d 47 (1997) 33 .

[4] H . Yu , S . Le e , J . Yu , C . Ao , Photocatalytic activity of disperse d TiO2 particle s deposite d on glas s fibers , J. Mol. Catal. A Chem . 24 6 (1 – 2) (2006) 20 6 –21 1 , https://doi.org/10.1016/j.molcata.2005.11.00 7 .

[5] S . Li u , N . Jaffrezi c , C . Guillard , Size effect s in liquid -phas e phot o -oxidatio n of phenol usin g nanomete r -size d TiO2 catalyst s , Appl . Surf. Sci. 25 5 (5) (2008) 2704 – 2709 , https://doi.org/10.1016/j.apsusc.2008.07.191 .

[6] M . Xi e , L . Jing , J . Zhou , J . Li n , H . Fu , Synthesi s of nanocrystallin e anatas e TiO2 by on e -po t tw o -phas e separate d hydrolysis -solvothermal processe s an d it s high activity fo r photocatalytic degradatio n of rhodamin e B , J. Hazard . Mater. 17 6 (1 – 3) (2010) 13 9 –14 5 , https://doi.org/10.1016/j.jhazmat.2009.11.00 8 .

[7] J . Ji u , F . Wang , M . Adachi , Preparatio n of highly photocatalytic active nano - scal e TiO2 by mixe d template method , Mater. Lett . 58 (30) (2004) 3915 –3919 , https://doi.org/10.1016/j.matlet.2004.08.017 .

[8] V . Patraval e , P . Dandekar , R . Jain , Characterization techniques fo r nanoparticulat e carriers , Nanoparticulat e Drug Delivery 87 –12 1 (2011) , https:// doi.org/10.1533/9781908818195.87 .

[9] A . E . Vladár , V . Hodoroab a , Characterization of nanoparticle s by scanning electron microscopy , Characterization of Nanoparticle s 7 –27 (2019) , https:// doi.org/10.1016/B978 - 0 -12 -814182 -3.0000 2 - X .

[10] S . Fukugaichi , Fixation of titanium dioxid e nanoparticle s on glas s fibe r cloths fo r photocatalytic degradatio n of organi c dyes , AC S Omeg a 4 (2019) 1517 5 –1518 0 .

Supplementary information

Methyl orange degradation using Ag-doped TiO_2, H_2O_2, and hydrodynamic cavitation

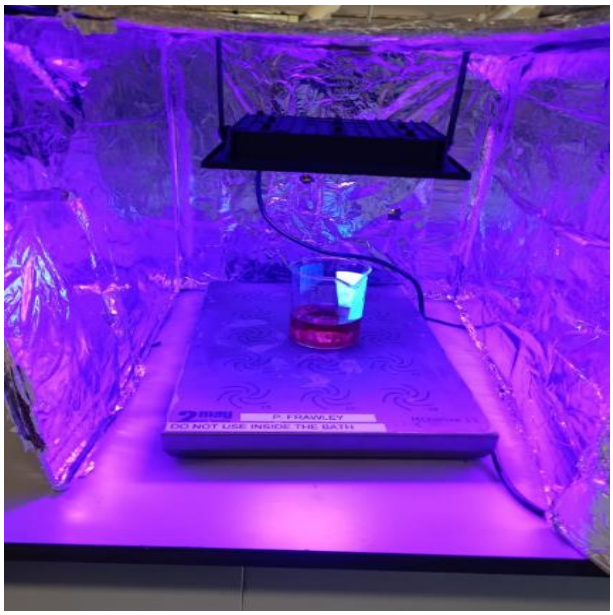

Fig.S1. Experimental setup of PC

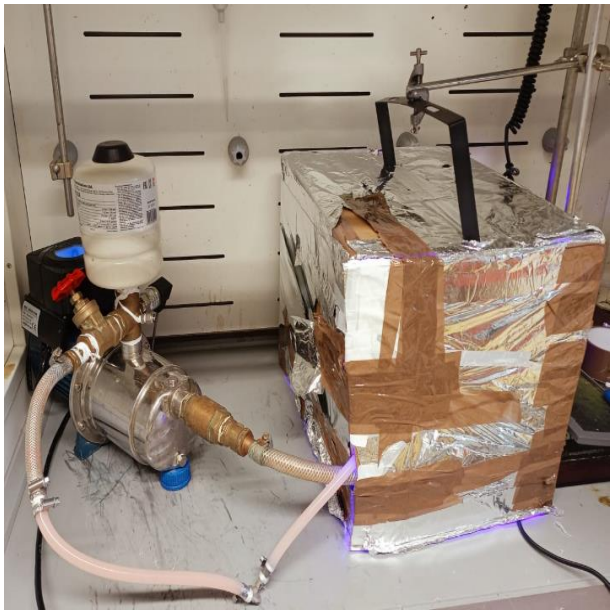

Fig.S2. Experimental setup of PC/HC

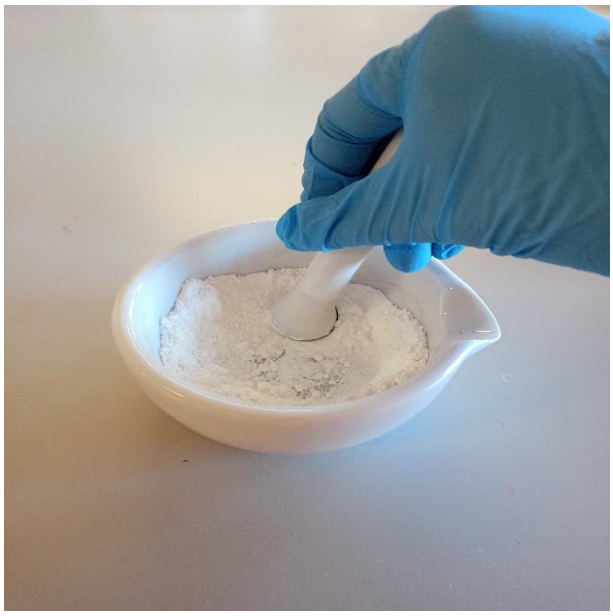

Fig.S3. Photocatalysts preparation process

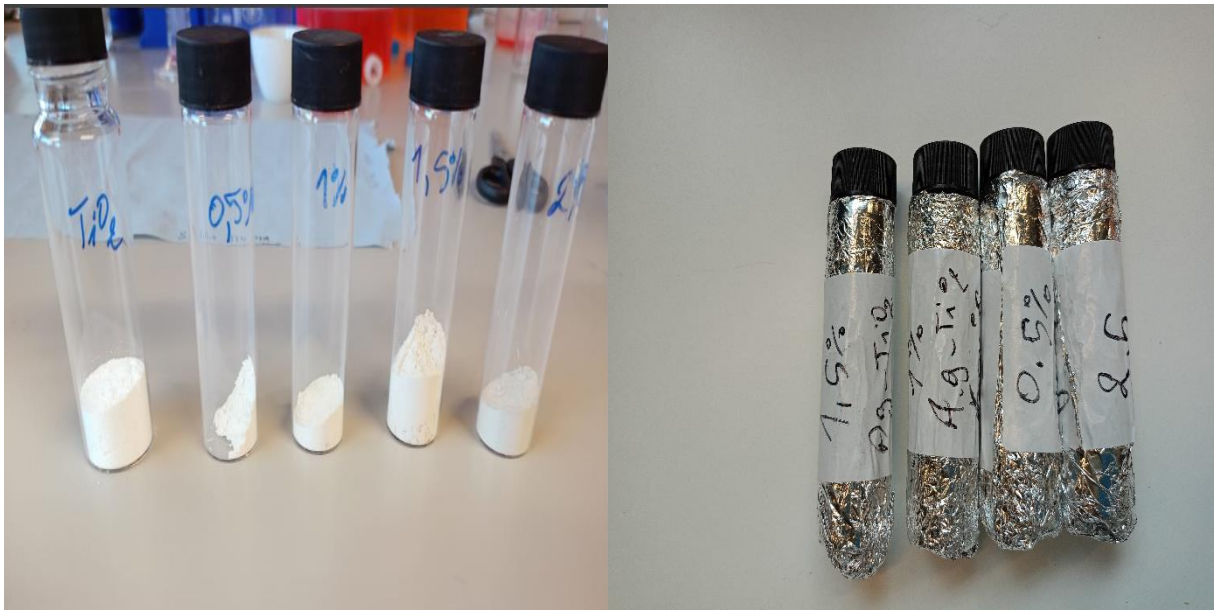

Fig.S4. Prepared Photocatalysts

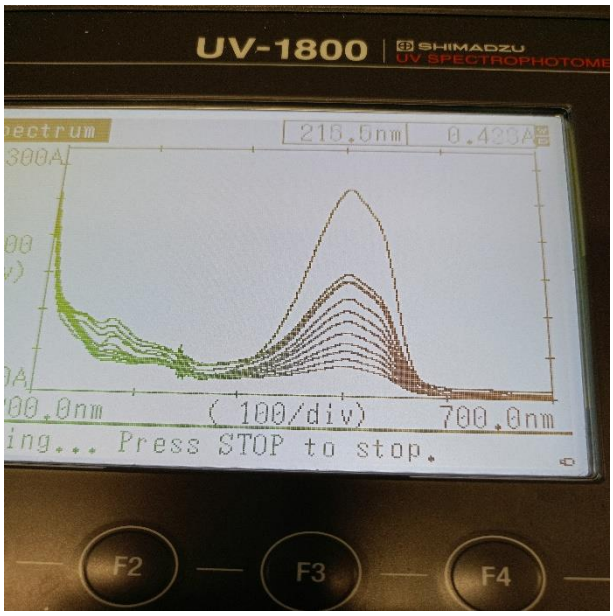

Fig.S5. UV spectroscopy analysis of MO samples using PC/0.01% v/v H_2O_2

S1. Calculation of synergy coefficient

$$\gamma_2 = \frac{k_{PC+H_2O_2+HC}}{k_{PC} + k_{H2O2} + k_{HC}}$$

The value of k_{HC} at 1.5 bar was calculated using previous work [280] as:

$$k_{eff} = \beta\Phi$$

$\beta = \frac{Q}{V}$ with Q=1.25 LPM, and V=2.5 L. The per-pass factor, Φ, was reported as 0.089. Thus,

$$k_{eff,HC} = \frac{1.25}{2.5} * 0.089$$

$$k_{eff,HC} = 0.0445$$

$$\gamma_{2,PC/0.01\%\ H2O2/HC} = \frac{1.9746}{0.0024 + 0.0003 + 0.0445}$$

$$\gamma_{2,PC/0.01\%\ H2O2/HC} = 41.85$$

Abstract

This thesis focuses on the development of advanced photocatalysts and their application in wastewater treatment, with a particular emphasis on the degradation of textile dyes. The primary objective was to enhance the efficiency of photocatalytic processes while facilitating their practical implementation.

First, an approach was developed to immobilize TiO_2 on a solid support, addressing the challenges associated with using the photocatalyst in powder form. The immobilized photocatalyst was then integrated into a hybrid process combining hydrodynamic cavitation and advanced oxidation, leading to a significant improvement in the degradation of organic pollutants.

A second approach involved doping TiO_2 with silver to optimize its photocatalytic performance. A simple, cost-effective, and environmentally friendly synthesis method was developed. The optimization of experimental conditions and the study of reaction mechanisms resulted in a highly efficient photocatalyst capable of ensuring rapid and effective degradation of contaminants.

The results obtained demonstrate the effectiveness of the proposed strategies and pave the way for practical applications in the treatment of industrial effluents. This work contributes to the advancement of water treatment technologies by proposing innovative solutions tailored to current environmental challenges.

Résumé

Cette thèse porte sur le développement de photocatalyseurs avancés et leur application dans le traitement des eaux usées, en mettant l'accent sur la dégradation des colorants textiles. L'objectif principal a été d'améliorer l'efficacité des procédés photocatalytiques tout en facilitant leur mise en œuvre pratique.

Dans un premier temps, une approche a été développée pour immobiliser le TiO_2 sur un support solide, permettant de surmonter les contraintes liées à l'utilisation du photocatalyseur sous forme de poudre. Ce photocatalyseur immobilisé a ensuite été intégré dans un procédé hybride combinant la cavitation hydrodynamique et l'oxydation avancée, ce qui a conduit à une amélioration significative de la dégradation des polluants organiques.

Une seconde approche a été explorée en dopant le TiO_2 avec de l'argent afin d'optimiser ses performances photocatalytiques. Une méthode de synthèse simple, économique et respectueuse de l'environnement a été mise en place. L'optimisation des conditions expérimentales et l'étude des mécanismes réactionnels ont permis d'obtenir un photocatalyseur hautement performant, capable d'assurer une dégradation rapide et efficace des contaminants.

Les résultats obtenus démontrent l'efficacité des stratégies développées et ouvrent la voie à des applications concrètes dans le traitement des effluents industriels. Ce travail contribue ainsi à l'avancement des technologies de traitement des eaux en proposant des solutions innovantes et adaptées aux enjeux environnementaux actuels.

الملخص

تركز هذه الأطروحة على تطوير المحفزات الضوئية المتقدمة وتطبيقها في معالجة مياه الصرف، مع التركيز بشكل خاص على تحلل الأصباغ النسيجية. كان الهدف الرئيسي هو تحسين كفاءة العمليات الضوئية التحفيزية مع تسهيل تنفيذها العملي.

أولًا، تم تطوير نهج لتثبيت ثاني أكسيد التيتانيوم (TiO_2) على دعامة صلبة، مما يساعد في تجاوز التحديات المرتبطة باستخدامه في صورة مسحوق. ثم تم دمج هذا المحفز الضوئي المثبت في عملية هجينة تجمع بين التجويف الهيدروديناميكي والأكسدة المتقدمة، مما أدى إلى تحسن ملحوظ في تحلل الملوثات العضوية.

ثانيًا، تم استكشاف نهج آخر من خلال تشويب TiO_2 بالفضة لتحسين أدائه التحفيزي الضوئي. تم تطوير طريقة تصنيع بسيطة واقتصادية وصديقة للبيئة. أدت عملية تحسين الظروف التجريبية ودراسة الآليات التفاعلية إلى الحصول على محفز ضوئي عالي الكفاءة قادر على تحقيق تحلل سريع وفعال للملوثات.

تُظهر النتائج المحققة فعالية الاستراتيجيات المطورة، مما يمهد الطريق لتطبيقات عملية في معالجة النفايات الصناعية. يساهم هذا العمل في تطوير تقنيات معالجة المياه من خلال تقديم حلول مبتكرة تتماشى مع التحديات البيئية الحالية.